High Resolution Methane Retrievals Using the PRISMA Spacecraft

Thesis Report

P. J. C. Bijl

Delft University of Technology
Faculty of Aerospace Engineering
Master profile Space Engineering

SRON
Netherlands Institute for Space Research

TU Delft

High Resolution Methane Retrievals Using the PRISMA Spacecraft

Thesis Report

by

P. J. C. Bijl

to obtain the degree of Master of Science
at Delft University of Technology,

Student number:	4492102	
Project duration:	September 1, 2021 – July 1, 2022	
Supervisors:	Dr. ir. J. M. Kuiper,	Delft University of Technology
	Dr. ir. J. D. Maasakkers,	SRON Netherlands Institute for Space Research
	Prof. dr. I. Aben	SRON Netherlands Institute for Space Research

TU Delft

Preface

The research project which is documented in this report took place in the context of my Master Thesis in Spaceflight, Aerospace Engineering at Delft University of Technology. The research project took place at The Netherlands Institute for Space Research (SRON) and as an intern I was part of the Earth Science Group.

I would like to thank my supervisors Bram and Ilse from SRON, as well as my supervisor from Delft University of Technology, Hans. Without them this project would not have been possible. In advance I would like to thank the other members of my thesis defence committee for taking the time to read my report and facilitating the defense.

Special thanks to Bram, who has been my supervisor for the past year and a half, starting with an internship that was continued into a thesis project. The very thorough feedback time and effort that he has put into this project did not only make it into a great success, but also taught me to be critical in every step of the process. Whenever I had any problem, issues or suggestions, Bram was always ready to provide feedback and help wherever he could.

My supervisors provided great assistance, but this project also relied on the expertise of experts and leaders in the field of instrumentation, atmospheric modelling and other fields, who provided me with assistance and interpretation of results. My thanks go out to Jochen and Tobias for providing me with insights and were available for feedback with regards to results obtained with SICOR. Thanks to Gerard Otter and Ruud Hoogeveen, who helped determine the problem with the fixed pattern noise in PRISMA measurements.

Not in the least my thanks to my fellow interns and PhD students and postdocs present at SRON, who I enjoyed working with. Special thanks to Allard, Lodewijck and Berend who helped me with results from their own projects to be compared to my own results. Big thanks to Acrab and Apus, who managed to survive my daily assault on their CPUs.

My last thanks to my family and friends who have helped me stay motivated and provided some relief from the hard work. I would like to extend gratitude towards my roommates, who accepted that I forsake my cleaning duties more often than not and who always had a nice dinner ready after a long working day. Shout-out to the Caldera, who did not manage to distract me enough to miss my deadlines.

P. J. C. Bijl
Rotterdam, June 2022

Abstract

It has become undeniable in recent years that the Earth is warming due to the emissions of greenhouse gases by anthropogenic activity [22]. Methane is the second most important anthropogenic greenhouse gas, after CO2, in terms of radiative forcing. The primary emission sources for methane come from the fossil fuel industry and from landfills, which are often concentrated as point sources. Detecting methane emissions from point sources can help fight climate change because the atmospheric lifetime of methane is relatively short. Recently it has been shown that the PRISMA satellite can be used to detect strong point sources of methane in the form of plumes [15]. This allows for high-resolution methane retrievals over selected scenes of 30x30 km.
The methane retrievals using PRISMA hyperspectral data are currently limited in their scope by the noise in the retrieval. Small sources are not visible due to this noise. The matched filter currently uses a linearized representation of how methane absorbs light, which was given more freedom after developing two new methods that allowed for an iterative approach to the problem. Analysis showed that the current matched filter retrieval is too restrictive for the estimation of enhancement concentrations around the sources of emissions.
The second retrieval method developed is a modified version of SICOR, the operational carbon monoxide retrieval method for TROPOMI data, which includes a step that estimates methane concentration. By adapting the inputs and changing the simulation settings it was possible to use it for PRISMA. It was shown to be able to detect methane emissions but with a higher level of noise. The source concentrations and emission estimates were higher for SICOR, showing the greater flexibility that a full inversion retrieval method has.
Analysis and comparison of the two models showed that the matched filter is better able to detect emissions, with a clearer distinction between enhancement estimates and the background noise. The best explanation for this is that it can the data of many spectra simultaneously, thereby reducing the noise. SICOR did allow for more flexibility and shows more adaptability to different areas, showing less susceptibility to areas with elevation changes. A combination of the two methods, where the matched filter provides plume identification and SICOR provides plume quantification, could be the best method to provide high-resolution methane retrievals and quantification estimates. Using part of the data for clustering allows for an albedo correction, which has shown to improve the retrieval of the matched filter, which could be extended in the future to SICOR.

Key Points

- A matched filter retrieval for PRISMA was implemented and improved, alongside with a full inversion retrieval method (SICOR) for methane adapted from TROPOMI.
- The models show that the matched filter is better at reducing noise in retrievals, but lacks the flexibility and independence that SICOR has.
- A combination between the two, using both strengths was deemed most effective for monitoring point-source emissions with high spatial resolution.
- Using hyperspectral data to provide for albedo corrections can improve results even more.

Keywords

PRISMA, Methane, CH4, Plume, Emissions, Matched Filter, Retrieval, Climate Change, Satellite

List of Figures

List of Tables

Abbreviations

ASI Agenzia Spaziale Italiana. 23

CH4 Methane. 17

CSF Cross-Sectional Flux. 40, 41

CTM Chemical Transport Model. 77

FFT Fast Fourier Transform. 65, 70

FWHM Full Width at Half Maximum. 23, 26, 30, 38, 39, 73

GHGs Greenhouse Gases. 13, 15, 16

GWP Global Warming Potential. 16, 17

ICU Internal Calibration Unit. 88

IMAP-DOAS Iterative Maximum A Posteriori–Differential Optical Absorption Spectroscopy. 53

IME Integrated Mass Enhancement. 27, 40, 43

ISRF Instrument Spectral Response Function. 58, 59, 70, 86

ISTA Iterative Shrinkage-Thresholding Algorithm. 24

LUT Look-up Tables. 39, 59, 70, 86

PAN Panchromatic. 22

PRISMA PRecursore IperSpettrale della Missione Applicativa. 13

PSNR Peak Signal to Noise Ratio. 34

RMS root-mean-square. 36, 42–44, 54, 74, 86

RTM Radiative Transfer Model. 23

SNR Signal-to-noise ratio. 21, 22, 24, 30, 32, 36, 43, 44, 84, 86, 88

SRF Spectral Response Function. 86

SVC Support Vector Classifier. 87

SWIR Shortwave Infra Red. 21, 22, 25, 66

TOA Top of the Atmosphere. 26

UTC Coordinated Universal Time. 23

VNIR Visible Near Infra Red. 22

Nomenclature

A_j Pixel area. 28

C Normalization constant. 59

N_A Avogadro's constant. 61

Q Source rate. 27, 28

U Wind speed. 28

Σ Covariance of the detector radiance spectrum. 24

δ Delta wavelength. 59

$\hat{\alpha}(\vec{x})$ Estimated enhancement. 24

λ Wavelength. 59, 61

τ Average residence time. 28

$\vec{\mu}$ Mean detector radiance spectrum. 24

$\vec{t}$ Target spectrum. 24

$\vec{x}$ Input detector radiance spectrum. 24

c Speed of light. 61

e_y Error vector. 25

h Planck constant. 61

x Atmospheric state vector. 25

Contents

1

Introduction

This report describes the thesis research of the project “High-Resolution Methane Retrievals Using the PRISMA Spacecraft”. The project is supervised by Dr. ir. J.M. Kuiper , assistant professor Space Engineering at Delft University of Technology, faculty of Aerospace Engineering. It is conducted at SRON Netherlands Institute for Space Research under supervision of Dr. Ir. J. D. Maasakkers (daily supervisor), Dr. S. Pandey and prof. Dr. I. Aben (overall supervisor).

Since the industrial revolution, fossil fuels have been the primary energy source for economic development. It has been proven that this continued use of fossil fuels has been the main driver of climate change [22]. Carbon dioxide and methane are the main drivers in terms of radiative forcing and are actively emitted by anthropogenic activity [19]. Monitoring of these Greenhouse Gases (GHGs) can help mitigate climate change by providing detailed source locations, which is especially useful for methane [26]. In recent years, several developments have been made in measuring GHGs from space, with observations being made by several satellites. These observations, however most often have a low spatial resolution or do not offer global coverage. Data from a new hyperspectral imager satellite, called PRecursore IperSpettrale della Missione Applicativa (PRISMA) offers targeted global high-resolution images over a wide array of wavelengths. While originally not meant for measuring methane, recent literature [15] has shown that it is possible to use this kind of data for methane retrievals and detection of large point sources of methane emissions. An issue with current methods is the detection limit. The high resolution retrieved methane enhancements are quite sensitive to noise and only large concentrated emissions are distinguishable from the background noise and are thus above the detection limit. Currently statistic methods are in use, while there are also more advanced methods for methane retrieval available. The question remains how much retrievals can be improved and where methane emissions can be discovered using PRISMA.

The report starts with a description of the theoretical background of the project in chapter 2. In this chapter, methane and its role with regard to radiative forcing is explained, along with how it can be measured from space. It concludes with the relevant retrieval techniques that will be explored further in this report and the techniques necessary to analyze retrievals in terms of quality and emission quantifications. This is followed by the research definition in chapter 3, where the opportunities and relevance of the project are explained together with the research questions that guide the research. Using the knowledge presented in the theoretical background and the research question a baseline and approach is presented in chapter 4, to provide a consistent framework with which to guide the project and answer the research questions. After establishing a theoretical background and the setup of the research the two developed methods for PRISMA methane retrievals will be discussed. The matched filter will be discussed first in chapter 5, starting with the original

implementation and newly developed methods. Obtained results and analysis will be presented along with tools that were developed to analyze PRISMA results. The second retrieval method is described and analyzed in chapter 6, which employs a different technique than the matched filter. Its applicability for methane retrieval is tested and results are presented.
The two developed retrieval methods are compared against each other in chapter 7. This is done by visually comparing results, discussing the difference in enhancements and quantification estimates and explaining where the differences originate from. Also in this chapter, the effects of hyperspectral denoising on methane retrieval are discussed, along with the effect of spectral calibration. From this analysis and the results of the chapters before the conclusion will be given along with an answer to the main research question in chapter 8

2

Theoretical Background

The theoretical background will describe the most important results from the literature study and focus on the underlying principles and theories that have been used throughout the project. In subsection 2.1.1 the causes and effects of global warming are discussed, of which methane is one of the most contributors. The observation of methane from space is discussed in section 2.2, which compares current missions in methane observations. section 2.3 describes the basics of hyperspectral imaging and more specifically the details of the PRISMA spacecraft and its data. The two relevant retrieval methods are explained in section 2.4 along with spectral calibration and quantification in section 2.5.

2.1. Global Warming and Methane

Global warming is caused by the radiative forcing of GHGs. Most of the emission of GHGs is caused by anthropogenic activity. This section will describe the greenhouse effect and the main contributors in terms of radiative forcing and what sources contribute to it.

2.1.1. Global Warming

It has become evident that the Earth is warming when compared to the pre-industrial era, as can be seen in Figure 2.1. This global warming and climate change can mainly be attributed to anthropogenic activity [19].

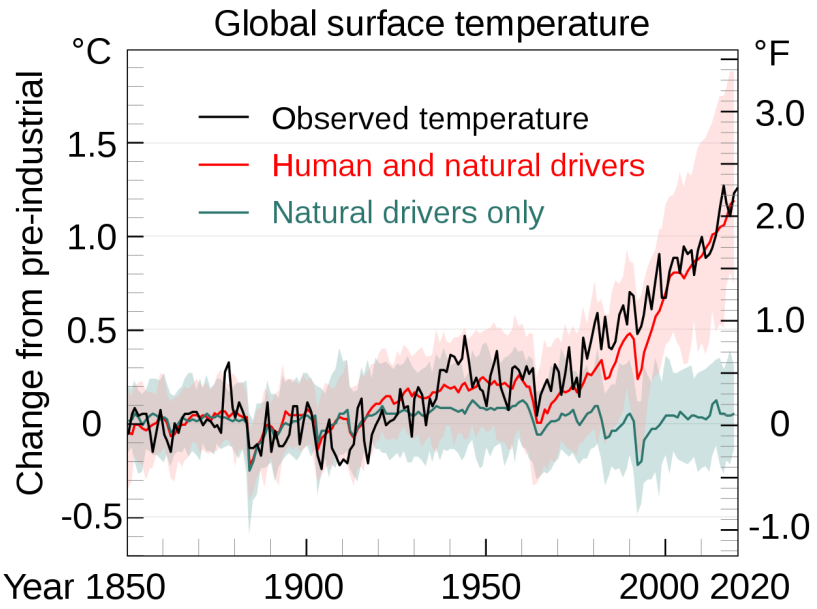

Figure 2.1: Global mean temperature change over the last 170 years [22].

The rise of Earth's temperature coincides with the unprecedented emission of GHGs due to anthropogenic activity [21]. As the concentration of these gases rises in the atmosphere, so does the temperature of the atmosphere. This leads to warming because these gases absorb terrestrial radiation with wavelengths from (5 to 50 μm) and emit them back to Earth. Earth's atmosphere naturally traps some radiation, primarily due to presence of water vapour. These GHGs add to this effect and radiation that would have escaped to space, is trapped by a "greenhouse effect" is created that heats the Earth with these gases. The proper term for this is called radiative forcing. The effect of radiative forcing has increased from 0.57 Wm^{-2} from 1971-2018 to 0.79 Wm^{-2} from 2006-2018, in line with the increased concentration and continued emission of several GHGs [21].
The reason that GHGs specifically cause this radiative forcing is that they have absorption and emission bands that correspond to the radiation that is coming off the Earth. The most important contributors to radiative forcing are in decreasing order of magnitude: CO_2, CH_4 and N_2O. A metric to quantify the effect that each trace gas has on the radiative forcing is the Global Warming Potential (GWP), which is defined as:

> The Global Warming Potential of a refrigerant is defined as the integrated radiative forcing over a "time horizon" of [20,100,500] years following an assumed release of 1 kg, divided by the integrated radiative forcing over the same period from release of 1 kg of carbon dioxide[20]. An overview for the three most important GHGs is given here below:

Table 2.1: GWP of the main greenhouse gases over different timespans [20].

GHG	Lifetime [yr]	GWP 20	GWP 100	GWP 500
CO2	-	1	1	1
CH4	11.8	81.2	27.9	7.95
N2O	109	273	273	130

> From this table, it becomes immediately apparent why the detection of methane plumes is so effective in short-term climate change mitigation. The short-term GWP of methane

is 81 times higher than that of carbon dioxide, meaning the amount of methane in the atmosphere decreases over time because the atmospheric lifetime of methane is shorter than that of carbon dioxide. Nitrous oxide has a higher GWP still. However, its overall radiative forcing is lower due to its lower concentration in the atmosphere, and it has a longer atmospheric lifetime [21]. Therefore, decreasing methane emissions in the atmosphere decreases the methane concentration significantly after only a few years and reduces the amount of radiative forcing on Earth.

2.1.2. Methane

Methane or Methane (CH4) is a naturally occurring colorless and odorless gas. It is slightly lighter than air and is the lightest alkane and the main constituent of natural gas, which is used as a fuel for combustion as well as heat. It is produced by both natural as well as anthropogenic processes. In the atmosphere, it exists as a gas, where it is the second most abundant anthropogenic greenhouse gas.

Properties

Under normal atmospheric conditions, it is in a gaseous form, but it becomes a liquid at -164°C. As stated before, it is most commonly found in natural gas, used as a fuel. While methane is odorless, an odor is added for safety reasons. Methane is flammable if the concentration of the gas in the air is 5-17%.

Methane has a molecular mass of 16.04 g/mol [24], which makes it slightly lighter than air. When assuming that the mass of the atmosphere is around $5.2 \cdot 10^{18}$ kg and that the mean concentration of methane in the atmosphere 1880 ppb, gives a total mass of atmospheric methane of $5.43 \cdot 10^{12}$ kg, or 5.43 Gt, while the unit Tg is also used, for which the value is 5430 Tg. Methane can generally be viewed as a well-mixed gas in the atmosphere, but its distribution over the Earth is not entirely homogeneous due to emissions and natural processes. The northern hemisphere has higher concentrations due to more emissions being located there. Over time the mean concentration also changes, which is because of the influence of nature on the sinks of methane [2].

The concentration of methane has risen from 722 ppb in 1750 to 1890 ppb in 2021. Throughout the year, methane values vary [27]. The main reason for this increase is the result of human activity. The main industries that contribute to rising methane levels in the atmosphere are agriculture and the exploitation of fossil fuels.

As shown before the concentrations of various gases influence the spectrum of radiation coming off from the Earth when seen from Space. Methane like any other molecule has specific wavelengths at which it can absorb and emit photons, which results in a transmittance spectrum in the atmosphere that can be seen on the next page:

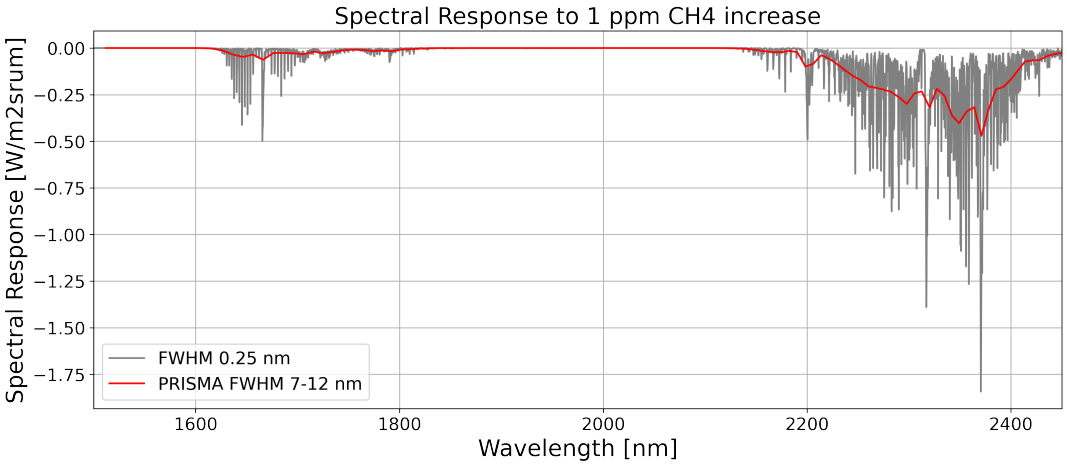

Figure 2.2: Overview of Methane spectrum.

Where the dips in the spectrum are caused by the absorption of methane. These fluctuations in transmittance can be used by a spectrometer to detect methane. The main absorption bands of methane that are of interest for PRISMA's data are around 2300 nm, with a less strong absorption band around 1650 nm.

Methane has three main sources: biogenic, thermogenic and pyrogenic. Biogenic entails all sources that are biological in nature. For example, rice paddies, wetlands, and landfills produce methane through microbes that produce methane (methanogens). Thermogenic methane is created by geological processes under high temperatures and pressures over millions of years and is most commonly found as fossil fuels. It is released naturally in the atmosphere by terrestrial and marine seeps and through mud volcanoes. Finally, pyrogenic sources are caused by the incomplete combustion of methane from fuels such as biomass, but also including fossil fuels [30].

Methane does not remain in the atmosphere indefinitely but is removed from the atmosphere through two processes: atmospheric reactions and reactions with soil. Since atmospheric reactions count for over 90% of the sinks for atmospheric methane, the focus will be on these reactions. The main reaction that removes methane from the atmosphere is its reaction with hydroxyl radicals (OH):

$$CH_4 + OH \rightarrow CH_3 + H_2O \tag{2.1}$$

This reaction explains the shorter atmospheric lifetime of methane when compared CO_2 and why it is a useful candidate for short term climate change mitigation. An overview of sources and sinks within the global methane budget is given below:

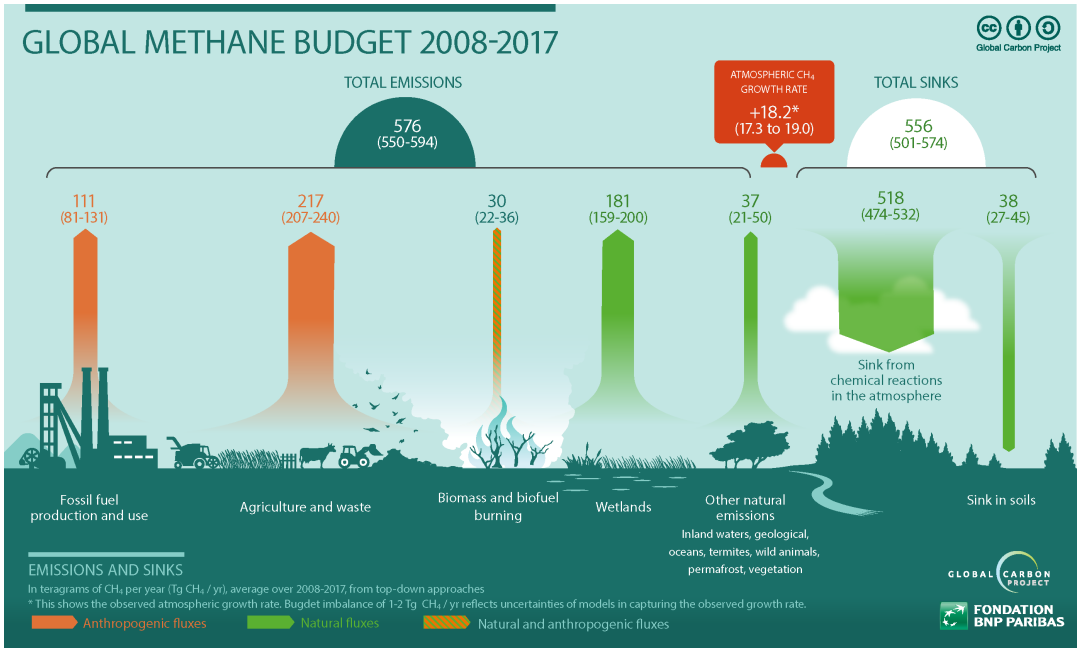

Figure 2.3: Overview of atmospheric methane sources and sinks [44].

It can be seen in the figure above that there is a net increase each year of the methane in the atmosphere. Of these sources, the fossil fuel production sites and distribution networks are the most interesting to investigate since these emissions are often point-sources and will produce high concentrations of methane that are observable from space [26] [9].

2.2. Measuring Methane from space

Earth has been monitored by satellites since the end of the 1950s, providing several services, ranging from telecommunications to information gathering for weather forecasts [10]. Environmental monitoring started with the European Remote-Sensing Satellite 1 and 2 in 1991 and 1995 respectively, with measurements about surface heights, wind speed and atmospheric water [7]. These have since been continued by ENVISAT and the Copernicus Program. In the previous chapter it was mentioned that environmental monitoring of the atmosphere can be done by measuring the spectrum of the reflected solar light reflected off Earth and using it for analysis. This is called imaging spectroscopy, and it has been recently used for atmospheric monitoring starting with the OMI instrument aboard the AURA mission and followed up by the TROPOMI instrument aboard the Sentinel-5P mission [46, 54]. With TROPOMI methane can be observed and monitored, alongside other trace gases on a daily basis at a global level. A more recent development still is the launch and use of private satellites that are able to monitor methane, such as the GHGSat constellation and the WorldView-3 satellite.

Additionally to the multispectral instruments of Sentinel-5P, Sentinel-2 and GHGSat, orbital hyperspectral instruments can be used for methane retrievals, even though they have not been designed for this capability [4, 15]. The difference between these two types of instruments is that a multispectral instrument measures only a limited number spectral bands that do not have to be continuous and a hyperspectral instrument measures over a continuous large spectral band [17]. Earlier it has been shown that this was possible using hyperspectral instruments using the airborne AVIRIS instruments

for methane emissions coming from point sources [49, 50]. Also a recent development is the use of WorldView-3 for high spatial resolution methane detections [43]. These imagers have different capabilities and specifications and are therefore also used in different ways. An overview of their specifications is given below:

Table 2.2: Overview of Methane monitoring satellites, values with regard to spectral/spatial accuracy and resolution have been given for values in the SWIR region * - bands are not continuous.

Satellite	TROPOMI [54, 36, 25]	Sentinel-2 [47, 45, 25]	WorldView-3 [6, 25]	GHGSat-D [28, 25]	PRISMA [31, 35, 25]
Orbit Altitude [km]	824	786	621	512	614
Revisit Time [days]	1	2-3	1	14	29
Spatial Resolution [m]	7000x5500	20	3.7	50	30
Field-of-View [kmxkm]	Global	Global	66.5x112	12x12	30x30
Spectral Resolution [nm]	0.25-0.55	100	40-50	0.1	7-12
Bands [nm]	270-2385*	400-2300*	400-2500*	1630-1675	400-2500
Instrument SNR	100-120	100	n.a.	200	100-200
Radiometric Accuracy [%]	2	3	n.a.	n.a.	<5
Pointing Accuracy [°]	0.03	0.07	n.a.	<0.3	0.07
Detection Limit [t/h]	25	1.8-25	0.1	1-3	0.5-2
Data Availability	open license	open license	no	no	open license

These missions are all interesting and relevant to compare, because they describe a wide array of methane monitoring possibilities. This starts with the global monitoring missions of TROPOMI aboard Sentinel-5P and the Sentinel-2 mission, which is a constellation of two satellites. TROPOMI was designed to monitor methane and therefore has great sensitivity and accuracy towards the retrieved methane concentrations, but it has a very coarse spatial resolution, which makes it hard to pinpoint emissions if they are spotted. Sentinel-2 improves on the spatial resolution part, but is less accurate, given the fact that it has very wide spectral bands that are less sensitive for the absorption features of methane discussed in the previous chapter. It was also not designed to detect methane, a capability that was shown only later [52] and a capability that only works for the largest methane plumes. WorldView-3 is similar to Sentinel-2, but has even higher spatial resolution still, but no open data policy given that it is a commercial satellite. GHGSat-D is a high spatial resolution targeted imager, which is designed to monitor methane emissions. It is targeted, meaning that it can only provide images of specific locations, it has a very high spectral resolution, which makes it very sensitive to methane. Its Field-of-View is small, which makes coordination important to spot emissions.

PRISMA is a hyperspectral imager, not designed to monitor methane. It falls between TROPOMI and GHGSat in terms of both methane sensitivity as well as coverage. PRISMA is a targeted imager, with high spatial resolution, but low spectral resolution. GHGSat-D and PRISMA are in many ways alike, having similar spatial resolution, field of view and revisit times, but their imagers differ substantially in terms of spectral resolution and the spectrum that they can observe, which corresponds more with that of the airborne AVIRIS instrument, which has already been used for methane retrievals [50, 49]. The most challenging aspect of PRISMA methane retrievals will be the fact that its spectral resolution is significantly lower than that of TROPOMI and GHGSat-D, this means that the methane signal will be smoothed out and that over the same given spectrum, fewer

datapoints can be used for retrieval. It will be important to verify if the Signal-to-noise ratio (SNR) requirement of the PRISMA mission of 100 is met in the Shortwave Infra Red (SWIR) region for PRISMA. This directly influences the detection limit, as an increase in noise will make it much harder to detect the dips in the electromagnetic spectrum and limit the detection of small methane emissions with PRISMA. An analysis of noise in the radiance measurement is done in subsection 6.4.1.

2.3. PRISMA

This section describes the PRISMA spacecraft and the hyperspectral instrument that it carries. Also discussed will be the data product that has been used throughout the thesis research.

2.3.1. Spacecraft

PRISMA (PRecursore IperSpettrale della Missione Applicativa) is a single satellite mission that allows for the near-global imaging of Earth, with a hyperspectral imager. It is a pointing imager, meaning that it images selected locations and does not provide complete global coverage like the Sentinel-2 and Sentinel-5P missions. Alongside the hyperspectral imager, there is also a panchromatic imager on board. The mission allows for imaging in the VNIR and SWIR bands with a spectral resolution of 10 nm, and a spatial resolution of 30x30 m.

The spacecraft is placed in a Sun-synchronous orbit with an altitude of 614 km and an orbital period of 98 minutes. This allows it to have a repeat interval of 29 days, but locations can sometimes be imaged at a shorter interval, by pointing the spacecraft towards the location, although the exact overpass will not be identical. It was launched on March 22nd of 2019 aboard a Vega rocket from the Guiana Space Centre in Kourou. [35]

The goal of the mission is to provide data that can be used to analyze the chemical physical composition of objects at the Earth's surface at the scene that the satellite is pointing at. This includes analyzing crops, environmental monitoring as well as surface classification, while also providing the geometric information of the objects below. The mission is also a technology demonstrator to show and verify that hyperspectral imagers work in space.

2.3.2. Instrument

The hyperspectral instrument of the PRISMA mission offers images with a 30m resolution along a 30km swath with 250 spectral bands that cover the visible, near-infrared, and short wave infrared, containing the absorption features of methane, carbon dioxide and carbon monoxide, with some overlap between the very near-infrared and the short wave infrared. Alongside the hyperspectral images, a panchromatic image is created with a sharper resolution of 5m. Below a schematic view of the PRISMA instrument can be seen. The instrument works as a targeting imager, where locations can be viewed upon request [31].

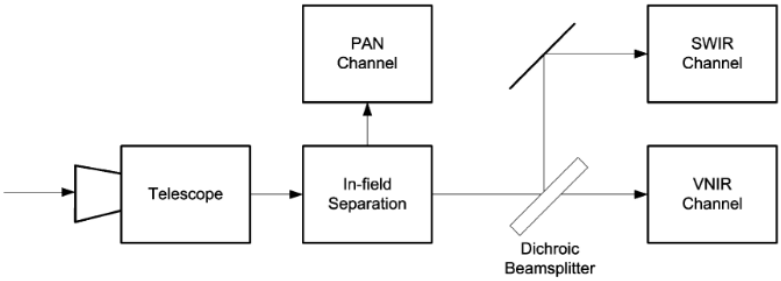

Figure 2.4: Block diagram of optics, that shows how incoming light is divided for the two different detectors [31]

From Figure 2.4 it can be seen that incoming light through the telescope is first separated. This is done by an in-field separation technique, which divides the incoming light for the Panchromatic (PAN) channel and the Visible Near Infra Red (VNIR)/SWIR channels. The second beam is then further split by a dichroic beamsplitter for the SWIR and VNIR channels. The VNIR channel has 92 spectral bands, and the SWIR channel has 170 spectral bands. Each channel has 1000 detectors. The Signal-to-Noise Ratio SNR for PRISMA is always larger than 100 and higher still at selected bandwidths. The PAN channel has an SNR of 240. The Hyperspectral/PAN Optical Head is fitted inside the spacecraft according to the block diagram below as follows:

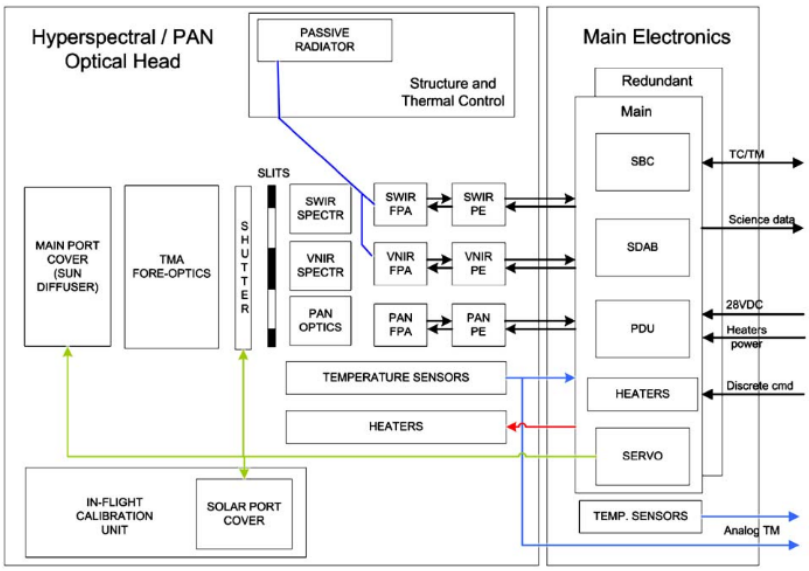

Figure 2.5: Block diagram of the PRISMA instrument [31].

In Figure 2.5 it can be seen how the electronics and thermal control interact with the main optical head. The thermal control keeps the SWIR detector in a range between 160 and 180 K, while the VNIR detector is kept cool between 240 and 250 K. It is also important to mention how the calibration unit functions. A dedicated solar port is used to allow sunlight to enter the instrument, before passing through a shutter in front of the optical slits, which also allows for dark calibration. This allows for sunlight to enter the instrument and verify if it still functions according to specifications. It is able to perform absolute and relative radiometric calibration as well as spectral calibration [31].

Every day the hyperspectral imager is able to take 223 30x30 km hyperspectral images and sends them to Earth via communication done over the X-band.

2.3.3. Data

PRISMA data is available on request as either level 0 products or level 1 products. For this thesis level 1 will be used as it is the lowest data level available through the PRISMA ASI portal. This is radiance data that has been radiometrically calibrated. Data is available in a hierarchical file format (.he5) and the main data is primarily divided into three separate fields: hyperspectral data fields, panchromatic data fields and geolocation fields. [41]:

- The panchromatic data field is a bi-dimensional array of 6000x6000 pixels that contains a panchromatic image of the scene with a resolution of 5m per pixel.
- The hyperspectral data field is a three-dimensional array, with the first dimension being the VNIR and SWIR bands (66 and 173 layers respectively), the second dimension being the detection in along-track direction. The third dimension is across-track and is where the different detectors are located. Data points are radiometrically calibrated radiance.
- The geolocation data field corresponds to the hyperspectral data field and contains the latitude and longitude of the pixels in two bi-dimensional arrays. Alongside the location, the Coordinated Universal Time (UTC) is also included .

Also added in separate fields are the central wavelengths of each detector and the Full Width at Half Maximum (FWHM) of each detector. Data is available on request provided on the PRISMA portal from Agenzia Spaziale Italiana (ASI), by selecting scenes based on locations and time windows and ordering them. This database consists of an archive of previous measurements.

2.4. Retrieval Methods

Two retrieval methods will be used for methane retrieval using PRISMA. These two methods are the matched filter, a method already in use for hyperspectral data[15] and SICOR, the operational CO algorithm using TROPOMI data. The matched filter is a signal processing technique, which correlates measurements to a known reference methane signal. SICOR on the other hand is a full inversion of a Radiative Transfer Model (RTM), which has more flexibility than the matched filter.

2.4.1. Matched Filter

The matched filter is a data-driven method where a target signal is correlated and matched to a measurement. In recent years it has been shown that this method can be used for methane retrieval from spectral data [48, 13, 50]. More recently, it was also shown that the same method could be used to perform methane retrievals from PRISMA data [15].

The target signal is acquired by simulating the spectral response by adding a unit enhancement concentration of methane to a representative atmosphere. This simulation is done by using the radiative transfer code provided by MODTRAN [1]. This spectral response is at a higher spectral resolution than that of PRISMA, so it is sampled per along-track column so that the right spectral specifications is used, which are stored inside the PRISMA data product [41] using the center wavelength of each detector and the FWHM.

The matched filter tries to maximize the SNR, by fitting a filter that tries to maximize the correlation between the measurement and the target signal and minimizing the noise. For a matched filter that uses a radiance spectrum as the target the following matched filter can be derived:

$$\hat{\alpha}(\vec{x}) = \frac{(\vec{x} - \vec{\mu})^T \Sigma^{-1} \vec{t}}{\vec{t}^T \Sigma^{-1} \vec{t}} \tag{2.2}$$

Where $\hat{\alpha}(\vec{x})$ stands for the estimated enhancement of methane in ppb, $\vec{x}$ stands for the radiance input spectrum of a detector that is matched to the reference spectrum, $\vec{\mu}$ and Σ is the mean and the covariance of the detector radiance signal. $\vec{t}$ is the reference signal, which is the elementwise multiplication of to the mean radiance spectrum with the unit spectral response, as shown in Figure 2.2. This input spectrum is similar to the one that can be found in Figure 2.2. In Equation 5.1 the dip in radiance with respect to the mean for every pixel of the detector is calculated, which then can be matched to the target spectrum, as they are now in the same form. Using the covariance of the radiance measurements of a single detector the matched filter is the least squares estimator for this problem.

The advantages of the matched filter method for methane retrievals are that it is computationally fast and immediately produces enhancements instead of concentrations, like other methods. By incorporating the different spectral characteristics of each detector-column in the matched filter problems with calibration of the instrument are also removed, which can negatively affect retrieval.

Sparsity Prior

In a typical scene of PRISMA only a small fraction of pixels contain relevant enhancements, even if the emissions cover thousands of pixels. Using this 'sparsity' might help isolate the enhancement pixels and better estimate their values, while 'ignoring' pixels that are not statistically significant and do not contribute to the signal. This practice is established in medical imaging, photography and other sensing disciplines [13, 37, 8].

The sparsity prior proposed in [13] uses l_1 sparsity, corresponding to the term used by the LASSO technique. This sparsity is implemented by assigning a regularization weight to each pixel. This regularization weight penalizes small enhancements and forces them to go to zero, so that only significant enhancements remain. The sparsity prior weights is defined as:

$$w_i^k = \frac{1}{\alpha_i^{k-1} + \epsilon} \tag{2.3}$$

Where α_i^{k-1} is the ith pixel enhancement at iteration k, ϵ is a small scalar that is added for numerical stability. The regularized weights can then be subtracted from either Equation 5.1 to regularize the matched filter. An iterative approach is used to implement the sparsity prior for the retrieval. The mean and covariance are recalculated in each step, along with the regularized weights, to ensure stability in a process called iterative shrinkage-thresholding algorithm Iterative Shrinkage-Thresholding Algorithm (ISTA) (ISTA).

2.4.2. SICOR

SICOR is the operational algorithm for the carbon monoxide product made using level 1 TROPOMI data. It uses a two-step retrieval approach, of which the first step provides an estimate for the methane concentration, which is used in a second retrieval step, which estimates carbon monoxide concentrations. It is different from the matched filter, because it uses an inversion of a Radiative Transfer Model. Whereas the matched filter is more a statistical model that tries to correlate a column of data to a linearized representation of absorption by methane. SICOR actually models the radiative transfer of radiation through the atmosphere, based on the trace gases that are included in its state vector. Not only methane is included in the model, but also other trace gases such as water vapour and carbon monoxide. It therefore has more flexibility than the matched filter, which cannot account for the influence of these gases. As mentioned above, SICOR uses a two step approach, where in the first step the methane concentration is estimated. This first step might be suitable for use for PRISMA data.

SICOR performs a pixel by pixel retrieval and introduces a state vector in which the concentration of all trace gases are included. This state vector determines how the radiative transfer is simulated and this is propagated in the following forward model.

$$y = f(x, b) + e_y \tag{2.4}$$

This forward model creates a measurement vector y that is a function of the atmospheric input vector x and ancillary parameter vector b, along with a measurement error vector e_y. SICOR uses a forward model that simulates the TOA radiance spectrum from 2315-2338 nm, which contains absorption of methane and carbon monoxide. Equation 2.4 is used to describe the measurement as a state of the atmosphere, which is retrieved by minimizing the following cost function:

$$\hat{\boldsymbol{x}} = \min_{x} \left\| \mathbf{S}_y^{-1/2} (\mathbf{F}(\boldsymbol{x}) - \boldsymbol{y}) \right\|^2 \tag{2.5}$$

Inversion is done by using a Gauss-Newton iteration scheme. For the second retrieval step, Equation 2.5 is used, which has the Tikhonov regularization in it. This regularization is added to account for the loss of sensitivity over the vertical profile and to ensure numerical stability. This iteration continues until the difference is below a set threshold or until the maximum number of iterations is reached. SICOR has four steps with two different retrieval steps that are used to retrieve the carbon monoxide concentration column along with a random error estimate:

1. Filter A: The first filter is used to check the L1B radiance data on quality and to remove observations that are too dark or have other quality issues.
2. Non-scattering retrieval: An initial retrieval for methane is performed, using the band of 2315-2324 nm. The forward model does not include any Rayleigh scattering because of its high computational load and also because in the SWIR scattering only constitutes 0.15% of the signal. The output of this step is the methane concentration of the state vector x.
3. Filter B: The retrieved methane concentration is used by comparing it against an accurate a-priori estimate. Measurements are only accepted if the difference between the two methane estimations falls under a threshold.

4. Physics-based retrieval: A second retrieval is performed to obtain the CO column concentration, for this a band is taken from 2324-2338 nm. For this retrieval the information obtained from the methane retrieval is used to infer the effect of atmospheric scattering by clouds and aerosols.

This algorithm returns the averaged CO column concentration, along with an estimation of the uncertainty [32, 55, 34]. An important part in the iterative scheme is the chi-squared score that is given to each iteration, where a lower score means a better fit for the measurements.

2.5. Spectral Calibration and Quantification

This section describes the spectral calibration possibilities for PRISMA and how quantification is used to estimate the source rate of emissions.

2.5.1. Spectral Calibration

The spectral calibration settings of the instrument are of the utmost importance for a retrieval. The FWHM of each detector corresponds to the width of that detector. This influences the retrieval as the simulated Top of the Atmosphere (TOA) radiance is convoled using these FWHM settings, alongside the center wavelength of each detector. Small differences in these values can have a significant influence in the retrieved concentrations of methane as well as the quantification of emissions from sources [16, 15].

A way of correcting the central wavelength and FWHM of each detector is to use scene-based calibration, by simulating multiple TOA radiance spectra for each detector column and use inversion to find the best fit between the across-track pixels [16]. This starts by generating the reference radiance spectra similarly to how the results from Figure 2.2 were generated and the target spectrum from the previously explained matched filter. These spectra are convolved with the nominal settings provided by the PRISMA data files. An iterative approach is used to discover the spectral shift and spectral widening of each detector to find the results that deliver the smoothest surface reflectance spectrum.

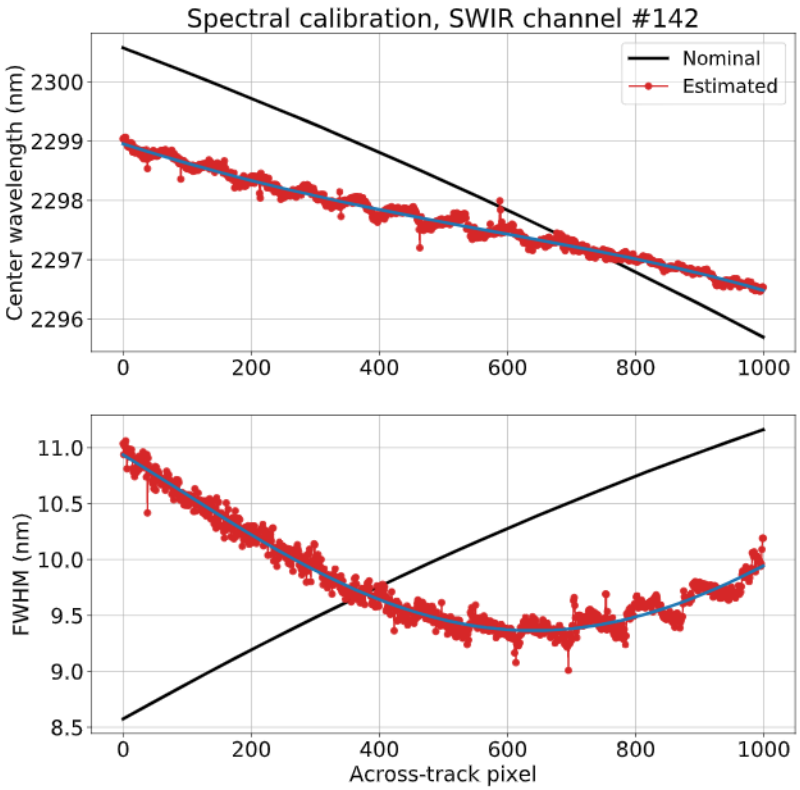

Figure 2.6: Across-track variation of central wavelength and FWHM, with updated values after using spectral calibration as shown in [15].

Above initial results of this calibration for a scene in Algeria are shown, where it can be seen that significant differences between the nominally reported values and the estimated values arise. It is interesting to test what the effect on methane retrieval will be by adopting the change in spectral settings for PRISMA.

2.5.2. Emission Quantification

An important part in the analysis of plumes is the quantification of the emitting source, how much methane is being emitted by for example a compressor station. In recent years several methods have been proposed to quantify emissions of which two will be discussed in more detail as they are most often used. These methods are Cross-sectional flux method and the Integrated Mass Enhancement (IME) method [53].

Cross-sectional flux

In the cross-sectional flux method the fluxes across the plume cross-section orthogonal to the plume direction are calculated. To calculate this, the following equation is used:

$$Q = \int_{-\infty}^{+\infty} U(x,y)\Delta\Omega(x,y)\mathrm{d}y \tag{2.6}$$

Where Q is the source rate, $U(x,y)$ is the wind field and $\Delta\Omega(x,y)$ is the methane enhancement per pixel. y is the axis perpendicular to the wind. In order to come to a practical solution the integral is discretised and taken over the width of the detectable plume, with an effective wind speed instead of a wind field, which is calculated using:

$$U_{\text{eff}} = 1.47 \cdot U_{10} \tag{2.7}$$

With U_{10} being the measurable 10-m wind speed. [53]

IME

The Integrated Mass Enhancement or IME relates the source rate to the total plume mass that can be detected from space. To get the plume mass first a plume mask is necessary, which highlights all the pixels that are part of the plume. The mass is then calculated using:

$$\text{IME} = \sum_{j=1}^{N} \Delta\Omega_j A_j \tag{2.8}$$

Which sums up the methane mass that is present in all pixels, with A_j being the area of each pixel of the plume and N the number of pixels. Before being related to the source rate Q:

$$Q = \frac{1}{\tau}\text{IME} = \frac{U_{\text{eff}}}{L}\text{IME} = \frac{U_{\text{cff}}}{L} \sum_{j=1}^{N} \Delta\Omega_j A_j \tag{2.9}$$

Where τ is the average residence time of the methane in the plume and L is the length of the plume, calculated as the square root of the plume area. The effective windspeed U_{eff} is calculated with the empirically retrieved relation:

$$U_{\text{eff}} = 0.34 \cdot U_{10} + 0.44 \tag{2.10}$$

3

Research Definition

3.1. Opportunities

There are several opportunities with this thesis project, the first of which is to verify if radiative transfer inversions can be used for hyperspectral data such as PRISMA to perform methane retrieval. The retrieval of methane with a hyperspectral instrument such as PRISMA can provide an additional link in a chain of satellites that monitor methane emissions, where global monitoring missions such as TROPOMI can provide locations of interest which a targeted imager such as PRISMA can use for further analysis. PRISMA has a high spatial resolution and this allows to pinpoint emissions to a facility level. With a 30 meter resolution it can be determined from which part of an oil/gas facility the emissions are coming from. While not designed for retrieving methane emissions, it provides a useful addition to other methane monitoring satellites, with targeted global coverage and detection capabilities between those of TROPOMI and GHGSat-D as shown in Table 2.2. Currently these detection capabilities are not equal around the world, expanding the detection capabilities is a useful tool in getting a better understanding where emissions are coming from and helping humanity tackle climate change. The last opportunity of this research is to expand the number of trace gases that can be retrieved with PRISMA, for this carbon monoxide is a prime candidate.

3.2. Relevance

In the previous chapters, the importance of the detection of methane plumes is explained, along with the potential of mitigating climate change through the timely detection and localization of these sources. Other satellites are currently already in use for the detection of these super-emitters. However, the development of using hyperspectral data from the PRISMA spacecraft is a very recent development [15]. It is capable of high-spatial resolution retrievals, which allows for source localization down to the facility level.

Current limitations prohibit extensive use of the PRISMA data with the matched filter retrieval method. Many locations on Earth provide too much noise for retrieval to be possible in all but the most extreme sources. Lowering the detection limit for more challenging scenes with less homogeneous surface features will expand the number of locations where emissions can be found. Improving the retrieval algorithms will hopefully reduce the noise and decrease the detection threshold. This thesis will test which

method works best for the use of hyperspectral data and allow for better retrieval, detection and quantification of methane plumes and whether the developed methods can be expanded to also include other trace gases, such as carbon monoxide.

3.3. Research Questions

The main research question of this thesis is:

> "Does a full inversion of a radiative transfer model improve over the matched filter for methane retrievals using hyperspectral PRISMA data and for what other tracers can it be used?"

The main research questions will be answered by first focusing on a smaller part of the problem, via the use of lower-level sub-questions.

- How does the matched filter need to be implemented for PRISMA methane retrieval to work optimally?
  - How does the matched filter retrieval method work?
  - What corrections can be made to improve previous results?
  - What is the effect of changing the spectral bands used in the matched filter on the retrieval?
  - Are retrieved enhancement concentrations and quantification estimates consistent with literature? How do these results differ over various types of scenes (Algeria, Turkmenistan and China)?
- How does an inverted Radiative Transfer Model (SICOR) need to be adapted for use for PRISMA methane retrievals?
  - What modifications need to be made for inputs to work with the spatial and spectral resolution of PRISMA?
  - Which parts of the algorithm to use for PRISMA methane retrieval?
  - How do results compare to the matched filter and results obtained from literature?
- How can the quality and accuracy of a PRISMA methane retrieval be determined?
  - What is a measure for background noise?
  - How can the SNR of a retrieval best be calculated?
  - What is the effect of changes in the spectral calibration of the central wavelength and the FWHM on the retrieval quality and accuracy?
- Is it possible to detect other tracers using developed methods for methane?
  - What tracers have absorption features in the detectable spectrum of PRISMA?
  - Which method is best suited for these detections?
  - What adaptions are necessary to make these detections possible?

4

Methodology

In this chapter the methodology behind this thesis project is explained, starting with a framework that entails the different parts of the project. This is followed up by the approach that was taken to come up with an answer to the research question. It closes off with the method behind assessing how and when this goal is reached.

4.1. Approach

The goal of the project is to get the most accurate retrieval possible of methane from PRISMA hyperspectral data. To help spot the challenges and set the approach for the project an overview of important characteristics of the three most relevant missions was made, using information obtained from Table 2.2 and ranked accordingly, shown in Table 4.1

Table 4.1: Ranked characteristics of the three most relevant methane monitoring satellites for this project. Green means the specications are the best, orange is in the middle and red means it is the worst. * bands are not continuous

Satellite	TROPOMI	GHGSat-D	PRISMA
Spatial Resolution [m]	7000x5500	50	30
Field-of-View [kmxkm]	Global	12x12	30x30
Spectral Resolution [nm]	0.25-0.55	0.1	7-12
Bands [nm]	270-2385*	1630-1675	400-2500
Instrument SNR	100-120	200	100
Radiometric Accuracy [%]	2	n.a.	<5
Pointing Accuracy °	0.03	<0.3	0.07
Revisit Time [days]	1	14	29
Coverage	Global	Targeted	Global

From this ranked table it can be seen that each satellite focuses on a different design, based off of different requirements. TROPOMI aboard the Sentinel-5P mission focuses on providing stable global measurements of many important trace gases, not just methane, which can be seen in its coverage, field-of-view and spatial resolution. GHGSat-D is the opposite, focusing on high resolution and very high sensitivity of methane, focusing just on a small band of 1630-1675 nm, where a methan absorption feature is located.

PRISMA is between the two in, in terms of coverage, field-of-view and pointing accuracy, but worse in terms of instrument SNR and spectral resolution. This highlights the biggest challenge, getting the most out of measurements that will likely have more noise than other instruments. This means that noise and artefacts from the retrieval must be minimized. A limiting factor in using PRISMA for the detection of methane emissions is that in some areas, primarily urban areas or areas that are situated near elevation changes (i.e. mountains) surface features are found in the retrieved methane enhancements. These are called artefacts as there is not a real methane enhancement at these locations. An example of what these artefacts look like can be seen below:

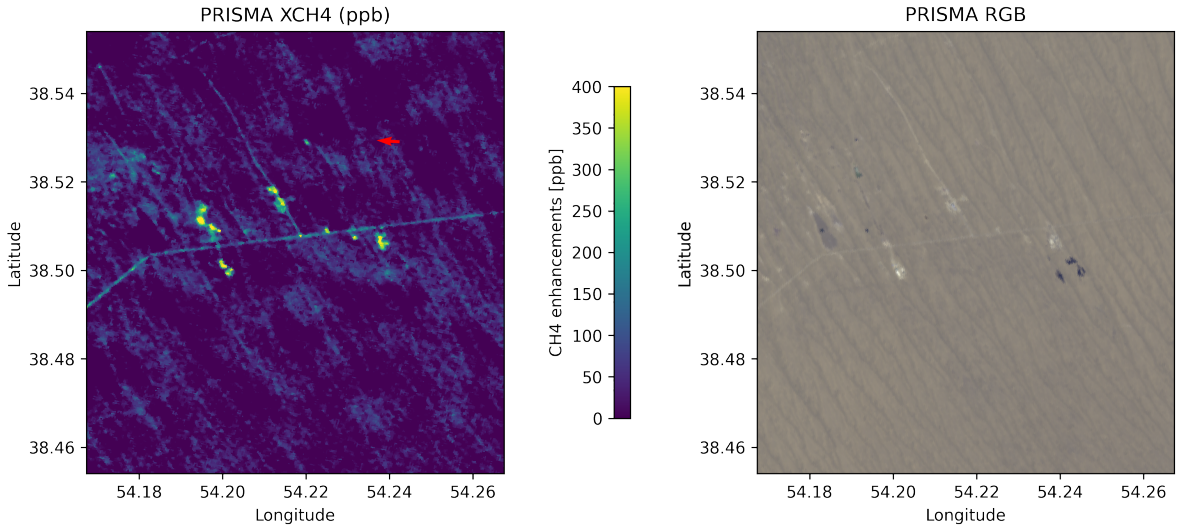

Figure 4.1: Example of road and facility artefacts in Korpezhe Turkmenistan from a retrieval done with the matched filter. Left is methane enhancements in ppb, the right image displays the RGB color image visible from PRISMA. Also parts of desert dunes are visible as noise in the methane enhancements. Red arrow indicates wind direction.

Through the center of the image, a road is visible, both in the visible (RGB) picture as well as the methane enhancements shown on the left. A road does not cause methane enhancements, meaning it is an artefact. The reason for these artefacts is that certain surfaces have an albedo that looks similar to the absorption feature of methane, which causes it to be picked up by the matched filter retrieval method for methane retrieval.

Besides causing artefacts noise is also a problem for current retrievals, which makes it hard to detect emissions, as the noise can overwhelm the true signal. Only strong emission sources can therefore be detected in some areas, because of these issues, raising the detection limit from where emissions are visible. Decreasing the noise and artefacts will allow more sources with lower emission rates to be visible, thereby decreasing the detection limit. This is ultimately the goal of this project, to expand the number of methane emitting sources that can be detected using PRISMA data.

For the approach, it is important to realize the characteristics and limitations of PRISMA, when comparing it to other instruments that detect methane from space. PRISMA is a hyperspectral imager, with a coarser spectral resolution than many other image spectrometers that are used to retrieve methane enhancements/concentrations, as shown in Table 2.2. This coarse resolution means that absorption lines of methane will be less deep than for example with other instruments such as TROPOMI, which has a higher spectral resolution. This makes detecting methane harder for two reasons, a coarser spectral resolution makes methane absorption lines more shallow and for a given spec-

trum there will be fewer data points. Every retrieval algorithm relies on data points to perform a retrieval and fewer data points mean in general that a retrieval will become less stable and/or accurate. Below a comparison between the methane absorption spectrum is shown for the spectral resolution of PRISMA and TROPOMI:

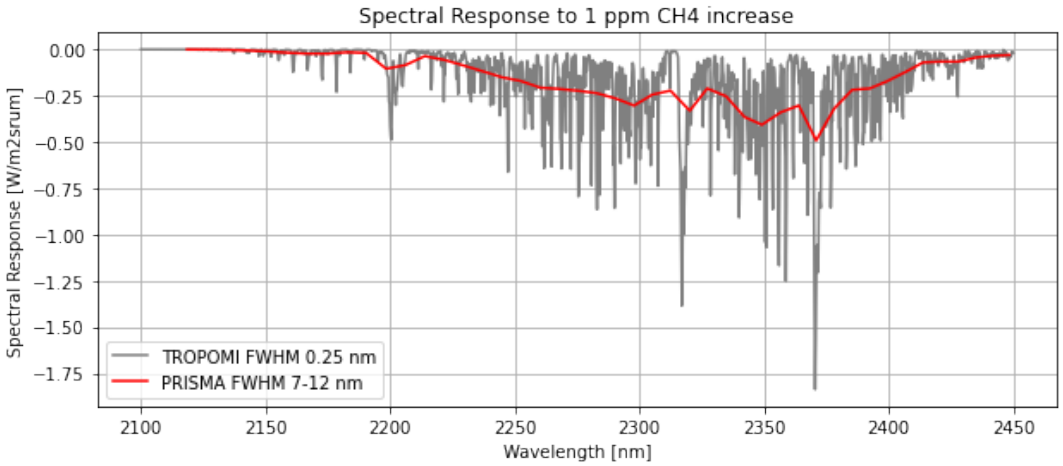

Figure 4.2: Comparison of absorption lines of methane between TROPOMI and PRISMA from 2100 to 2450 nm. It can be clearly seen that TROPOMI better captures the fine absorption details of methane. It must be said that TROPOMI does not measure the entire spectrum that is shown here, this figure is purely to show the comparison in spectral resolution between the two instruments for the entirety of the methane absorption feature around 2300 nm.

From this figure, it is immediately visible that a lot of detail is lost at the spectral resolution of PRISMA, which makes retrieval more difficult, as there are fewer data points to perform a retrieval with. That is why the focus of this project is to use the data points that we have in an intelligent way to get the most out of the PRISMA data. PRISMA will most likely be less sensitive for methane, but because of its high spatial resolution it will deal with much more concentrated emissions and concentrations than TROPOMI. The approach is to make sure that these methane enhancements from emissions are visible and that the emission quantifications that result from them are as accurate as possible.

4.2. Framework

The project consists not only of the retrieval of methane but also the preprocessing of data and further analysis such as emission quantification, analysis of noise and a comparison with other instruments. That is why the project can roughly be divided into three steps, which are Data, Retrieval and Analysis. The data step deals with correcting the data and settings. This consists of two steps, with spectral calibration updating the spectral settings of the satellite and hyperspectral denoising removing noise from the radiance data. The retrieval part consists of the two methods that have been developed for methane retrieval. The analysis part of the project deals with using the methane enhancements to perform emission quantification and assess the quality of the retrieval. Parallel to the PRISMA retrieval work by others on TROPOMI and Sentinel-2 data can be used to compare the emission quantification and concentration estimates and assess the methane retrieval performance of PRISMA. An overview of how these processes are divided can be seen below:

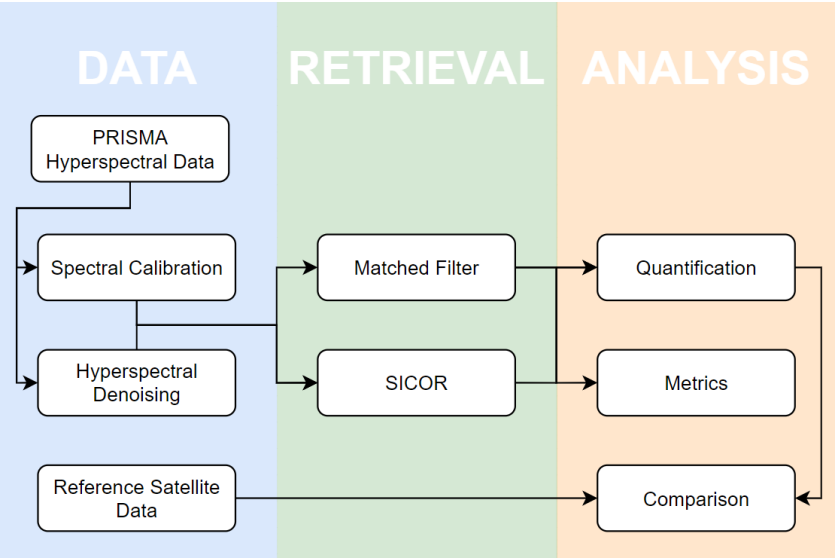

Figure 4.3: Overiew of the project structure. The individual boxes indicate separate parts of the project or inputs.

The hyperspectral denoising process is part of a separate thesis that coincides with the same project, part of the Master of Science of Econometrics and Data Science at the Vrije Universiteit Amsterdam. The methodology and results of that research, will not be repeated in detail in this report, except for the effect that hyperspectral denoising has on methane retrieval using PRISMA. The idea behind hyperspectral denoising is that the received measurements contain noise, that have a detrimental effect on retrieval. The assumption is that there is a 'real' observation which can be found by applying denoising algorithms, making use of certain properties of hyperspectral data. Several methods were tested, by adding various types of noise to measurements received and measuring the increase in Peak Signal to Noise Ratio (PSNR) after denoising the 'noisy' image. The best algorithm from that research is used for actual performance concerning emission quantification and analysis in this thesis.

4.3. Baseline

To provide a baseline for terminology and the data this section describes how the data will be used and what is meant by certain terms. Below in Figure 4.4 the orbital setup of the PRISMA spacecraft can be seen. It makes use of a pushbroom configuration, where one spatial dimension and one spectral dimension are directly measured by the 2D matrix detector and the temporal along-track flight provides the second spatial dimension for measurements. The y spatial dimension corresponds to across-track and the x spatial dimension to along-track measurements. Each y-λ column acts as a spectrometer.

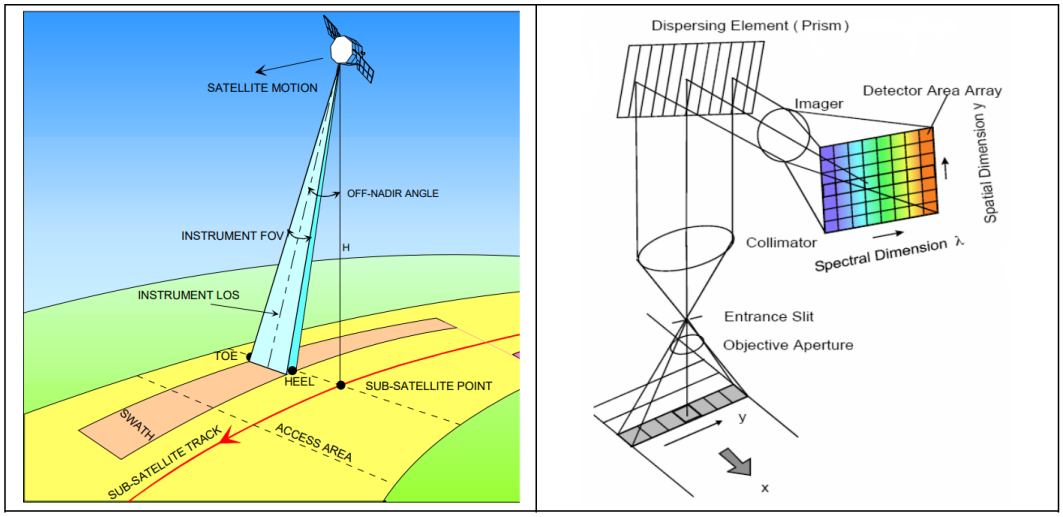

Figure 4.4: Overview of the data acquisition by the pushbroom configuration of PRISMA and how the matrix detector captures incoming light. [41]

It can also be seen in the figure that PRISMA is a targeted imager, as it can be seen that it performs measurements with an Off-Nadir Angle. This is different from other missions such as Sentinel-5P and Sentinel-2. When comparing the pushbroom configuration used in PRISMA to whiskbroom configurations used for example in high-resolution airborne spectrometers it is important to note that the pushbroom configuration can have problems with the spatial uniformity and cross-contamination of the spectra, which need to be corrected, which is done for the PRISMA data [41].

A PRISMA scene is a 30x30 km^2 image taken over the swath of the imager, which corresponds to 1000x1000 x and y spatial pixels. For the methane retrieval, the SWIR datacube will be used, which has 170 spectral pixels in its spectrum over the λ dimension. When a channel is mentioned one of the 170 layers/spectral pixels of the λ dimension is meant, corresponding to a certain wavelength range of the measured PRISMA spectrum. A channel can be used for a slice of the entire hyperspectral image or just an along-track column. With an along-track column, the column in the x-direction is meant.

4.4. Evaluation

In order to determine what the performance of the developed methods is a common logic needs to be applied for evaluation of different scenes and the two retrieval methods. While for an instrument such as TROPOMI the concentration estimates are important, for detecting emissions the enhancements are important, meaning levels above

the background concentration. For the matched filter enhancements are directly retrieved from the retrieval, for SICOR an additional step is necessary, which will be discussed in chapter 6.

The detection limit shown in Table 2.2 is directly linked to the SNR of the instrument and the resulting noise of the retrieval. A measure for noise is the root-mean-square (RMS) deviation, which uses all methane enhancement values of a retrieval. Most of the methane enhancements are not due to significant methane concentrations in the atmosphere, but due to surface features or instrument noise. The measure of noise also logically leads to a measure of plume visibility, by combining the enhancement value of a plume with the measure of noise to form a measure of peak-signal-to-noise ratio. It is important to do this for both the highest enhancement within a plume, as it shows how well the likely source is visible against the background, as well as for the median plume enhancement, as this determines the plume visibility and detection limit.

The third way of evaluation is that of comparing the retrieved emission quantification with that of other instruments and controlled releases. This ties together both the accuracy of retrievals with regard to the enhancement estimations as well as the ability to properly distinguish a plume from the background. The relative difference between the reported difference between controlled releases and PRISMA will be taken as a metric for available scenes as well as a comparison with the emission quantifications of other instruments and experiments, such as Sentinel-2. This evaluation logic will be used when comparing various methods and parameter settings and to help determine what the best procedure is to perform a methane retrieval using PRISMA and to help answer the research questions.

5

Methane Retrieval Using the Matched Filter

In this chapter the matched filter retrieval method for PRISMA will be discussed, starting with the implementation of the base method and the improvements made in section 5.1. This is followed by the processing of the enhancement data into plume masks and quantification estimates in section 5.2. Parameter tests and method tests were done to verify which settings and methods work best, the results of this and the preliminary conclusion are discussed in section 5.3. These results are further analyzed using a representative set of PRISMA scenes, that show the capabilities of the matched filter and quantifications are presented in section 5.4. The application of the matched filter to other trace gases is discussed in section 5.5. At the end of the chapter a preliminary conclusion is provided with regard to the matched filter with regard to the sub-research questions.

5.1. Implementation

The matched filter was initially implemented according to the specifications of [15], which uses a target signal of methane generated by a radiative transfer code. This is explained in subsection 2.4.1. The retrieval using the matched filter starts with a reference signal. This reference signal is an absorption spectrum of methane that has been normalized for a unit increase of 1000 ppb methane in the atmosphere over the average column concentration of methane in the atmosphere for medium latitudes. This spectrum is created by simulating two radiance spectra, one without added methane in the simulated atmosphere and one with the added methane. The difference between these two is normalized using the radiance spectrum without added methane, which also removes the effect that average albedo has over the spectrum, assuming that the albedo is constant, which might not be the case as will later be discussed in section 6.3. This means that the reference signal of methane is linearized around an input enhancement. A problem with this is that the relative absorption of methane in the atmosphere of radiation is not linear, but more logarithmic. The matched filter uses this reference signal by comparing it against the difference of each pixel spectrum against the average spectrum of an along-track column and correlating it with the methane signal. A step by step explanation is shown below:

1. Compute the methane reference signal
2. For every along-track column:
   (a) Calculate the covariance of the radiance measurements
   (b) Convole the reference signal to the specific PRISMA central wavelength and FWHM
   (c) Calculate the enhancements using Equation 5.1

The main limitation of the matched filter is that it assumes that the reference signal behaves linearly with added methane, but this is not the case. For low input methane enhancements, the specific absorption of light is higher than for high input enhancements. This leads to overestimation for high methane enhancement reference signals and underestimation for low methane enhancement reference signals. Allowing more freedom and flexibility in the matched filter might allow for more accurate methane enhancement estimation.

The first improvement to the matched filter that was made for this research was to give it more freedom in its reference signal. This led to the creation of the iterative matched filter. In this method, a reference signal starts with a standard input, which is the same for every detector. It will perform the normal matched filter and get back the enhancements for that detector column. It will then move the reference signal towards one with an input closer to the maximum retrieved enhancement and continue to do the retrieval with an updated reference signal. This continues until convergence is reached. A pseudocode algorithm is shown below:

1. Compute the methane reference signal for various input enhancements
2. For every along-track column:
   (a) Calculate the covariance of the radiance measurements
   (b) Convole the reference signal to the specific PRISMA central wavelength and FWHM
   (c) Calculate the enhancements using Equation 5.1
   (d) Use the maximum enhancement from the along-track column to generate a new methane reference signal and continue iterating until the change in enhancement is smaller than a set threshold.

The second method allows even more freedom to the matched filter, which extends the iterative method to the individual pixels, which is why it is called the pixel iterative matched filter. This freedom might be necessary, because within an along-track column there can be large differences with methane enhancements. Pixels with low enhancement pixel uses the same reference input as the high enhancement pixels in the iterative matched filter, meaning that their enhancement concentration might be overestimated. A downside of this added flexibility to the individual pixel level is the added computational costs. For every column retrieval a convolution is necessary in order to go from a high spectral resolution reference signal to a convoluted signal that uses the central wavelength and FWHM of the specific detector-matrix pixels of PRISMA, this adds significant added computational cost if iterations for every individual spatial pixel are done. To mitigate this added computational cost, a similar method used for the iterative matched filter was used for the reference signal, but now for the convolution. A detailed implementation of the pixel iterative matched filter is shown below:

1. Compute the methane reference signal for various input enhancements
2. For every along-track column:
   (a) Calculate the covariance of the radiance measurements
   (b) Calculate the initial enhancement estimates using the regular matched filter.
   (c) For every pixel in the along-track column:
      i. Convolve the reference signal to the specific PRISMA central wavelength and FWHM
      ii. Calculate the enhancements using Equation 5.1
      iii. Use the enhancement from the pixel of interest in the along-track column to generate a new methane reference signal and continue iterating until the change in enhancement is smaller than a set threshold.
      iv. Extract the enhancement value of the pixel of interest and save them in the result array.

The pixel iterative matched filter uses the same approach for its reference signal, by creating Look-up Tables (LUT) and using linear interpolation to create the signal for each input methane concentration. A second interpolation with LUT is needed for the convolution of the reference signal for each detector, which saves significant computational resources. The main difference between the iterative matched filter and the pixel iterative matched filter is that the iterative matched filter calculates the enhancements for an entire column and delivers that as output, while the pixel iterative matched filter does calculate the enhancements from the entire column, but only delivers back the enhancement of the pixel of interest for which the reference signal was optimized. This way the strength of the matched filter (using many pixel-spectra simultaneously) can be combined with the flexibility of doing a separate retrieval for each pixel.

5.2. Processing

After retrieving the methane enhancements for the PRISMA scene it is important to come up with metrics and processed results to say something about the quality of the retrieval and the spotted emissions.

5.2.1. Plume Mask

It is important to distinguish the plume from noise and artefacts to provide meaningful emission quantifications and analysis. In order to select pixels a method called plume dilation is used. Here a starting location is needed from which the plume mask dilates outwards while checking for every pixel if it is above a predetermined threshold. The starting location should be the source location, but if this is not clear a location in the head of the plume can be used. The threshold is determined separately for each scene, as the amount of noise and/or artefacts differs per region, but for initial plume mask generation is set to 1.5 the estimate for the background noise.

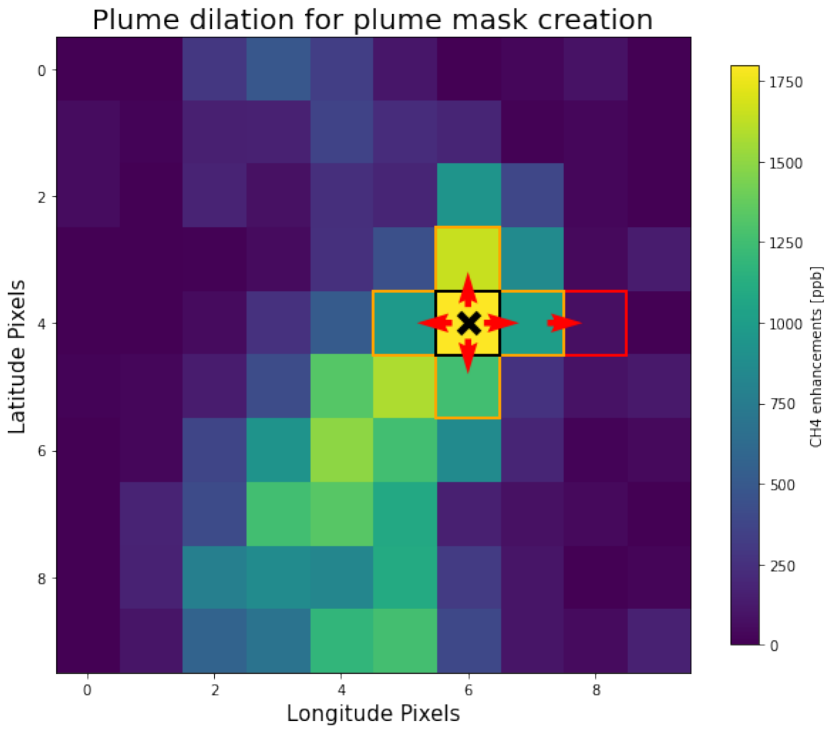

Figure 5.1: Example of plume mask dilation. The highest methane enhancement pixel (shown with the black cross and box) is chosen as a starting point where the dilation start (shown with the red arrows), if they are above the set threshold they are included in the plume (orange boxes), but if they fall below they are discarded (red box). This continues until no new pixels can be added or if the maximum number of iterations is achieved.

5.2.2. Emission Quantification

For quantification as shown in chapter 3 two methods are used, IME and Cross-Sectional Flux (CSF).

The IME for quantification could be implemented straightforward, as it needed only the enhancements, the plume mask and an effective wind speed. Windspeed is provided by coupling the GEOS-FP wind dataset to the retrieval so that it uses a representative wind speed for the day and time (within 1 hour) that the scene was obtained by PRISMA [38]. The GEOS-FP dataset has global wind data, but for a coarser spatial resolution than PRISMA. That is why the closest value to the center of the PRISMA scene is taken as a representative value for the entire scene. For IME quantification only the enhancements of the plume mask are taken, not enhancements that are the result of noise or artefacts. The windspeed retrieved from GEOS-FP is not without error and that is why an uncertainty of 50% was used in the windspeed for estimating the uncertainty of the

emission quantification [15, 52, 4].

CSF requires more input from a user, not only a clear starting point, with which the transects cover the plume, but also the length and width of the plume. A visual inspection is needed to make sure that the correct start location is chosen and the right length and width. A third thing to consider is the angle with which to take the cross-sections. This can be done automatically with the wind angle, but this is not always the axis by which the plume is best aligned. That is why this angle is best determined by hand, most of the time being relatively close to the wind angle. An example of the cross-sections being applied for use in CSF is shown below:

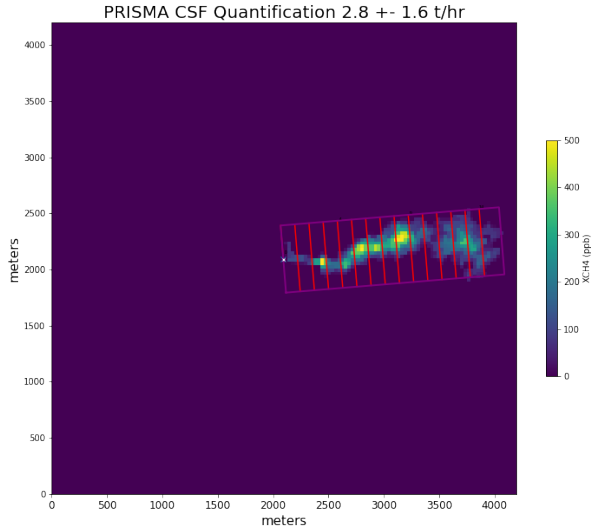

Figure 5.2: Overview of CSF quantification, for a controlled experiment done by Stanford. The starting point in this case is not the highest enhancement pixel, but it does capture the entire plume. The width and length of the cross sections are set by the user. The red stripes indicate the cross-sections.

In here it can be seen that the white point (the start of the cross-sections) is not the highest enhancement pixel, but it does allow for the cross-sections to fully cover the plume mask.

5.3. Parameter Testing

In order to get the most out of the matched filter tests were done to verify which parameters and settings were optimal for a retrieval. For these tests, a wide variety of scenes was necessary that include various types of surfaces and emissions were necessary. An important factor in this regard is the presence of surface features that can lead to artefacts in the methane signal, main contributors to this are elevation changes and albedo changes over the spectrum.

Scenes both with and without emissions are necessary for testing, as retrieved methane where no sources are suspected should be avoided. Emissions from known locations are selected, including Turkmenistan, Algeria, China, USA and others. A full list of scenes that have been used can be found in Appendix A.

For all the scenes that contain emissions, plume masks were created after using the original matched filter settings to retrieve methane enhancements. These plume masks are used to consistently select the emissions over various parameter settings and methods. Different bands or methods might result in different visible plumes, but this will

raise other problems when comparing the plumes and is less feasible to do, as to do so would mean a manually generated plume mask for each test.

The parameters that will be tested are the input channels and methods. The input channels determine which radiance spectrum data will be used for the retrieval and the methods are the normal matched filter and the two iterative methods that have been developed for this research. Testing will determine which method and band will work best for PRISMA methane retrievals.

Band Tests

The first parameter test is to determine what part of the spectrum will be used for retrieval using the matched filter. In order to compare results, relative differences for two metrics will be compared to the original implementation of the matched filter with a spectrum of 2110-2450 nm. The two metrics that will be compared is the relative difference of the mean plume enhancements divided by the RMS of the scene, which is called the mean plume ratio and the relative difference in emission rate Q, using the IME method. These two metrics are chosen because the mean plume ratio includes both a measurement for noise as well as a measurement for how strong a plume is. These two combined indicate how 'visible' a plume is against the background noise enhancements. The mean enhancements are taken and not the maximum enhancements as we are interested in more than just the source of the plume. The emission rate Q change is used as a metric because quantification of emissions is the ultimate goal of doing these retrievals and it is interesting to see how this differs from the original implementation of the matched filter. A selection of relevant band experiments is shown below:

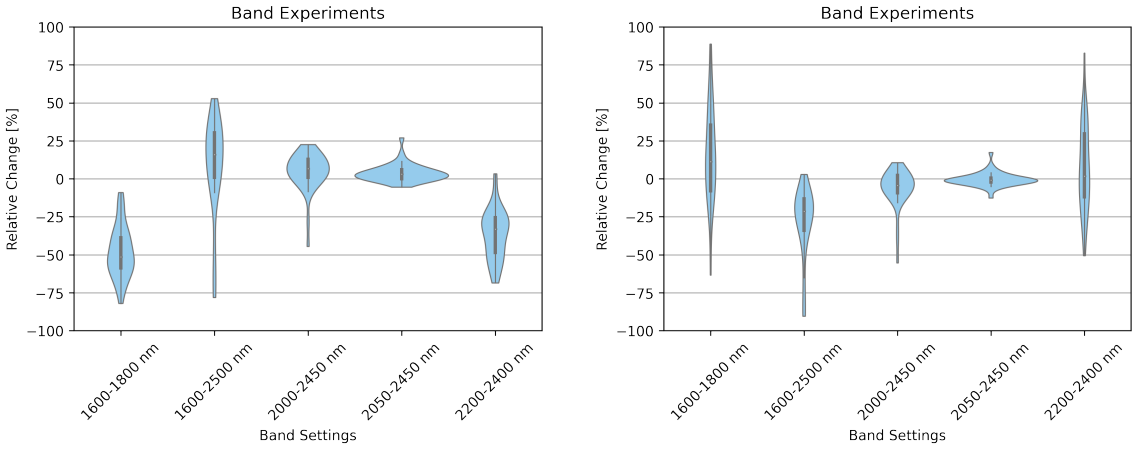

(a) Mean Plume Ratio Change

(b) IME Quantification Change

Figure 5.3: Comparison of selected metrics of the iterative matched filter and pixel iterative matched filter to the results of the original matched filter with a reference input signal of 1000 ppb methane enhancements. Width of the violin plot indicates the relative number of plumes for that value, with the total area being equal to 40 plumes.

From these results, it can be seen that using the weak absorption feature of methane from 1600-1800 nm delivers a weakly visible plume, and an uncertain estimation of emissions, which is expected. The same can be said for the 2200-2400 band, which focuses on a band with more absorption in the strong absorption feature of methane. The 1600-2500 nm band shows an increased mean plume ratio, but with a large spread, but it can be seen in the right figure that the quantification estimates are significantly

lower, which is caused by the on average lower enhancement estimates. The 2000-2450 nm band and the 2050-2450 nm band show increased mean plume ratios and no significant changes in emission quantification estimates, but these changes are not very significant as the mean plume ratio only increased for 50%-75% of the selected plumes. That is why the original band of 2110-2450 nm will be kept for further tests.

Method Tests

For the method tests, the two newly developed methods are compared to the original reference implementation. Six metrics have been calculated to determine whether the new methods improve over the initial implementation:

- RMS: The RMS is a measure for the noise of the scene and important to see how the changes in algorithms influence the average RMS of the methane enhancements of a scene.
- Mean Plume Enhancement: The mean enhancement of the plume mask is useful to see how average methane enhancements behave with changes to settings.
- Max Plume Enhancement: The maximum methane enhancement is taken as a proxy for the source concentration as it is useful and interesting to see how the source enhancement estimations change.
- Mean Plume/RMS Ratio: A measure of SNR for the average enhancement in the plume compared to the RMS metric. This provides a base metric for visibility of the plume against the background noise.
- Max Plume/RMS Ratio: A measure of SNR for the maximum value in the plume to the RMS metric. It is important to also take this metric into account as the maximum enhancement of a plume can be significantly higher and behave differently than the mean enhancement.
- Q IME: Emission estimate using the IME method. Like mentioned before it is important to notice how the quantification behaves when comparing it to other metrics, as a known plume may be more visible when comparing it to the background noise, but it is expected that the emission quantification should not change too much.

These metrics can be very different between plumes, as some have higher concentrations than others and the quantification estimate can differ an order of magnitude. That is why the relative change of the metrics will be used to compare methods. For each plume and method they are calculated and compared against the original implementation of the matched filter to arrive at the following results:

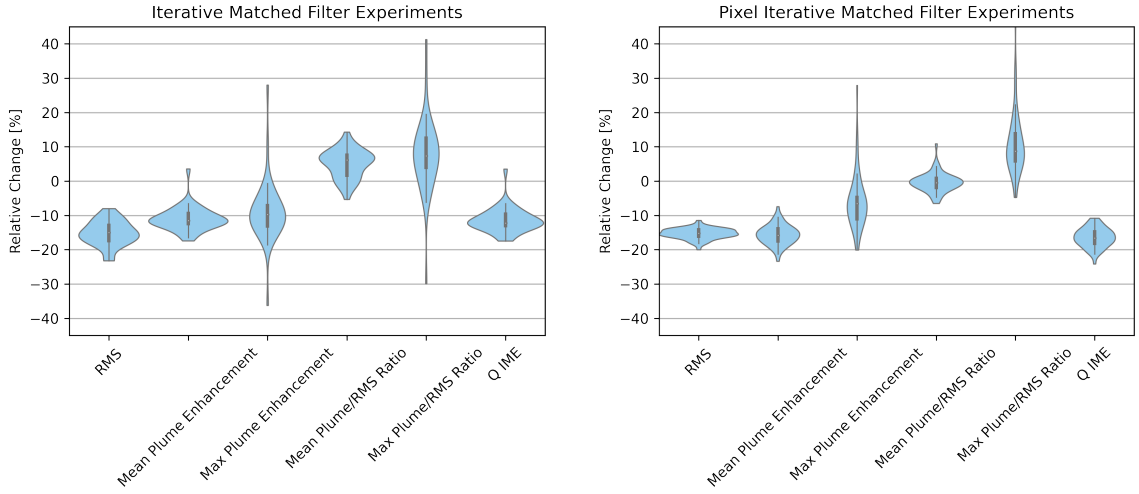

(a) Iterative Matched Filter

(b) Pixel Iterative Matched Filter

Figure 5.4: Comparison of selected metrics of the iterative matched filter and pixel iterative matched filter to the results of the original matched filter with a reference input signal of 1000 ppb methane enhancements. Width of the violin plot indicates the relative number of plumes for that value, with the total area standing for all the plumes.

From the figure above it can be seen that the relative noise/RMS decreases for both methods more so even for the iterative matched filter than for the pixel iterative matched filter. The pixel iterative matched filter does show more consistency in decreasing the noise/RMS, with a lower spread around a mean decrease of around 15%. It also decreases the mean plume enhancement, something which the iterative matched filter does less so. The iterative matched filter performs better for the mean plume/RMS ratio than the pixel iterative method, which is logical, because it generally has higher enhancements in the plume mask, because it iterates using the highest enhancement value as input in its reference signal. This is however not always desirable as is shown in Figure 5.5. While the SNR is on average better for the iterative matched filter it is evident that the pixel iterative matched filter provides a more consistent improvement, seeing as the relative change spread is lower for almost all metrics, except for the RMS. The higher spread for RMS is expected as the pixel iterative matched filter has the flexibility to lower the enhancement estimates for pixels without a meaningful presence of methane, something which the iterative matched filter is less able to do. The reason for this is the ability for the pixel iterative matched filter to change the input methane reference signal also for lower input methane enhancements. To show the difference between the iterative matched filter, the pixel iterative matched filter and the regular matched filter a visual comparison is shown in Figure 5.5.

From the difference plot it can be seen that the pixel iterative matched filter minimizes some enhancements that are the result of artefacts, but also those found in the tail of the plume. In general the pixel iterative matched filter will reduce methane enhancements in size if they are lower than the original input enhancement of 1000 ppb and increase enhancements above 1000 ppb. The methane enhancements close to the source of the plume are therefore estimated higher for the pixel iterative matched filter.

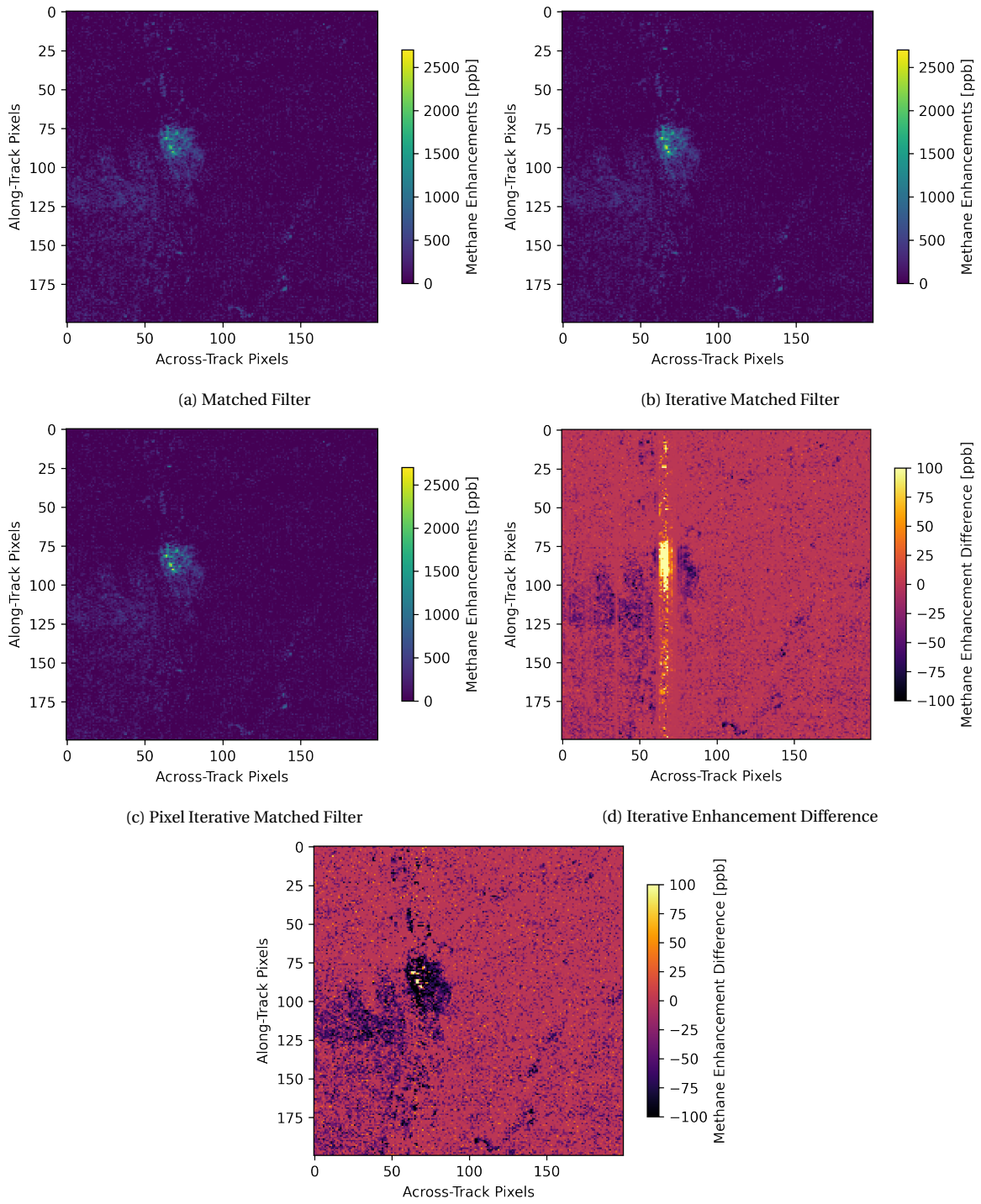

(a) Matched Filter

(b) Iterative Matched Filter

(c) Pixel Iterative Matched Filter

(d) Iterative Enhancement Difference

(e) Pixel Iterative Enhancement Difference

Figure 5.5: Comparison of enhancements retrieved over a strong methane plume in Shanxi, China. The difference is calculated by subtracting the matched filter enhancements from the iterative and pixel iterative matched filter enhancements. It can be seen that in the center of the plume the concentrations are estimated significantly higher when using the pixel iterative method against the matched filter method, but that the rest of the plume is estimated significantly lower.

A limitation of iterating only per along-track column and not every pixel is visible from the difference plot of the iterative matched filter. All the pixels in the along-track columns

with very high enhancements (>2000 ppb) are estimated much higher because for all pixels the same reference signal with higher input enhancements are used. A limitation of both the iterative and pixel iterative matched filter is that they cannot distinguish between low plume enhancements and artefacts. Other methods such as MAG1C, where a sparsity prior is employed, that try to limit the number of spatial pixels where significant enhancements are present, suffer from similar issues [13, 15]. A consequence of this for methane retrieval is that for the pixel iterative method the majority of the pixels in a plume have lower estimations than with the regular matched filter, which translates into lower emissions, as can be seen in Figure 5.6

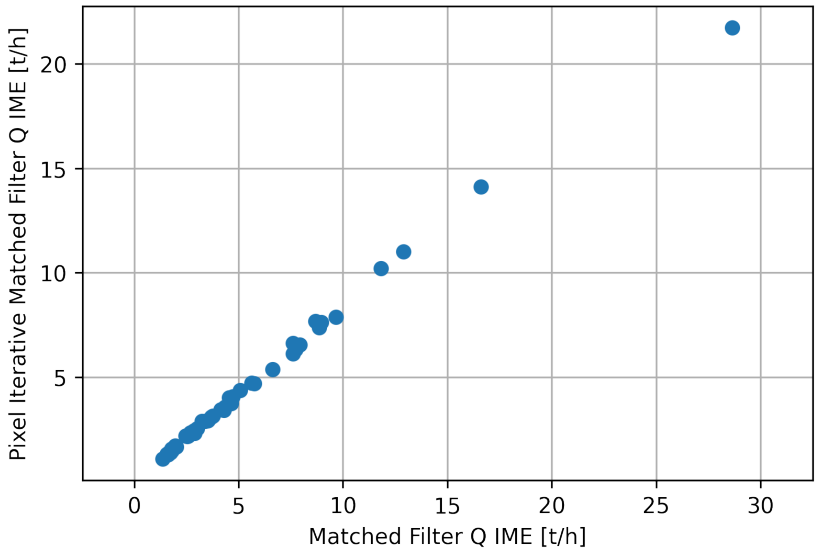

Figure 5.6: Emission Quantification comparison between the pixel iterative matched filter and the regular matched filter.

From this comparison it can be seen that the pixel iterative matched filter estimates the emission quantification about 20% lower than the matched filter and does this consistently so. This can be explained by the fact that the median plume enhancement is around 100-200 ppb and this will be estimated lower for the pixel iterative matched filter. For this reason and because of the minimum improvement in plume visibility the original matched filter will be used for further results and analysis. The reason why the enhancements are estimated consistently lower is investigated further in Table 5.4.

5.4. Results and Analysis

In this section, the results from the original matched filter will be shown. The original matched filter will be used to compare it to results found in literature. Using known locations of methane emissions several PRISMA scenes containing methane plumes were found and analyzed. Four of these will be studied in more detail and later compared to the second methane retrieval method and are shown below:

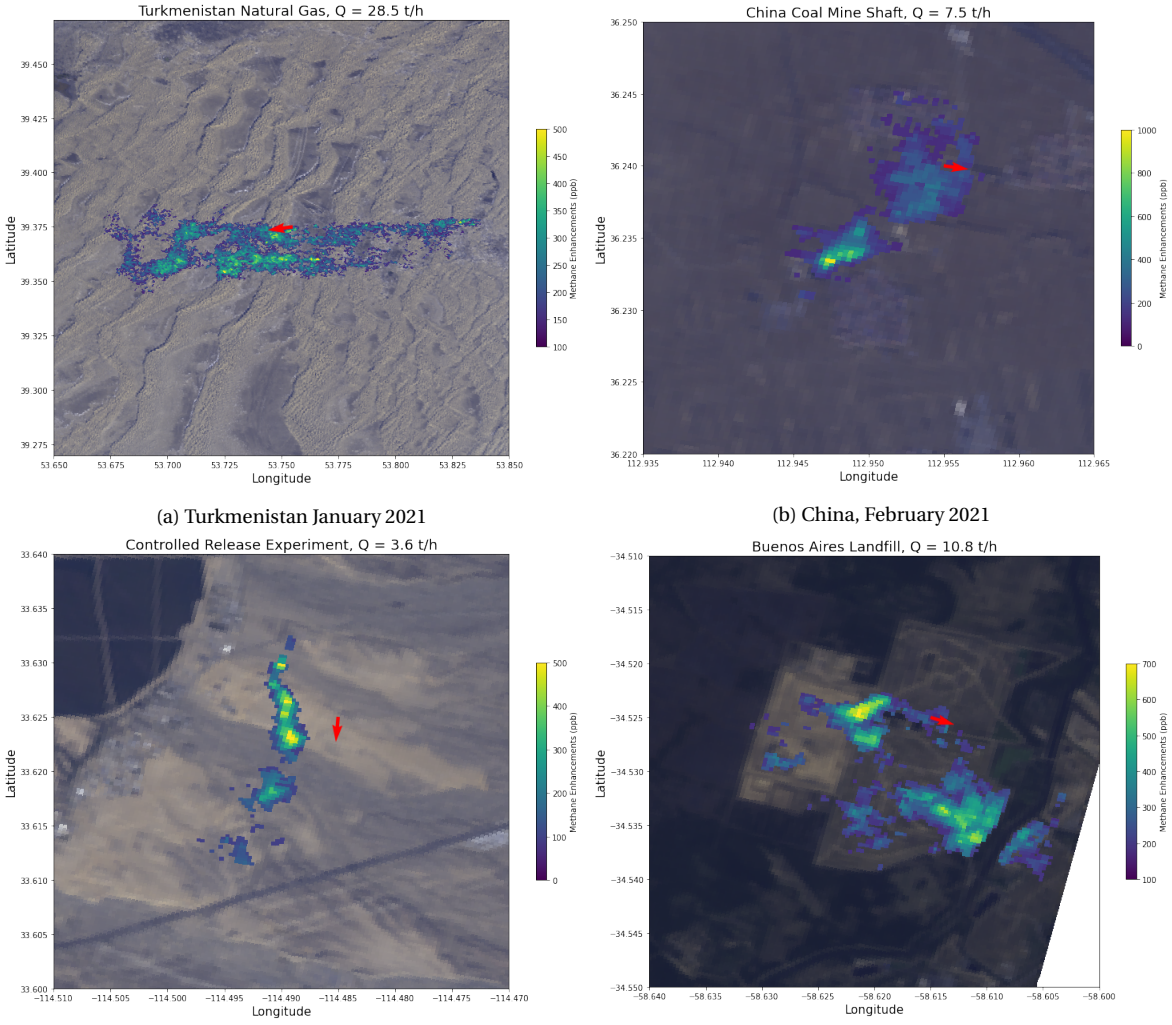

(a) Turkmenistan January 2021

(b) China, February 2021

(c) Arizona USA, December 2021

(d) Buenos Aires, January 2022

Figure 5.7: Plume masks and quantification estimates for four different type of methane emission sources and scenes of interest. Methane enhancements have been filtered using a median filter for illustrative purposes. The RGB background was created using PRISMA measurements in the visual spectrum.

It can be seen that the matched filter can be used to retrieve enhancements and quantify emissions from various types of emission sources, ranging from natural gas facilities to mine shafts and even large emissions from landfills. The type of scene that can be used for methane retrievals is also quite varied, ranging from the Turkmenistan desert to more mountainous regions in China and regions with lots of vegetation in Buenos Aires. In order to verify that the quantification methods have been properly implemented a comparison was made to results from PRISMA retrievals obtained from literature:

Table 5.1: Comparison of retrieved plumes with values obtained from literature [15, 23], a * indicates that the plume mask could not be exactly replicated. From the resutls it can be seen that the CSF method consistently overestimates when compared to the IME method. Emission quantification estimates (with IME) for the pixel iterative matched filter method are also included.

PRISMA Observation	Q Ref [kg/h]	Q IME [kg/h]	Q CSF [kg/h]	Q Pixel [kg/h]
Turkmenistan 2020-04-19*	6600 ± 1300	4100 ± 1600	5600 ± 1800	3400 ± 1300
Turkmenistan 2020-06-22 #1	7700 ± 3400	5100 ± 2000	9700 ± 5400	4400 ± 1500
Turkmenistan 2020-06-22 #2*	5700 ± 2500	2700 ± 1100	4900 ± 2600	2400 ± 1000
Turkmenistan 2020-06-22 #3*	6400 ± 2800	4600 ± 1800	7600 ± 3900	4000 ± 1500
Turkmenistan 2020-07-21	18300 ± 6800	16600 ± 6600	19100 ± 4500	14100 ± 5600
China 2021-02-06 #1	8700 ± 3500	7500 ± 3300	11300 ± 4700	4900 ± 2300
China 2021-02-06 #2	9600 ± 3800	8900 ± 3600	15000 ±4700	7400 ± 3000
China 2021-02-06 #3	7700 ± 3100	7900 ± 3200	16300 ±6000	6600 ± 2900

From this, it can be seen that the IME method is mostly within the confidence bounds for quantification, albeit that it is on average below the values found in literature. The main probable reason is differences between plume masks that are used, with the implemented method being fairly conservative with plume masks generally being smaller than results found in literature, which explains the lower emission quantification estimates. The CSF method generally overestimates the emissions and has significant higher standard deviations for its estimates. The results also show that the pixel iterative method consistently estimates emission quantifications lower than the regular matched filter for both methods, owing to its lower mean enhancement in the plume. The disparity between the CSF and IME methods is investigated further by comparing more methane emissions around known locations of emissions, which can be seen below:

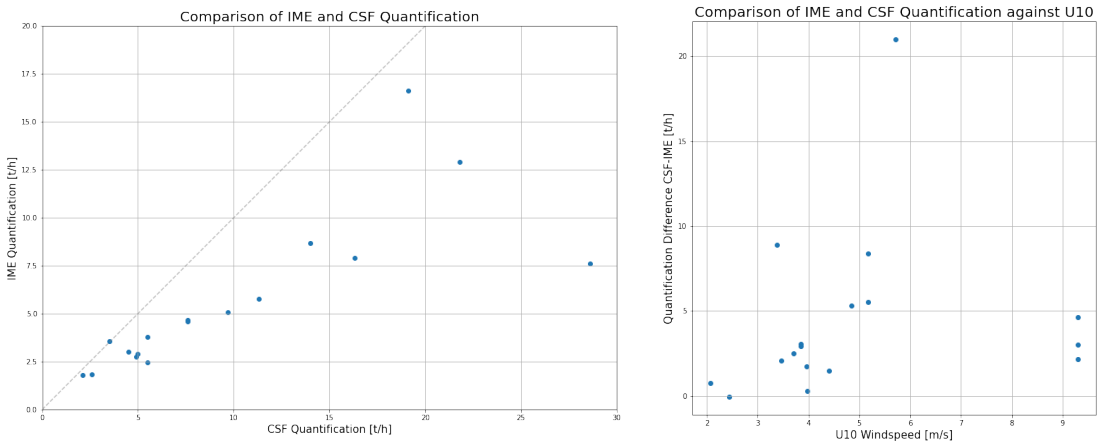

(a) CSF and IME quantification plotted against each other.

(b) Difference between CSF and IME against U10.

Figure 5.8: Comparison of quantification results of PRISMA with the CSF method against the IME method on the left picture (a). It becomes clear that there is a consistent scaling between the two, except for a few outliers for the higher emissions. The dashed grey line signifies a 1:1 ratio between CSF and IME. On the right an overview of IME and CSF quantification estimates plotted against the U10 windspeed of the GEOS-FP data is shown. There is a weak correlation between increased windspeed and an increase in the disparity between CSF and IME.

From the figure above it can be seen that there is a consistent difference between the CSF and IME methods. A possible explanation for these disparities is the implemented effective wind speed U_{eff}, which might not be calibrated properly for retrievals us-

ing PRISMA. A last experiment with regard to quantification was done by analyzing PRISMA scenes of controlled release experiments, done by Stanford. In these experiments, methane was purposefully released into the atmosphere at the time that PRISMA was performing an overpass. The release was measured at the ground and can also be estimated using the matched filter enhancement results:

Table 5.2: Controlled Release Experiments compared agains the PRISMA retrieved emissions using the matched filter. All values are given in kg/hr. First three columns signify the controlled release experiments. The IME quantification estimate for the pixel iterative matched filter is also given as a reference.

Date	Min Q	Mean Q	Max Q	PRISMA Q IME	PRISMA Q CSF	PRISMA Q Pixel
2021-10-21	3939	4177	4417	3560 ± 1420	3500 ± 1600	2900 ± 1200
2021-10-27	3274	3484	3670	3000 ± 1200	4500 ± 2500	2800 ± 1300

These results provide an initial indication that the matched filter provides quantification estimates that are accurate within confidence bounds, but with a slight underestimation for the IME method and a larger uncertainty for the CSF method. With more tests like these a more conclusive answer can be given that PRISMA provides accurate emission quantification estimates, but these initial results are promising.

Comparison Between Instruments

To verify that the quantification of emissions is realistic, a comparison was made between observations made by PRISMA and another methane observing satellite. The comparison satellite is Sentinel-2 as its spatial resolution is similar to that of PRISMA and it provides global coverage which is freely available. With the help of another student at SRON, a comparison was made between PRISMA and Sentinel-2 for four different plumes found over Algeria, for which the observation times of PRISMA and Sentinel-2 were within a day from each other. For both methods, the IME quantification method was used, to get the most consistent results possible.

Table 5.3: Emission quantification comparison between SENTINEL-2 and PRISMA. Retrievals were done using the matched filter only, as the methane emissions were located in the radiance pattern affected part of the PRISMA scene.

Location	Sentinel-2 IME estimate [kg/hr]	PRISMA IME estimate [kg/hr]
ALG0301 22/06/2021	2730 ± 1100	1700 ± 700
ALG0302 22/06/2021	2940 ± 1180	2000 ± 800
ALG0301 19/08/2021	2390 ± 960	1620 ± 640
ALG0302 19/08/2021	6540 ± 2610	4340 ± 1740

From these results, it can be seen that PRISMA estimates the emission quantifications lower than the quantification of Sentinel-2. These difference can be explained by a calibration difference for the effective wind speed of the IME, as it was also observed that the PRISMA IME consistently estimates the quantification lower when comparing it to the CSF quantification.

Matched Filter as Least Squares Estimator

One of the properties of the matched filter is that it can be interpreted as the least-squares estimator for the task of retrieving the enhancements of an along-track column to the methane reference signal. That means that the matched filter tries to minimize the squared residual between the measurements and the reference signal. In a

column of 1000 spatial pixels only a few pixels will be part of a methane plume that contains emissions. A possible effect concerning methane enhancements is that high enhancement pixels will be estimated with a lower value than what they, in reality, should be. This is because the matched filter tries to minimize the squared residuals and a few methane enhancement containing pixels do not contribute that much, even though they are outliers that have a larger effect on the residual than the average pixel. When looking at what influences the calculation of methane enhancements using the matched filter it helps to group the different components:

$$\hat{\alpha}(\vec{x}) = \frac{(\vec{x} - \vec{\mu})^T \Sigma^{-1} \vec{t}}{\vec{t}^T \Sigma^{-1} \vec{t}} \tag{5.1}$$

In blue the matrices and vectors containing PRISMA are given, which is an input that cannot be changed, in green the reference signal convoluted to the specific PRISMA spectrum is given, which is an input that can be changed but does not solve the problem that outliers are penalized heavily. In red the covariance matrix of the channels is given, calculated from all the measurements. This is an input that can be changed because if all measurements are used then the covariance is mainly determined by pixels that do not contain any methane enhancements. To test if the matched filter indeed suffers from this penalization for high enhancement pixels the covariance was estimated using pixels that contain an enhancement higher than 100 ppb for a column which had a known source location in it in Turkmenistan, the results of which are shown in Table 5.4

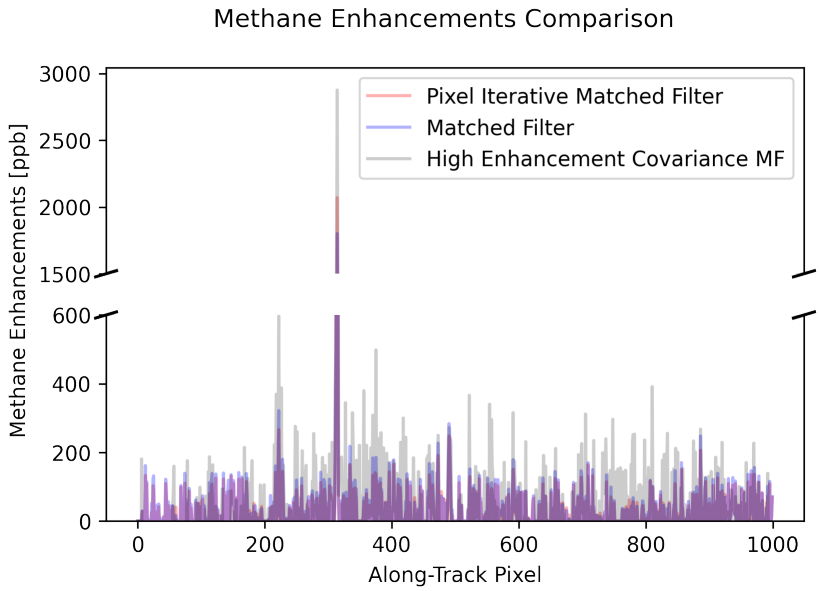

Figure 5.9: A comparison between the matched filter with a regular covariance estimation and a covariance that only used high enhancement measurements. It can be clearly seen that at along-track pixel 315-320 that significant enhancements are present, which are amplified with the high enhancement covariance. It is also apparent that the noise increases, now that the matched filter no longer uses the covariance estimated by the complete data column.

It can be seen that the high enhancement covariance matched filter estimates the highest enhancement of the plume (pixel 314) much higher than the matched filter and even

the pixel iterative matched filter. It does come at a cost, with the non plume enhancements being much higher, up to 3 times as high. In this example the benefit of the pixel iterative matched filter is shown over the matched filter for cases with very high enhancements. The highest enhancement (likely plume source) is estimates higher than the matched filter, but the non plume enhancements (noise) are estimated lower. The increase in enhancements is however only about 10% and much less than the high enhancement covariance matched filter estimate. These results do show a limitation of the matched filter, that cannot be solved by performing iterations, as the problem lies with how the reference signal is correlated to the data and not in the reference signal itself. This is a reason to try a different model, one with more flexibility, a possible candidate is to employ the use of a sparsity prior, but testing showed that could not make a distinction between artefacts and real methane signals. It is also clearly visible that deviating from the original covariance does indeed result in more noise, as the high enhancement covariance has significantly more noise. It might be interesting to look at ways to rewrite the matched filter and incorporate information about the expected distribution of enhancements in the matched filter retrieval.

5.5. Expansion to Other Trace Gases

This section explores the possibility of other trace gas retrieval using the matched filter. Two other interesting gases that are useful for analysis in greenhouse gas emissions are carbon monoxide and carbon dioxide. Carbon monoxide, because it is an indication of air pollution and carbon dioxide because it is the greenhouse gas that is responsible for the largest amount of radiative forcing on Earth [22]. These two gases have different absorption spectra which are shown below.

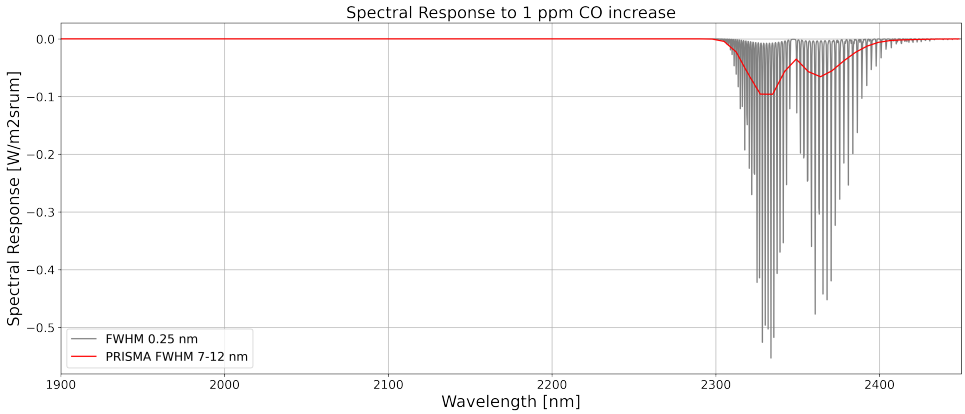

(a) Carbon Monoxide

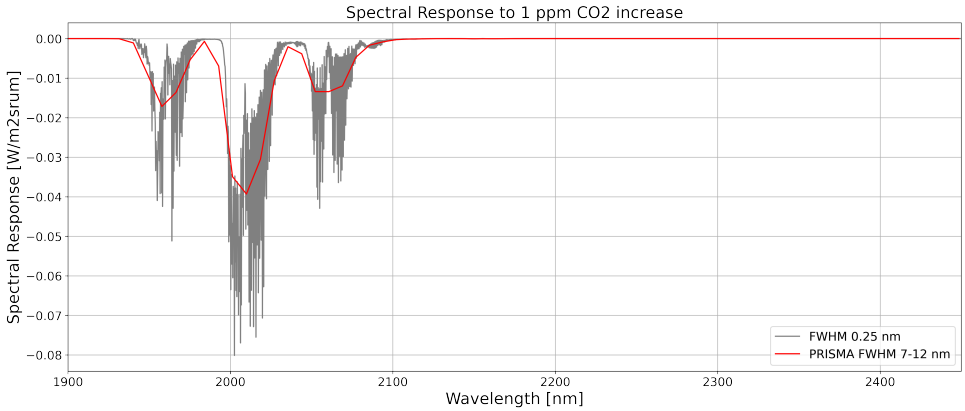

(b) Carbon Dioxide

Figure 5.10: Comparison of absorption spectra of carbon monoxide and carbon dioxide. Notice the difference in scales between the two trace gases.

From this figure, it can be seen that the spectral response from carbon monoxide is higher per molecule, but its absorption feature is more narrow compared to that of methane and carbon dioxide. carbon dioxide has a lower specific spectral response, but its higher concentration in the atmosphere makes the total spectral response of carbon dioxide higher in magnitude.

Carbon Monoxide

Based on the absorption spectrum that can be seen in Figure 5.10, the band for carbon monoxide retrieval needs to be different from that of methane Implementation, using Figure 5.10 a spectrum of 2300 nm to 2450 nm was used, as this is where the spectral response of carbon monoxide can be found. As test cases multiple PRISMA scenes were acquired for the Bhilai steel plant, a known emitter of carbon monoxide.

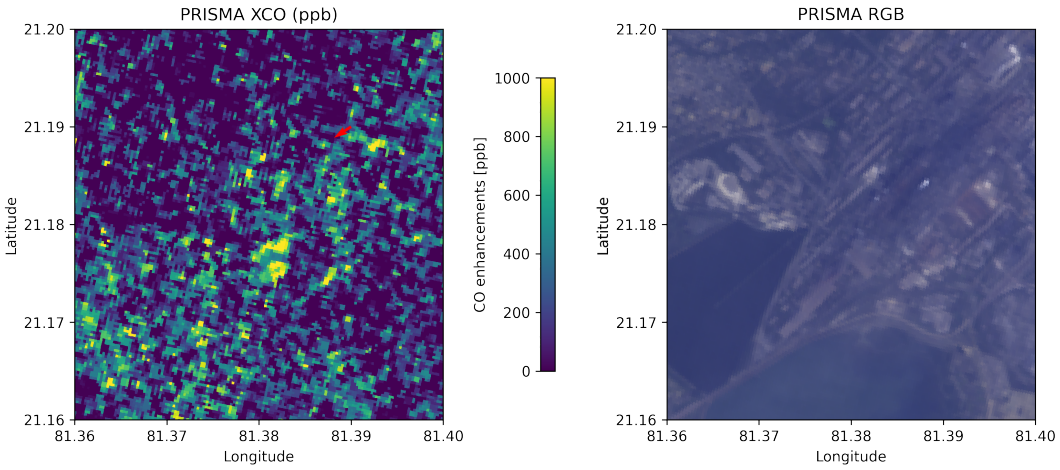

Figure 5.11: Carbon monoxide enhancement retrieval using the matched filter on the left side and the RGB image on the right side. The image is centered around the Bhilai steel plant. Wind direction is indicated with a red arrow.

From the results above it can be seen that the amount of noise in the retrieval is very high. The RMS metric returns a value of 615 ppb, which is considerably higher than values retrieved for methane.

Carbon Dioxide

Recently it has been shown that PRISMA can also be used for detecting carbon dioxide emissions, using Iterative Maximum A Posteriori–Differential Optical Absorption Spectroscopy (IMAP-DOAS) methods [5]. It is interesting to see how the matched filter compares against these results and if it is possible to detect carbon dioxide emissions. Using the spectrum shown in Figure 5.10 it was determined to include radiance data for a matched filter for carbon dioxide from 1900-2100 nm as that is where the majority of carbon dioxide absorption is present. The reference signal for the matched filter for carbon dioxide uses a different input enhancement than the methods for methane and carbon monoxide because the atmospheric concentrations and emissions of carbon dioxide are significantly higher than either two. An input enhancement of 300 ppm was used, based on the enhancement concentrations found in [5]. Two PRISMA files over a power plant were used for a retrieval which can be seen in Figure 5.12

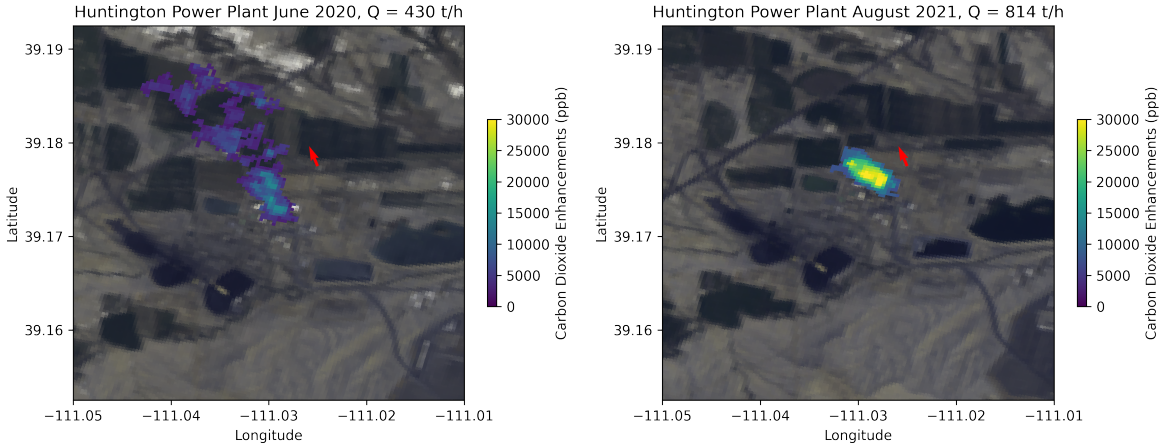

(a) Huntington Power Plant Plume June 2020

(b) Huntington Power Plant Plume August 2021

Figure 5.12: Comparison of two carbon dioxide retrievals over the Huntington Power Plant in Utah, USA. The left plume was found also in literature and the right plume was found by analyzing a new PRISMA file. Both plumes clearly originate from the facility, which is in the centre of the image. Wind direction is shown with the red arrow.

For the left image quantification was found in literature and determined to be 614 t/h [5]. The matched filter thus has a lower emission quantification estimate than with other models but in the same order of magnitude. The right image has a higher emission, which is possible as emissions with the GAO satellite have estimated emissions of up to 1430 t/h [5]. It is, therefore, possible to retrieve carbon dioxide emissions with the matched filter using PRISMA, but it is important to keep in mind that these quantifications need to be verified with more known sources.

5.6. Conclusion

The results in this chapter show that the matched filter using PRISMA data can be used for methane retrievals and help to detect methane emissions from multiple types of sources. The matched filter is used by implementing it per along-track column and retrieving enhancements directly. To quantitatively evaluate a retrieval multiple metrics were devised to assess a retrieval, the most important of which were a proxy for noise: RMS and the plume to noise ratio. After testing multiple bands it was found using experiments that keeping the original band from 2110-2450 nm was ideal, as deviating from this resulted in a less visible plume and more uncertain emission quantification estimates. A limitation of the matched filter is that it uses a linear relation for specific methane absorption, which is not how it behaves in reality. This can partially be solved by giving the matched filter more flexibility, as shown with the iterative matched filter and the pixel iterative matched filter methods. The improvements however do not result in significant improvements in the detection limit as the pixel iterative matched filter also estimates the median plume enhancement lower than the original implementation of the matched filter. For further analyses, the base implementation of the matched filter will be used, with a band of 2110-2450, unless stated otherwise.

The absorption features of other trace gases are also present in the spectrum that PRISMA measures. These include carbon monoxide and carbon dioxide. For carbon monoxide, the absorption feature of 2200-2400 nm was used by the matched filter, but it was too faint to be detected by PRISMA. Carbon dioxide can be detected, using a band from 1900-2100 nm, but the estimated enhancement concentrations and emission quantifi-

cations are lower than what is expected from other results obtained with PRISMA from literature. This might be explained by the absorption of water vapour in that same band, or be a limitation of the matched filter.

When testing the implementation for the matched filter, results were in line with those from literature, with the quantification estimates being slightly lower than expected, but within the confidence bounds. Disparities can be explained by more conservative plume masks than those found in literature. Methane emissions could be found over different kinds of scenes and from multiple types of emission sources. When comparing results quantification results with that of a different satellite, Sentinel-2 it shows that the quantification estimate of PRISMA with the matched filter is lower, which might be explained by a calibrated effective windspeed used in the IME method.

For some scenes, especially over areas with buildings and other surfaces that have albedo spectra that have similar features like methane the matched filter was unable to spot methane emissions. A limiting factor in detecting more methane emissions is the fact that the matched filter is sensitive to changes in albedo over the spectrum that is used for a retrieval. Over the 2110-2450 nm band, the albedo can change significantly, which is currently unaccounted for. For strong sources over a homogeneous area, this is not a big problem as these sources can easily be detected (Turkmenistan, Algeria), but sources such as landfills are much harder to detect.

When analyzing the matched filter as the least-squares estimator it was found that the matched filter might underestimate high enhancement pixels, as using a different approach for covariance estimation, using only high enhancement pixels showed that enhancements close to the source of a plume might have much higher concentrations. The developed iterative adaptations to the matched filter suffer the same limitation, but show a slight ability to estimate higher enhancement for these pixels close to strong sources. A more flexible model such as SICOR might be needed to estimate the concentrations of these high enhancement pixels.

6

Methane Retrieval Using SICOR

This chapter describes the PRISMA methane retrieval done with SICOR, the design philosophy and aim of SICOR are described in section 6.1, which is followed by the necessary modifications to the model in section 6.2. The parameter tests that were done to optimize the settings are shown in section 6.3, which is followed by the results and extension to other trace gases in section 6.4 and section 6.5. The chapter closes off with a conclusion presented in section 6.6.

6.1. Design Philosophy

SICOR is a retrieval model designed for TROPOMI carbon monoxide retrievals, that works quite differently than the matched filter and while both aim to retrieve methane they have different methods and pitfalls. The matched filter uses the difference in radiance per column to estimate methane enhancements for an entire along-track column at once, while SICOR does this for each pixel and spectra individually. The matched filter only uses a radiative transfer model to model a signal with which the PRISMA measurements are compared and SICOR uses this as an integral part of its iterative solving methods to retrieve the state vector that contains the methane concentration for a single spatial pixel.

As such SICOR has less information (i.e. individual data points from detectors) for each pixel retrieval, but it has more flexibility to deal with variation in altitude, temperature and water vapour content in the atmosphere. This flexibility is a double-edged sword, while it allows for solving problems with areas that are prone to albedo artefacts and correcting for mistakes, it also is susceptible to them, as it reviews methane on a pixel by pixel basis.

That is why it is important to ensure the stability of SICOR. This can be done by focusing on the quality of the modelled and measured spectra and providing corrections where necessary. An important part of this is the focus on the chi-squared score that the model retrieves, which indicates the goodness-of-fit, with lower scores indicating a better fit of the model to the measurements.

6.2. Modifications to Model

SICOR originally is a two-step model that retrieves carbon monoxide, with a non-scattering methane retrieval as a first step. This first retrieval will be the focus of this chapter as it will be modified to work with PRISMA data to perform a methane retrieval. To adapt SICOR to work with PRISMA the inputs need to be identified along with the changes that are necessary to make them compatible. Below an overview of the two-step retrieval is shown along with the necessary inputs in green:

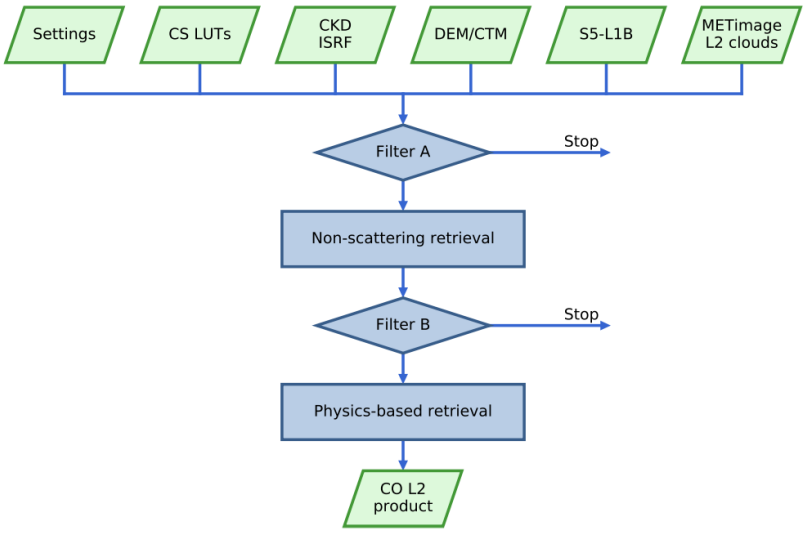

Figure 6.1: Overview of inputs and steps of SICOR. The inputs are given at the top of the figure with green. For the PRISMA adaptation of SICOR only the non-scattering retrieval will be used, as it provides an estimation of methane concentration. The filters are applied to pixels that contain either clouds (A) or for which the retrieval did not converge properly (B). [33]

An overview of the input types is provided below:

- Settings: The settings file includes all settings that are necessary to make SICOR work.
- LUTs: Look-Up Tables are used to provide cross-sectional absorption values for the trace gas molecules included in the radiative simulation.
- ISRF: The Instrument Spectral Response Function (ISRF) provides the response of an instrument to incoming light at different wavelengths.
- DEM/CTM: Meteo data containing information about the atmosphere on the day of the retrieval are included for the radiative simulations.
- L1B data: The L1B data contains the PRISMA radiance measurements, which need to be adapted, but also information regarding the orbit and instrument.
- METimage L2 clouds: Clouds are not included in the model and scenes are selected without clouds before processing.

Settings

SICOR works with a settings document in which the settings for the radiative simulations are stored and the locations of reference files are stored. The settings for radiative simulations have been changed to work with the spectral resolutions of PRISMA and the generated LUTs. The settings for the iterations of the model have been changed to be less restrictive than for TROPOMI, with SICOR originally only allowing for a 50% deviation from the apriori methane concentration estimate, which is too restrictive for PRISMA. The reason for this is that the spatial resolution of PRISMA is much higher than TROPOMI, which means that concentrated emission enhancements are much higher than for TROPOMI. PRISMA observes concentrations that can go well above 150% of the background concentration of methane, meaning its estimations are likely less certain and more likely to be above the original 50% deviation. The maximum deviation has been set to 10000%, as to make sure that many spatial pixels can be used in the retrieval, with filtering at later stages being possible to remove pixels that have not converged well or arrive at nonsensical values. In order for SICOR to work information regarding the solar spectrum is needed. Since PRISMA does not measure the solar spectrum a reference spectrum is needed, which is referred to in the settings.

LUTs

The original LUTs of SICOR only cover a part of the methane absorption features as shown in Figure 2.2. These LUTs cover the molecular absorption cross-sections of the most important trace gases used in the radiative transfer simulations of SICOR. Therefore they need to be generated, which was done for carbon monoxide, water, semi-heavy water and methane for bands ranging from 2050-2500 nm, with a spectral resolution of 0.1 cm^{-1}], covering the strong methane absorption feature. To calculate these values python scripts from SRON were used, which were also used to calculate the original LUTs for the TROPOMI SICOR retrieval, used for carbon monoxide.

ISRF

The ISRF is essential for estimating how the PRISMA detector reacts to incoming light. The spectral response for TROPOMI has been measured before the mission using monochromatic light sources and on-board it can be measured by five diode lasers [51]. The ISRF used in SICOR is thus very well known for TROPOMI. For PRISMA these measurements are not available and thus they need to be approximated. This is usually done using a Gaussian Response Function [14, 16].

$$S = \exp\left[-\left(\frac{(\lambda - \lambda_c(i) - \delta)}{C\sigma_i}\right)^2\right] \tag{6.1}$$

With λ being the reference wavelength, λ_i being the central wavelength of the detector-pixel and δ being the delta wavelength, C is a normalization constant and σ_i is the FWHM of detector-pixel i. This has been done for all detector pixels using the spectral settings that have been provided by PRISMA. The Gaussian function uses a delta wavelength domain of +20 and -20 nm. Because of the way the input data is structured for SICOR a single-centre wavelength had to be used as input, which resulted in a diagonal shift of the ISRF across-track, similarly how the center wavelength moves across-track. An example of how the ISRF looks like for a channel of PRISMA is shown below:

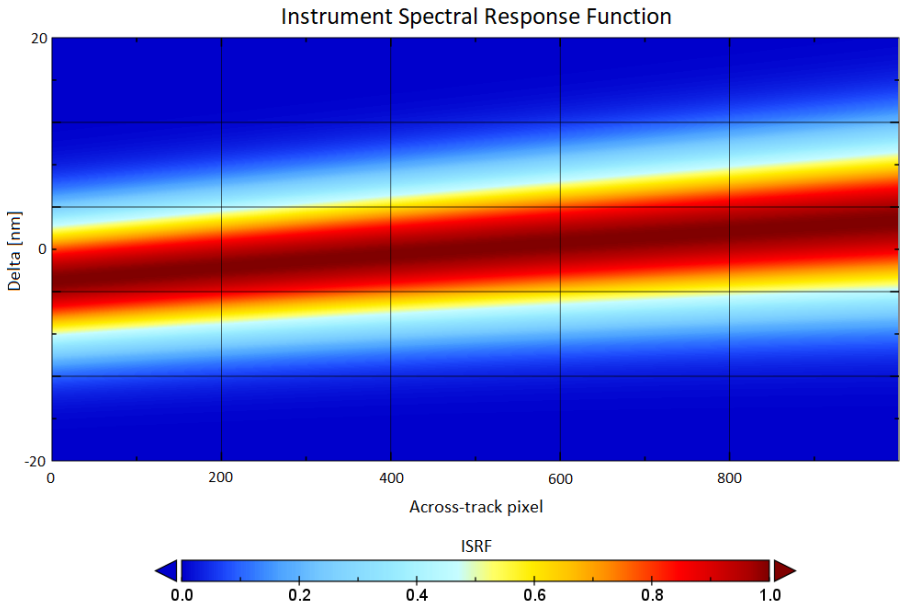

Figure 6.2: Modelled ISRF for PRISMA channel 60 at 2050 nm. The difference in central wavelength and FWHM for the different detector pixels can be clearly seen as the ISRF moves across-track.

METEO, Priors, Orbit

One of the inputs for the retrieval is meteorological data, including surface pressure, temperature gradient and the humidity of the air. The data used for SICOR is that of the GEOS-FP dataset, provided by NASA [38]. This is a dataset that has daily global meteorological data for these variables. Data is sampled for the proper latitudes and longitudes of PRISMA scenes. The number of atmospheric layers used in the GEOS-FP dataset does not match the number of layers in SICOR, so a linear interpolation is used between the two, to arrive at matching shape and values of the data.

For both the methane as well as the carbon monoxide retrieval a prior is needed with which to start the retrieval process, to initialize the state vector. This is done by creating two separate files with a prior for each individual pixel of PRISMA. Since no high-resolution methane prior database exists the average concentration of methane from a reference atmosphere is taken instead. The same is done for carbon monoxide.

The orbit file for SICOR consists of data fields that describe the coordinates of the corners of each spatial pixel on the ground and its positioning concerning the Sun and PRISMA and includes the viewing angles and solar zenith and azimuth angles.

Radiance

The TROPOMI radiance input is different from that of PRISMA, because it measures the number of photons in mol at a certain wavelength per steradian per nanometer, instead of Watt per steradian per nanometer. That is why a conversion is necessary to conform to the input for SICOR. This is done by using Planck's Law to calculate the average energy of a photon for the measured radiance by PRISMA, by using the specified central wavelength of the PRISMA detector pixel as the wavelength of the photon. This results in the following conversion:

$$L_{TROPOMI} = \frac{L_{PRISMA}}{\frac{hc}{\lambda} N_A} \tag{6.2}$$

Where L_{PRISMA} is the measured radiance from Tropomi, h is the Planck constant, c is the speed of light, λ is the wavelength of the PRISMA detector-pixel and N_A is Avogadro's constant. As mentioned in the section regarding the settings a reference solar spectrum is used, which is also adapted using the formula shown above.

6.3. Parameter Optimization

Like with the matched filter a systematic approach was used to determine the optimal settings for a methane retrieval using a variety of different scenes, containing both plumes as well as empty scenes. A difference with the matched filter is that not only the results of the enhancements matter but also how well SICOR can fit the spectrum. SICOR uses the chi-squared metric for this, which indicates goodness-of-fit for the measured and modelled spectrum. SICOR estimates the concentration of trace gases in its state vector, but enhancements are needed. To calculate enhancements either the global background concentration of methane can be subtracted from measurements or an estimated mean concentration. Using the background concentration might not be suitable, because that would require SICOR to accurately estimate the mean concentration of methane using PRISMA data, which is known to be noisy. That is why a different method is proposed by estimating the mean concentration of each along-track column, thereby eliminating the effect that individual across-track detector columns have on the enhancement calculation and subtracting that from the concentration estimates from each spatial pixel.

In order to use the right parameters a systematic approach will be used where in the parameters will be estimated in the following order:

1. State Vector, determining which trace gases and state variables are included in the iterations.
2. Albedo, determining what albedo profile is suited for a retrieval.
3. Bands, determining what spectrum will be used by SICOR to retrieve the state vector.

The reason that these parameters are estimated successively is the long computational time for each retrieval. Estimating these parameters successively allows for time savings and still retains the ability to measure the effect of each parameter. From testing, it became quickly evident that only methane and water vapour could be added as trace gases as the absorption of carbon monoxide and semiheavy water vapour is too faint at the PRISMA resolution to provide stable iterations in SICOR. The concentration values of carbon monoxide and semiheavy water often tend to go to zero or even negative values, meaning that SICOR is unable to properly include them. That is why it has been decided to only include water vapour and methane as trace gases in the state vector of SICOR, alongside the estimated albedo coefficients.

The next step was to determine how the albedo profile should be estimated in the retrieval. Albedo plays a significant role in the estimation of methane concentrations, which is even more important in SICOR, because it performs the retrieval for each individual pixel separately. It is important to take this into account because the possible

spectrum that is going to be used (2100-2450 nm) is larger than the original SICOR spectrum. The albedo can differ strongly between one spectral area and the other, which interferes with the methane signal. Originally the effect of albedo was modelled with a constant and a linear trend, but that might not be sufficient. That is why the albedo was estimated for an area in Turkmenistan to see how that would compare to results found in literature. To do this a zeroth order polynomial was estimated for several spectral bands over a larger spectrum. This way an albedo profile could be estimated and compared to measured results:

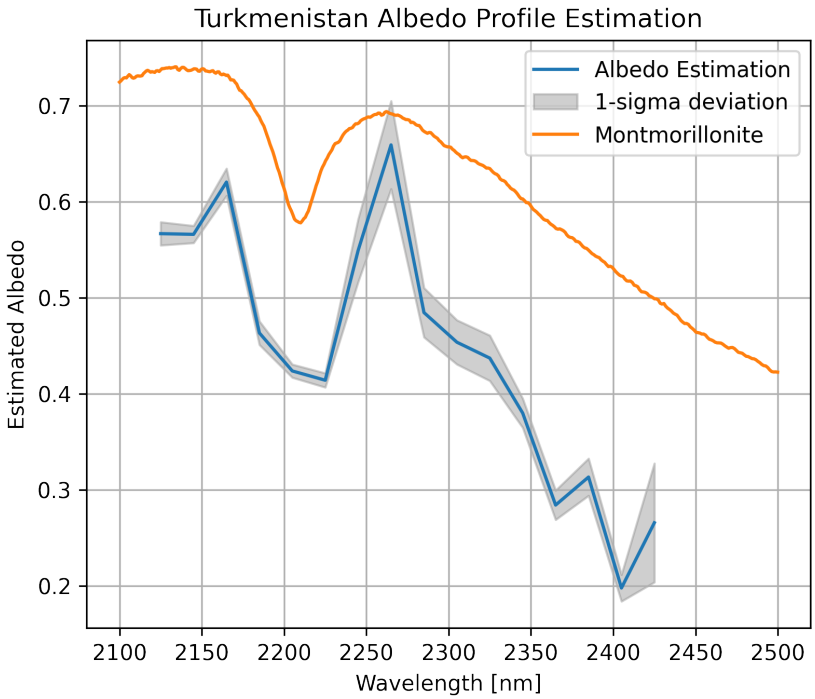

Figure 6.3: Comparison of an estimated albedo profile of pixels in Turkmenistan and that of a measured clay mineral Montmorillonite. The estimated albedo spectrum was created by estimating the albedo using SICOR for bands of 50 nm with intervals of 20 nm. The two show a similarity in shape, indicating that a simple line is not sufficient to model the larger shape.

From this, it can be seen that there is a significant variation in albedo over the spectrum where also the methane absorption feature is present. A linear fit for this albedo dependence is most likely not sufficient, which was confirmed by increasing the polynomial from 1 to 2 for SICOR, which decreased the average chi-square value with 1.15 for tests in China, Turkmenistan and Algeria. The last parameter that needs to be determined is that of which bands are included in the retrieval. This was done by performing tests with different bands for five different scenes that all contained methane emissions.

Table 6.1: Relative changes for three metrics when comparing to a band of 2110-2450 nm. From this it can be seen that reducing the band size from 2110-2450 can have significant change on the fit of measured and modelled spectra. All given values are in %.

Band	RMS Change	Mean chi-squared change	Mean enhancement change
2110-2400 nm	12.34	-42.53	10.11
2110-2350 nm	-16.12	-56.52	-13.26
2150-2400 nm	0.87	-27.96	-1.16

From the results shown above, it can be seen that by reducing the band given to SICOR the iterations improve significantly. It must be said however that these changes are highly location-dependent, with homogeneous scenes such as deserts being less affected by changing bands and heterogeneous scenes such as those found in China and Buenos Aires being highly affected. For desert scenes using the full band of 2110-2450 nm gives the best result, but for scenes where vegetation or urban areas are present reducing the band size to 2110-2400, or even 2110-2350 nm, might result in a better retrieval. That is why it is important to verify with a smaller test which band works best.

The chi-squared score gives a metric of the goodness of fit of how well SICOR can fit the data to the measurements, with lower scores meaning a better fit. Based on experiments and results it became visible that high chi-squared scores can result in significant methane concentration estimates, most of these being caused by albedo artefacts. Using this chi-squared score a filter can be applied to remove these high methane concentrations and replace them with the median value of the detector column. For the controlled experiments in Arizona, this was immediately useful.

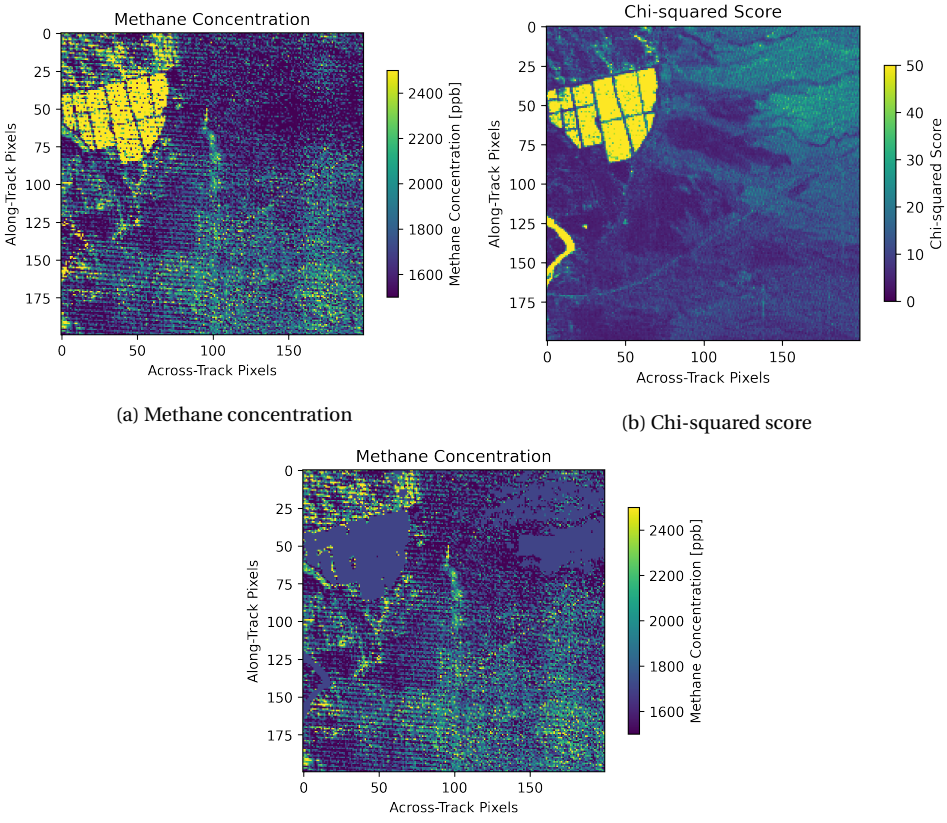

(a) Methane concentration

(b) Chi-squared score

(c) Filtered methane concentration

Figure 6.4: Comparison of methane concentration estimates using SICOR and the chi-squared score per pixel. In the middle a plume from a controlled experiment is visible. On the left a strong correlation between high methane concentrations and a high chi-square score is visible. This correlation can be used to remove artefacts from the data as is shown on the right image, where high chi-squared scores are used to replaced retrieved concentration with the median concentration obtained in the same along-track line, in order to facilitate the calculation of enhancements.

6.4. Results and Analysis

After finding the parameters that lead to the clearest methane enhancement concentrations several retrievals were done over various areas, including several known locations with emissions. When running tests over Algeria an anomaly in the data was discovered, which is discussed in subsection 6.4.1, this is followed by the results and analysis in subsection 6.4.2.

6.4.1. Instrument Radiance Issues

When working on enhancement retrievals using SICOR a pattern seemed to emerge in the methane enhancement pictures that showed correlation between different locations. This pattern showed a predominantly across-track correlation, but it could not be explained by just a stripe, because it was at an angle. This pattern would only emerge at some of the detectors of PRISMA and not at others. The pattern was predominantly visible in regions of the spectrum with significant absorption of water vapour, meaning that the measured radiance was low. To investigate the cause of this pattern measurements were gathered where the measured radiance was expected to be low, so that the pattern, which was assumed to be fixed in nature would be most visible. A scene over the sea in Norway in February 2020 was taken as a reference for this, for which two radiance images are compared in Figure 6.5.

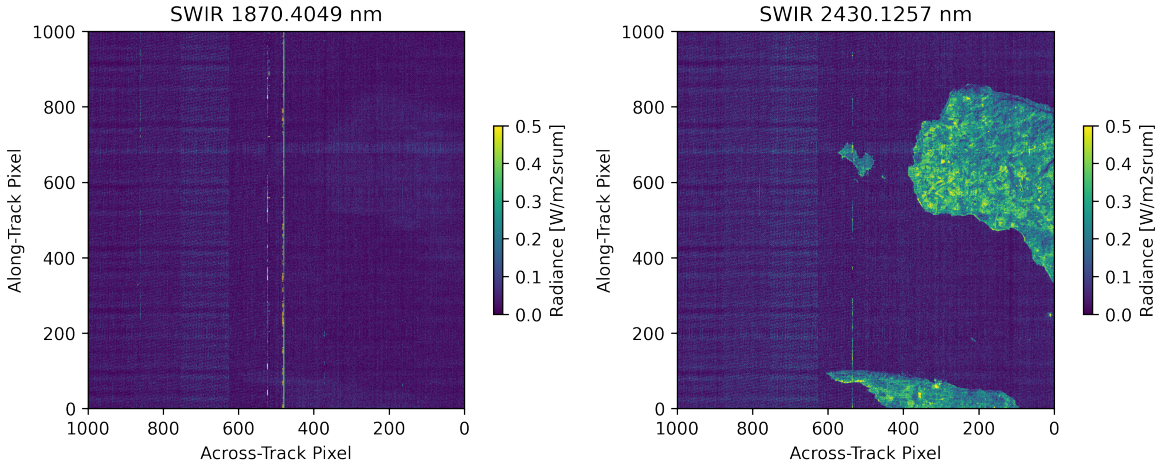

Figure 6.5: An example of the radiance pattern for two different wavelengths, one at 1870 nm in a water absorption band, showing that almost no radiance is measured at the land, and one at 2430 nm, in the part of the spectrum that is used for methane retrieval. The magnitude of the radiance pattern stays roughly the same, independent of the wavelength.

Because the pattern does not change in form or intensity, it is unlikely that it is the result of an optical issue in the instrument. It looks like fixed pattern noise and was also noticed recently in literature [40]. It can also be seen that the intensity of the noise changes across-track, with intervals of 125 pixels. This can in fact be explained by the design of the detector. The detector in use aboard PRISMA is the Sofec Saturn SW detector, which has 8 outputs with 125 columsn each. It consists out of two halves which also explains why the fixed pattern noise is primarily present in the left halve of the image. The pattern does not obscure the true radiance data completely but seems to be added to a 'true' measurement, meaning that it is likely to be in the offset of the measurements.

When adding all the channels together they form a wavelike pattern, that can be observed in the methane concentrations and enhancements, where the dips and bumps are seen by the inversion model as traces of methane. Because the wavelike pattern is in the along-track direction and thus changes in time it is likely that it is the result of an electronic issue with reading the data. A possible problem with this is the frame rate that is currently in use for PRISMA. For 1000 spatial along-track pixels with a resolution of 30 m the frame rate would be around 250 Hz, which is above the limit of the Saturn SW detector, which is rated for 240 Hz [39, 12].

The problem with this data is that the pattern is not 'hard', meaning that it is not a single stripe that can be corrected by filtering. Individual layers have to be processed to remove the pattern, which only fully appears when all layers are combined in the retrieval. Several methods have been experimented with to see which would result in the best removal of the pattern. The methods investigated were median filtering, wavelet decomposition filtering and Fourier analysis. Fourier analysis was the only method that had a decent performance in pattern removal, by using the Fast Fourier Transform (FFT). An example of how this approach works in practise is shown in Figure 6.6

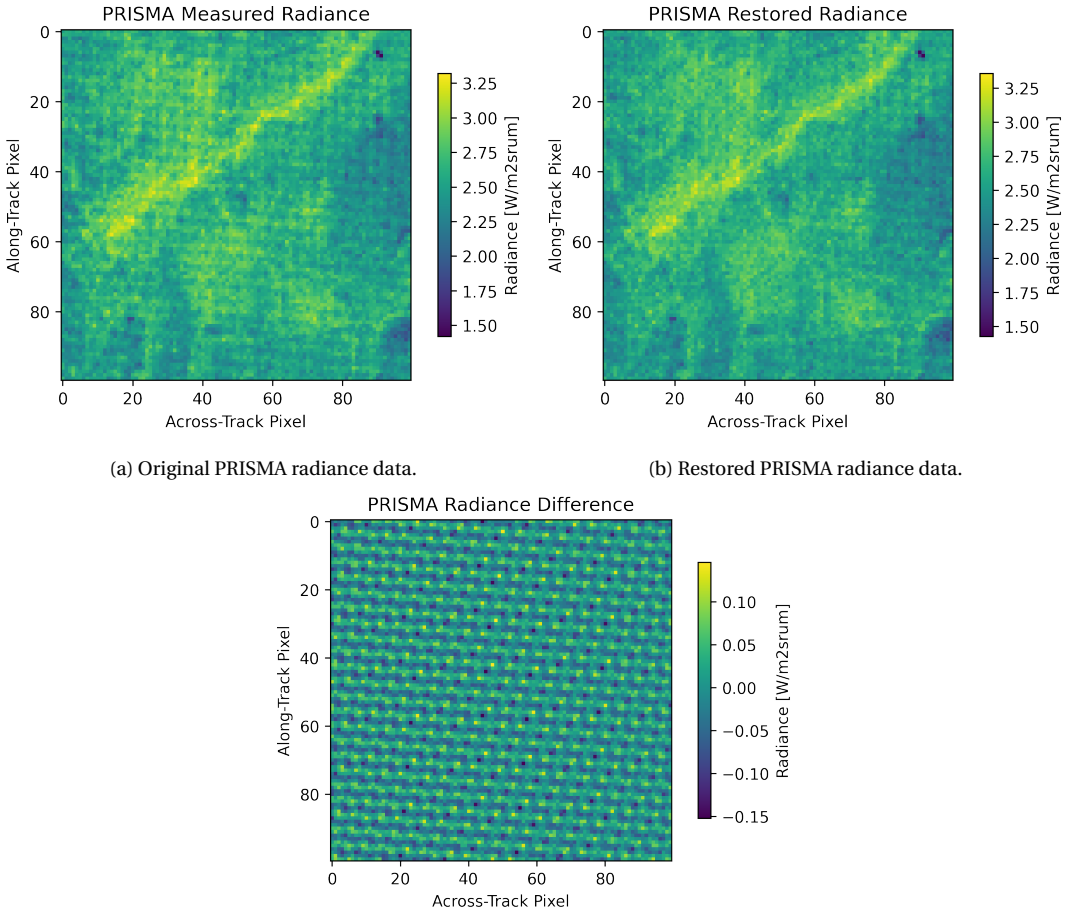

(a) Original PRISMA radiance data.

(b) Restored PRISMA radiance data.

(c) Radiance difference.

Figure 6.6: Example of how the removal of certain frequencies in the FFT domain can help remove fixed pattern noise in the radiance data. These three pictures show a part of a PRISMA scene in Algeria where multiple plumes are present. Radiance measurements here correspond to 2465 nm.

In this analysis, the Fourier transform is utilized to find frequencies with high energies.

High energy frequencies in the Fourier transform often signify noise, or in this case a pattern. These noisy frequencies are removed by setting them to zero, after which the data can be recreated by utilizing the inverse Fourier transform. Through testing, a level of cutoff energy was determined that would remove frequencies that cause a pattern. Not all high energy frequencies are linked to the pattern, that is why some areas in the Fourier transformed data are not allowed to be set to zero, to preserve information. From the figure the magnitude of the pattern is seen, which seems to be around 0.15 $W/m2srum$ in magnitude, which corresponds to 3-6% of the measured radiance at 2465 nm. This would violate the design requirement of an SNR of 100 in the SWIR region. The effect of using this FFT analysis is shown below, where it can be seen that the pattern in the methane enhancements is less severe than before:

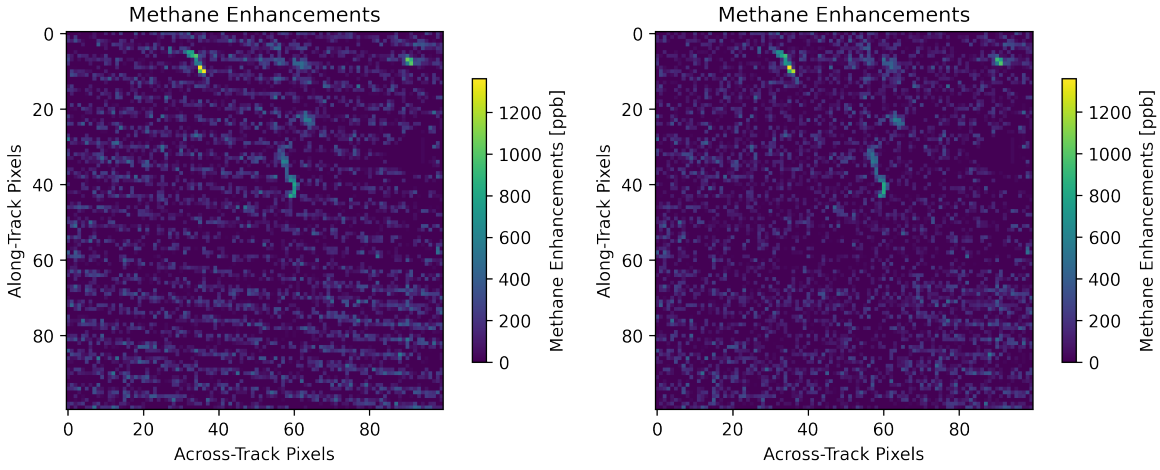

(a) Enhancement pattern as seen in Algeria

(b) Enhancements using the pattern removed radiance data.

Figure 6.7: An example of how FFT can be used to remove frequencies that cause a pattern to emerge in the enhancements. It can be seen on the right picture that the pattern is not entirely removed, but it does help in distinguishing the plume from the background noise.

While the pattern can partially be removed it does still limit the plume mask dilation capabilities as the pattern is still picked up in the enhancements. That is why emissions primarily from the unaffected area are used in further analyses unless stated differently.

6.4.2. Results

Initially, several retrieval runs were done to verify that the estimated concentration was in line with the background concentration of Earth. The background concentration estimated with SICOR varies scene per scene, with scenes with high vegetation or elevation changes being estimated with higher concentration. The enhancements are calculated by subtracting the median value of each column. An example of how methane concentration is retrieved and how it results in enhancements is shown below:

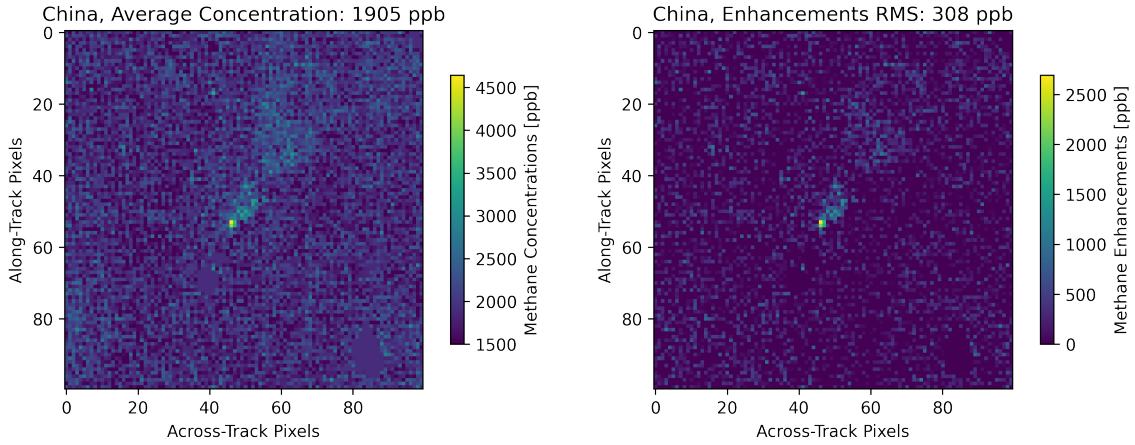

(a) Retrieved methane concentrations over China.

(b) Retrieved methane enhancements over China.

Figure 6.8: Methane Concentrations over China on the left and enhancements on the right. A plume like shape is visible.

An advantage of SICOR is the fact that a chi-squared score is given to each individual spatial pixel of the observation, indicating the goodness-of-fit. This is used to filter out artefacts and is done for pixels that have a chi squared score higher than 1.5 times the mean chi squared score of the scene, but for scenes with high chi squared scores a manual approach is sometimes necessary. These pixels are replaced by the median concentration of the scene. This is done so that the enhancement estimates are not skewed by the high concentration estimates of measurements that SICOR found difficult to fit.

After finding good parameters for SICOR to use several tests were done over known plumes that had been detected using the matched filter. These include emissions in China, Turkmenistan and a landfill in Buenos Aires. These scenes all have emission sources located in the unaffected parts of the scene, so no radiance pattern interferes with the enhancements. Enhancements have all been calculated by subtracting the median concentration of each along-track column. Results are shown on the next page:

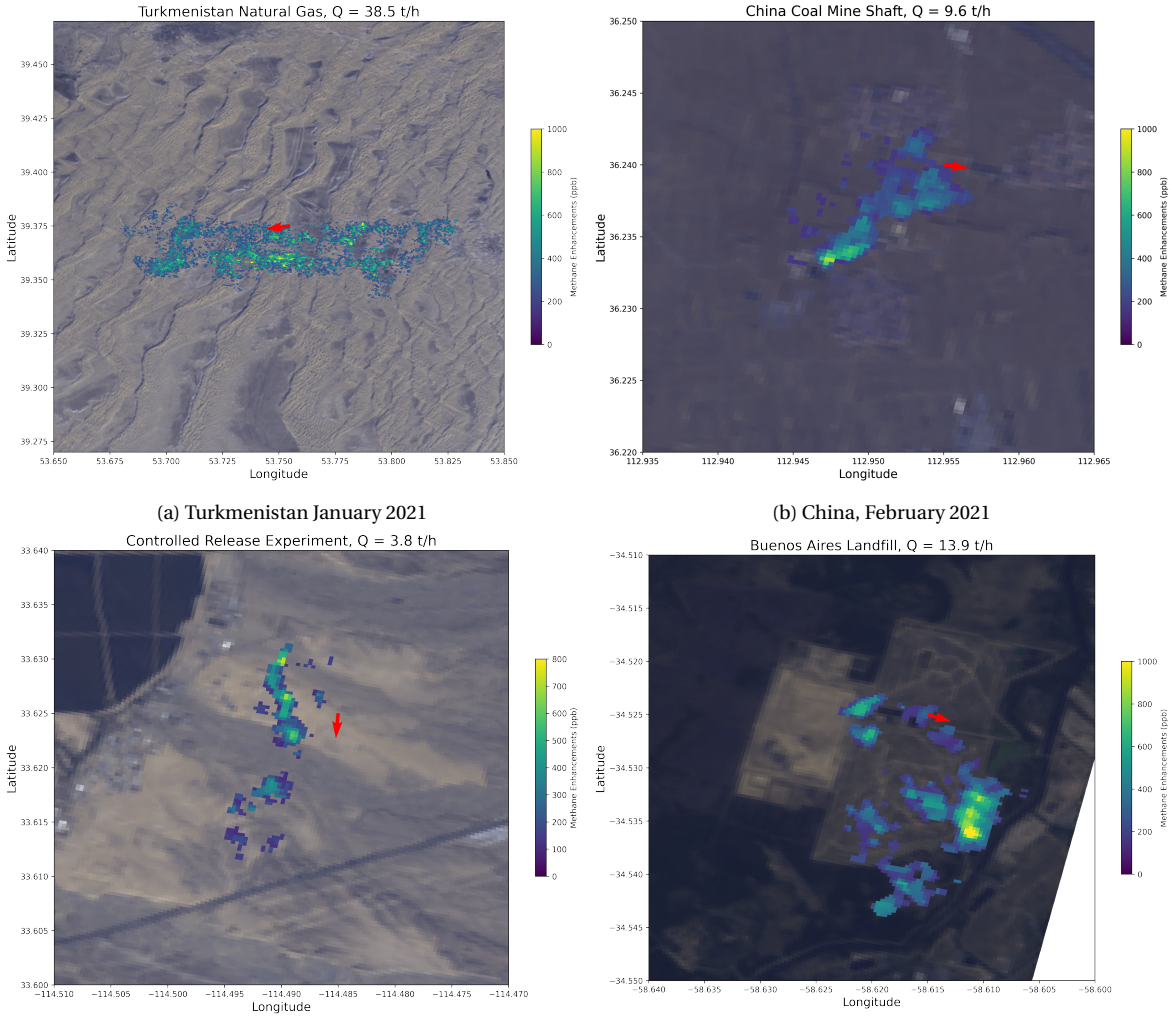

(a) Turkmenistan January 2021

(b) China, February 2021

(c) Arizona USA, December 2021

(d) Buenos Aires, January 2022

Figure 6.9: Plume masks and quantification estimates for four different type of methane emission sources and scenes of interest using SICOR. Enhancements shown have been made using a median filter of retrieved methane enhancements for illustrative purposes.

From this, it can be seen that SICOR is also able to retrieve plumes from PRISMA data. Overall the concentrations are higher, especially at the source of the plumes, which have higher enhancement concentrations than with the matched filter. This also results in higher emission quantification estimates. Plume mask generation is more difficult than with the matched filter, this being most visible for the controlled release experiment and the plume visible in Turkmenistan. Like with the matched filter a comparison was made with quantification estimates of the controlled release experiments done by Stanford and the retrieved PRISMA emission quantifications done by SICOR retrieved enhancements.

Table 6.2: Controlled Release Experiments compared agains the PRISMA retrieved emissions using SICOR. All values are given in kg/hr. First three columns signify the controlled release experiments.

Date	Min Q	Mean Q	Max Q	PRISMA Q IME	PRISMA Q CSF
2021-10-21	3939	4177	4417	3830 ± 1530	3200 ± 1500
2021-10-27	3274	3484	3670	3560 ± 1400	4000 ± 2400

From these experiments, it can be seen that the quantification estimates for SICOR are slightly higher than those of the matched filter and come closer to the presented values from the controlled release experiment. The CSF quantification estimate is also closer to the reported value, but the confidence level stays similar. While two experiments are not sufficient to conclude that a methane retrieval using SICOR is better it does provide a good outlook for using a method like this for quantification and with more tests, a more conclusive answer can be given.

6.5. Extension to Other Trace Gases

SICOR was initially designed to retrieve carbon monoxide from TROPOMI and it is interesting to see whether it is possible with PRISMA to show some sensitivity concerning carbon monoxide in a retrieval. From the matched filter it could already be seen that this is a very difficult task, as the carbon monoxide signal is much weaker than that of methane. This makes it difficult to fit, resulting in significant noise in the retrieval. The initial approach for SICOR is to first fit methane and then carbon monoxide, making use of two different bands from 2315-2324 en 2324-2338 for methane and carbon monoxide respectively. For PRISMA this is not possible, as using these bands would result in only 2-3 spectral pixels being available for each retrieval, resulting in a very unstable retrieval.

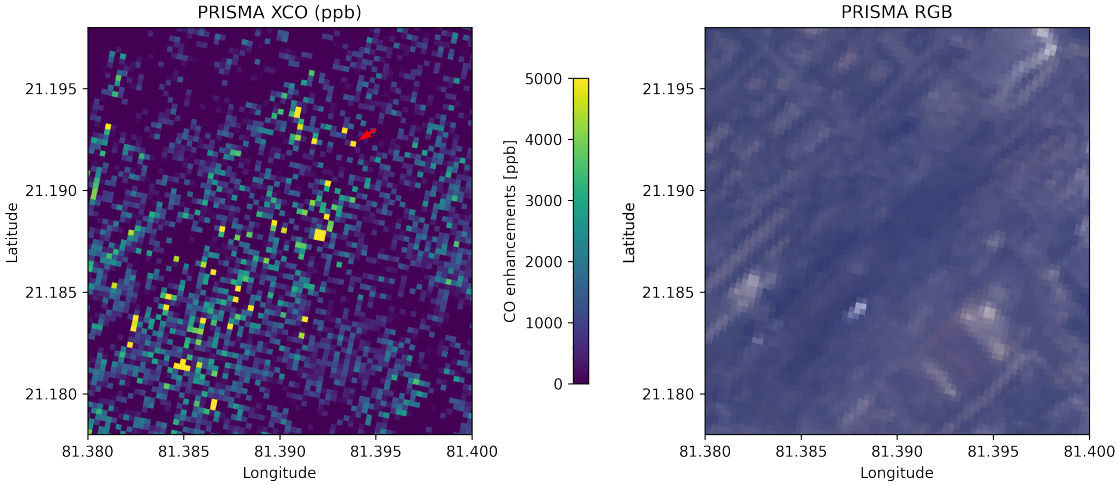

Figure 6.10: Results for CO retrieval over Bhilai steel plant. As can be seen from the colorscale of the image the noise of the retrieval is very high. In reality such concentrations of carbon monoxide would not be realistic as concentration values are usually around 100 ppb [11]. It can also be seen that no plume is visible.

The settings for this retrieval have been set from 2200-2400 nm with carbon monoxide being included in the state vector. The retrieved concentrations are an order of magnitude larger than expected values and no plume structure is visible. From this it can be concluded that PRISMA is not suitable for the retrieval of carbon monoxide, using SICOR. Carbon dioxide was considered as well, but not all input files for SICOR were available for carbon dioxide. Retrieval of carbon dioxide is likely to be more successful as the total absorption of carbon dioxide is significantly larger than that of carbon dioxide, which makes the dip in the PRISMA measured data more measurable.

6.6. Conclusion

This chapter started with the modifications that were necessary to make SICOR, the operational algorithm for carbon monoxide retrieval for TROPOMI data, work with data from PRISMA. A list of modifications was made, with the most important being the changing of model settings, the adaptations of radiance data to TROPOMI format and generating the ISRF and LUT. SICOR uses a two-step approach in which the first retrieval step estimates the methane concentration of a spatial pixel. This first step will be used to retrieve methane using PRISMA data.

Tests were done that confirmed that only water vapour and methane should be included as trace gases in the retrieval, as the other trace gases had to faint signals to be able to properly estimated using PRISMA data. It was shown that SICOR retrieves methane concentrations that are similar to the background concentration, but with high variation over different scenes. Enhancements however are estimated fairly consistent, which are estimated by subtracting the median concentration value for each along-track column from the along-track concentrations. Based on tests using different bands it was shown that SICOR behaves differently over various types of scenes, with the fit improving over scenes with a smaller band than the original 2100-2450 nm band used from the start. SICOR also takes an albedo profile estimation into account and from tests it was shown that the original linear trend for this albedo was not optimal for the retrieval, using a second-order polynomial resulted in a more optimal fit with lower chi-squared values.

From tests, it could be seen that SICOR is also able to retrieve methane enhancements from PRISMA data and shows the presence of plumes. From tests over Algeria, it was shown that PRISMA suffers from fixed pattern noise in part of its measurements, which correlate with methane concentration and enhancement estimates. This can partially be fixed by applying a FFT and removing some frequencies in the FFT domain. Emissions that are not affected by this pattern were used to determine the quality of SICOR retrievals. These have shown that SICOR can also be used to retrieve methane from PRISMA data and show emissions from point-sources. From the retrieved plume masks, it can be seen that the SICOR methane retrievals are noisier than those of the matched filter and that performing plume dilation is more difficult. Quantification estimates are in line with results from the matched filter, but on average are a bit higher, with SICOR being closer to reported values of controlled release experiments.

From this, it can be concluded that the proposed adaptations work to modify SICOR to work with PRISMA data, by using the first retrieval of SICOR, which estimates the methane concentrations. Emissions can be recovered, but results are noisy and SICOR is sensitive to the pattern noise that was found in the radiance data.

7

Analysis

This chapter analyzes the different steps of the project as outlined in chapter 4, as part of the preprocessing step of this project the effect of hyperspectral denoising and spectral calibration will be discussed in section 7.1 and section 7.2. Continuing, both methods for methane retrieval will be discussed and compared against each other in section 7.3 and its current capabilities and applications in section 7.4. To close the chapter off a final extension is discussed to improve performance in section 7.5 and preliminarily concluded in section 7.6.

7.1. Hyperspectral Denoising

Hyperspectral data can be noisy and this noise affects retrievals. In order to improve the quality of the hyperspectral data denoising can be applied. Statistical techniques such as wavelet shrinkage and matrix approximation techniques make use of properties of hyperspectral data to try and identify the 'real' measurement and remove the noise. This noise can be the result of temperature imbalances, instrument patterns or from other sources [42]. Hyperspectral denoising has already been used for classifying surface types, but not for methane retrievals [42]. The application of hyperspectral denoising techniques on PRISMA data is the subject of a second thesis at the VU, coinciding with the thesis of this report. Two methods have been developed which employ different strategies to remove noise and keep the measurement. The first method is that of PCA wavelet shrinkage [3], and the second is Noise-Adjusted Iterative Low Rank Matrix Approximation or NAILRMA for short, a matrix approximation method [18]. Out of this research, it was found that the NAILRMA method is best suited for hyperspectral denoising. The good thing about NAILRMA is that it is able to allow for different levels of noise to exist in the hyperspectral data and adapt to them as it can model this noise for different wavelengths. As a reference scene, a PRISMA scene over coal mines in China was chosen. This is because this region is generally a difficult one to perform retrievals for. The noise in the methane enhancements is generally higher here, making it more difficult to spot emissions. The reason for this is because of the elevation changes and many surface changes over an area (buildings, vegetation, mountains and roads). The assumption here is that this is reflected in the instrument receiving more noise than over a homogeneous region and that denoising can improve the retrieval capabilities of PRISMA. NAILRMA was implemented as a pre-processing step and the denoised radiance data was used to perform a matched filter retrieval:

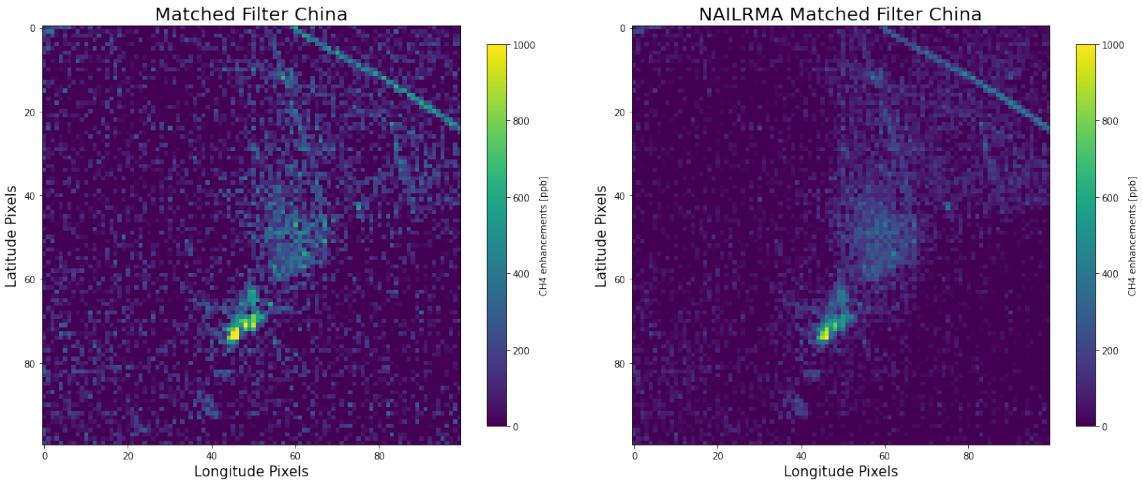

(a) Original Matched Filter, Max enhancement CH4: 1278 ppb, RMS: 114 ppb

(b) NAILRMA Matched Filter, Max enhancement CH4: 996 ppb, RMS: 79 ppb

Figure 7.1: Experiment over a coal mine in China with the NAILRMA. On the left side the original data is used with the matched filter and on the right the NAILRMA is implemented to denoise the input radiance data. It can be seen that the noise around the plume is decreased significantly, but also that the plume has become more faint.

From the figure above it becomes evident that the noise far away from the plume is decreased significantly. This is less so with noise just around the plume or noise that has more structure to it. Artefacts such as roads and buildings are not removed. The methane enhancements are decreased as well, most probably because some information is lost in the denoising process. The amount of noise however is decreased more than the methane enhancements, as the level of noise is decreased by 31% and the max enhancement only 22% and less so for the median plume enhancements. This is useful for purposes such as plume mask generation as the plume stands more out, because the background noise is suppressed. For methane retrieval using SICOR the results are a bit different:

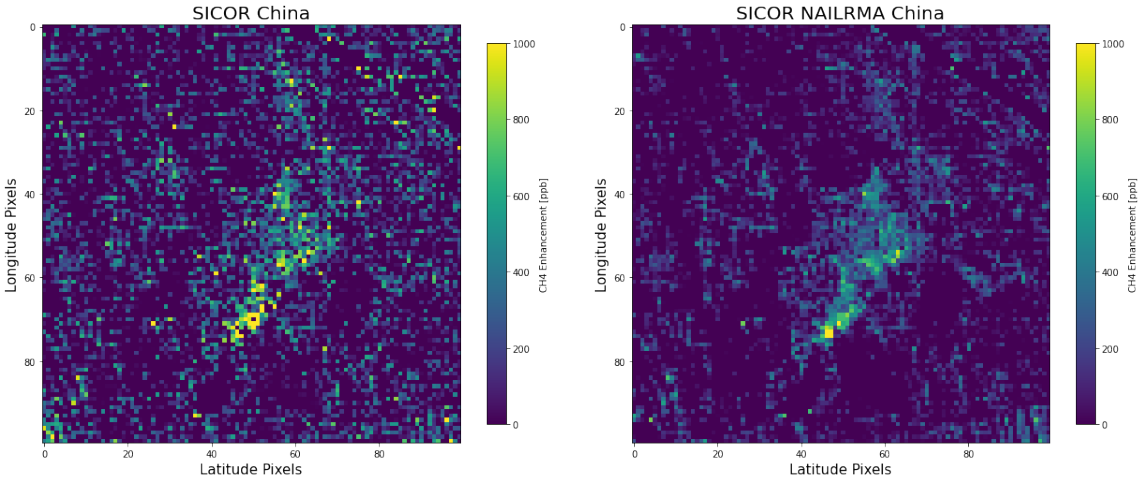

(a) Original SICOR, Mean CH4: 1792 ppb, Max enhancement CH4: 2373 RMS: 310 ppb, Mean chi-squared: 9.241

(b) NAILRMA SICOR, Mean CH4: 1785 ppb, Max enhancement CH4: 1476, RMS: 179 ppb, Mean chi-squared: 5.112

Figure 7.2: Experiment over a coal mine in China with the NAILRMA. On the left side, the original data is used and on the right, the NAILRMA is implemented to denoise the input radiance data. Both images use SICOR to retrieve methane concentrations and enhancements. With NAILRMA it can be seen that the algorithm removes a significant amount of noise and tries to uncover the plume structure, concentrations do however decrease for the left image.

The effect of NAILRMA denoising is even greater on the retrieval using SICOR. While on the left it cannot be seen that a plume shape is visible on the right it has a clear plume structure. The reason why this difference exists between the matched filter and SICOR is again that the matched filter simultaneously estimates the enhancements for an entire along-track column and SICOR performs a retrieval pixel-by-pixel. The results of the matched filter are already a bit smoother and the effect of NAILRMA is less. The denoising does not have a large effect on the average estimated concentration of methane, but it does have a large effect on the maximum enhancement, noise level using RMS and the chi-squared score. From the results it can be seen that the maximum enhancement of the plume decreases significantly, This is primarily because the maximum enhancement for the original SICOR retrieval (left) is so large compared to the rest of the enhancement within the plume. Even so, the noise reduction is larger than the loss in enhancement as it decreases by 42% and the max enhancement decreases only by 37%, with again median values in the plume being less affected.

7.2. Spectral Calibration

In the original implementation of the matched filter for methane retrievals using PRISMA [15] a section on spectral calibration was included. In here the effects of changes in the central wavelength and FWHM on the enhancement and quantification was included but it did go into much detail what effect calibration has on these results. That is why experiments were done for both the matched filter as well as for SICOR. For the spectral calibration experiments, the spectral calibration result for a scene in Algeria were taken from experiments done by Luis Guanter. The method used is discussed in subsection 2.5.1. For the matched filter these values can be added fairly straightforward and the experiments can be done. For SICOR an additional step is necessary as the ISRF needs to be generated using the updated settings, which use the same steps as mentioned in Figure 6.2.

For the matched filter the results differed only slightly, which might be explained by the fact that it estimates enhancements for an entire along-track column, increasing its robustness to change in spectral settings.

Table 7.1: Comparison of matched filter retrieval with and without spectral calibration over Algeria. It can be seen that calibration only performs better for the estimated noise, but scores worse for all other metrics.

Calibration Settings	RMS [ppb]	Mean Enh [ppb]	Max Enh [ppb]	Q IME [kg/hr]
No calibration	42	141	587	1532
CW and FWHM	41	126	521	1721

SICOR shows a similar story with changes in the spectral settings, due to spectral calibration. Noise estimates are higher for the updated settings, with the goodness of fit also being slightly worse.

Table 7.2: Comparison of no calibration vs spectral calibration for SICOR over Algeria. Again it can be seen that spectral calibration does not result in a better retrieval, but with differences being small.

Calibration Settings	RMS [ppb]	Mean Concentration [ppb]	Chi squared
No calibration	117	1560	5.01
CW and FWHM	127	1598	5.08

From this, it can be concluded that the spectral calibration does not result in an improvement for methane retrieval, for both the matched filter and SIGOR. This is concluded because they do not result in an improvement in the metrics that determine the quality of the retrieval. The results are insufficient to show that spectral calibration will never work for methane retrieval using PRISMA, but further experiments are outside the scope of this project.

7.3. Comparison Between Methods

Both methods have been developed and optimized according to the approach set out in chapter 4. Both methods have a different approach to solving the problem at hand, retrieving methane concentrations from PRISMA measurements. The matched filter employs a statistic technique to retrieve 1000 pixel enhancements simultaneously. SICOR employs a pixel by pixel method by doing a full-physics inversion retrieval.

7.3.1. Metrics Comparison

From the analysis of the retrieved enhancements of the matched filter and SICOR, it could be seen that in general SICOR had higher enhancements in the plume mask and with more noise. In this section, the comparison will be made between the two methods with regard to all relevant metrics including maximum source enhancement, median plume enhancement, RMS and IME quantification. A selection of plumes were made, all of them located in the unaffected part of a PRISMA scene, except for one. They represent different types of sources from different regions and with different source rates. IME quantification was used, because it could be implemented automatically and consistently. Results are shown below:

Table 7.3: Comparison of important metrics for selected plumes for the original matched filter and SICOR. All values for max, median and RMS are in ppb and all quantifications in tons per hour. * indicates a plume that was located in the affected part of PRISMA with the fixed noise pattern. RMS has been calculated using the same spatial pixels for both methods.

Method	Matched Filter		SICOR		Matched Filter		SICOR	
	Max	Median	Max	Median	RMS	Q IME	RMS	Q IME
Turkmenistan 22	945	207	3252	367	149	28.5	356	38.5
China 6	1279	151	2438	202	110	7.5	320	9.6
Controlled 2	799	144	1386	177	113	3.6	303	3.8
Argentina 1	899	290	1820	441	123	10.8	375	13.9
China 2	987	222	1570	379	134	7.9	343	10.2
China 7	2167	441	5720	789	218	11.8	551	16.3
Algeria 5*	587	110	961	197	54	1.7	150	3.6
Turkmenistan 16	824	142	1630	319	72	3.2	226	3.7
Turkmenistan 17	590	132	1527	254	72	3.6	226	4.5
Libya 1	469	75	989	153	52	2.2	240	2.9
Iraq 1	571	116	862	153	82	5.8	245	5.1

From this table, it can be seen that the noise is higher for all SICOR retrievals, but also the maximum concentration in the plume mask. When looking at the distribution of maximum enhancements in the plume mask it becomes clear that there is more variation in the SICOR retrievals than for the matched filter. The median values of the

plume are much more similar, meaning that SICOR does not just scale all enhancements higher than those of the matched filter. This reinforces the property of SICOR that it is more flexible, also when taking the distribution of enhancements into account shown in Figure 7.5. When determining which method is better based on the metrics that were set out in chapter 4 the matched filter is in general better for plume detection, especially when taking into account that for some plumes no successful SICOR retrieval could be done, such as in Australia and for many plumes in Algeria, which were detectable using the matched filter.

7.3.2. Response to Artefacts and Noise

The two retrieval methods employ different techniques to retrieve methane enhancements and as such respond differently to surface features, one of which is landfills, which often cause artefacts for the matched filter, but less so for SICOR, as can be seen in Figure 7.3.

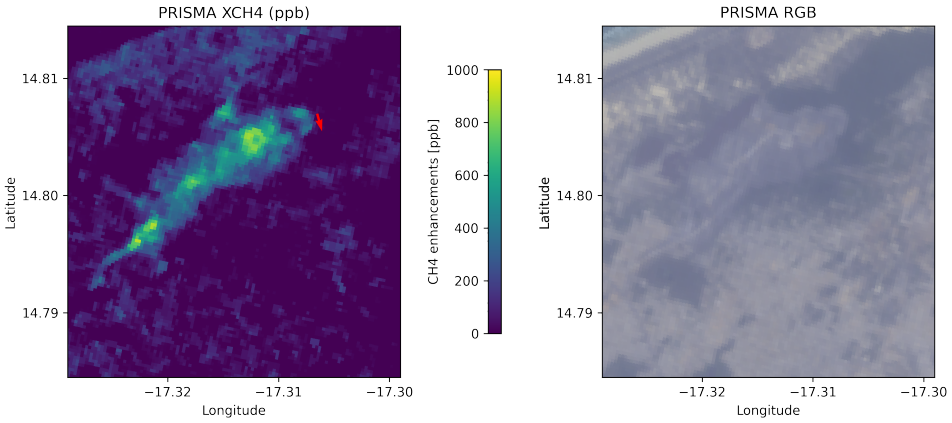

(a) Dhakar matched filter retrieval June 2021, with RGB

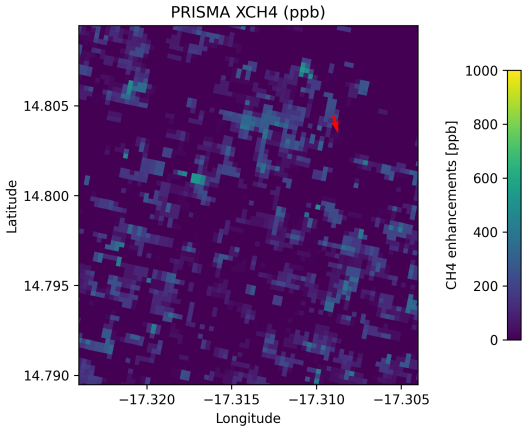

(b) Dhakar SICOR retrieval June 2021

Figure 7.3: Comparison of matched filter retrieval and a SICOR retrieval over a landfill in Dhakar. It can be clearly seen that the matched filter has a correlation with albedo, as it follows the shape of the landfill very closely, as seen in the RGB on the right, even though the wind is directed nearly perpendicular. While SICOR is not able to retrieve any methane emissions, it is not correlated with the albedo as much as the matched filter.

A major difference between SICOR and the matched filter is that the matched filter is largely able to filter out the radiance pattern that appears in the methane enhancements. This pattern is visible in the methane enhancements retrieved by in SICOR in a

part of the PRISMA scene. A possible explanation is that the matched filter is designed to suppress noise and uses multiple measurements (spatial pixels) simultaneously. In Figure 7.4 the same scene over Algeria is shown, where multiple plumes are present.

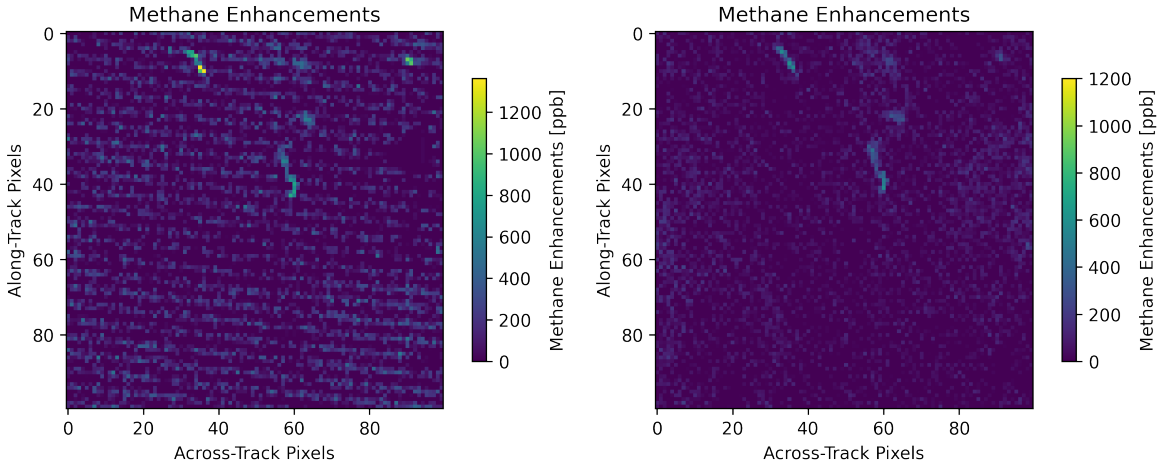

(a) SICOR methane retrieval over Algeria in August 2020

(b) Matched filter methane retrieval over Algeria in August 2020

Figure 7.4: Comparison between SICOR and matched filter of the pattern found in Algeria. It is immediately visible that SICOR is more affected by the radiance pattern than the matched filter.

The pattern is much less visible in the methane enhancements, but some regularity can be found in the matched filter methane enhancements, with a faint diagonal pattern being present. In SICOR however the methane pattern is nearly as strong as the emissions itself, severely affecting the capability of plume mask generation as the distinction between plume and pattern is hard to make by an algorithm.

With regard to visibility and plume detection, it varies per scene. The matched filter is the faster of the two methods, returning a retrieval for the entire PRISMA scene within a few minutes, something which will take more than 24 hours for SICOR. The speed of the matched filter allows for scanning the entire image, which is useful for scenes where the exact location of emissions is not known. For areas where plume detection is more difficult and a source location is already known it becomes more advantageous to use SICOR as it is less sensitive to changes in the surface albedo.

Both methods have their advantages and disadvantages and a combination of both results

7.3.3. Enhancements

From the previous sections, it became clear that there is a distinct difference between the matched filter and SICOR, as they do not show the same enhancements and are affected differently by the radiance pattern found in PRISMA data. To better analyze these differences the enhancements for four known plumes that were visible for both retrievals were plotted as a histogram to visualize the enhancement density of the plume:

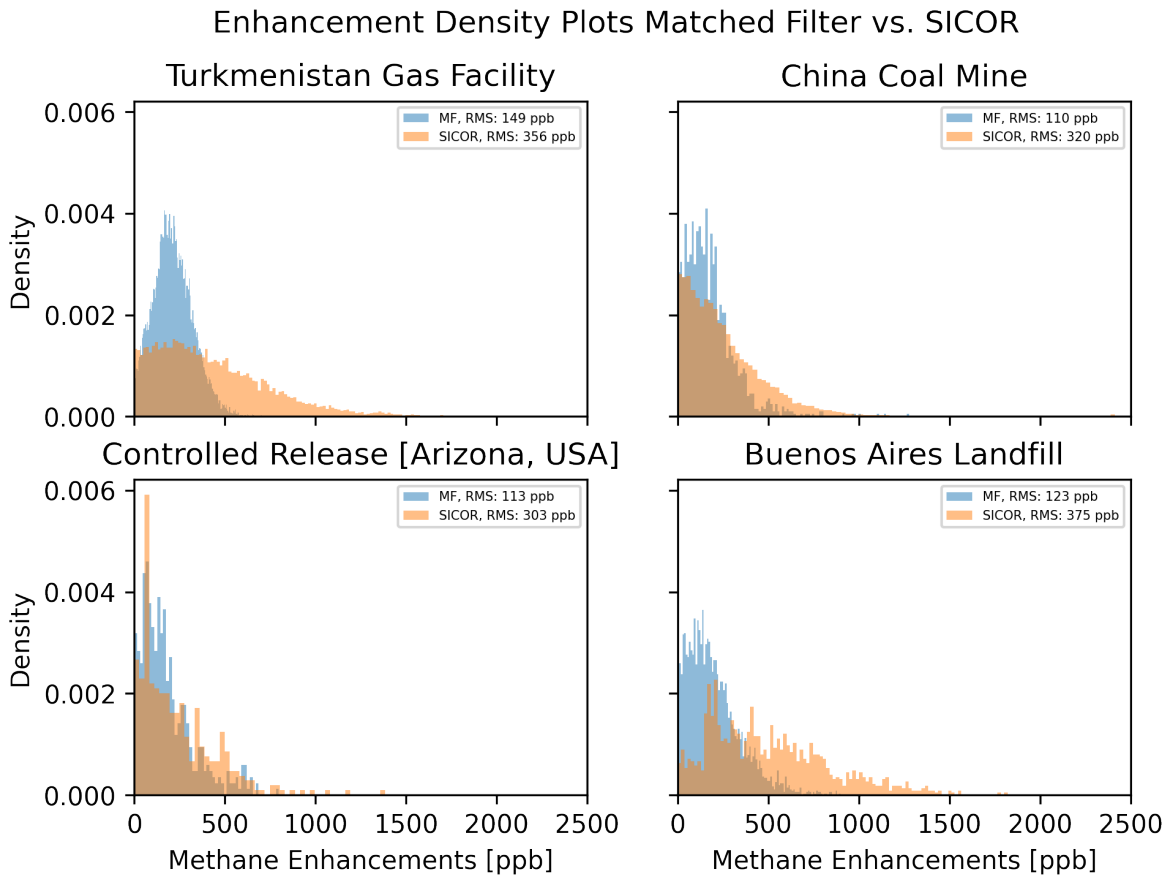

Figure 7.5: Comparison of histograms for matched filter and SICOR retrieved enhancements for four scenes that represent a different kind of methane emission sources. It is clear that the enhancements from SICOR are noisier, signified by the heavier tails of the distribution, but they are also different in distribution because the peak of the distribution does not always overlap with those of the matched filter. The Buenos Aires distribution is radically different, most probably because enhancements were less concentrated at a single source.

From the figure above it can be seen that the distribution of enhancements for the matched filter is very similar for all four scenes. They follow the same shape and seem to have their peaks at a few hundred ppb of enhancement. The SICOR distribution is different for each plume, with the Buenos Aires Landfill plume differing the most from the matched filter distribution. For the matched filter and SICOR a plume mask was created that looked similar in terms of shape but that was generated independently from each other. These differences between distributions show that SICOR has greater independence to fit the methane to the measurements than the matched filter, but that this also results in higher amounts of noise as the distributions have heavier tails.

A way to determine which method most accurately describes the enhancements within a plume is to compare the obtained retrieval results to that of a modelled plume. WRF is a Chemical Transport Model (CTM) that can model how trace gases disperse in a wind field and is often used to model plume emissions. Enhancements were obtained for a simulated plume and histograms were created for the distribution of these enhancements for 20 hours of emissions (intervals of 30 seconds).

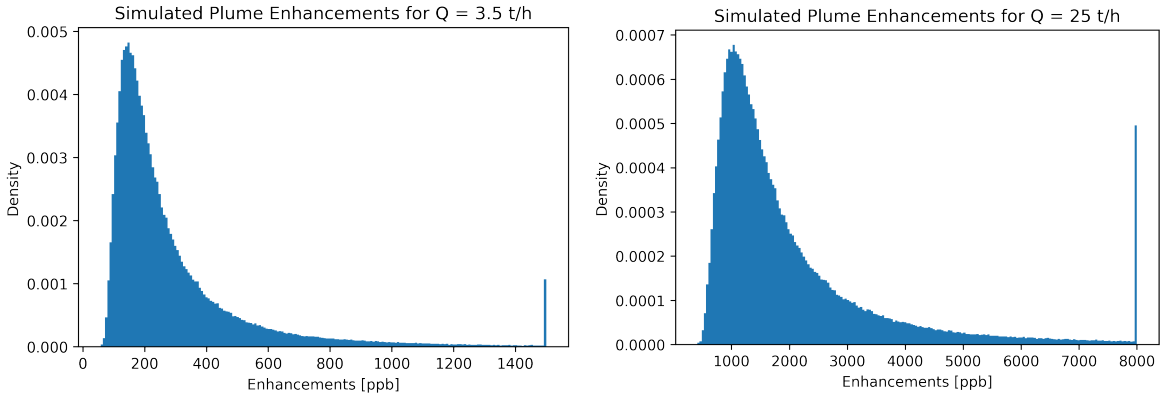

(a) (b)

Figure 7.6: Histograms of estimated plume enhancements for simulated plumes with a source emission rate of 3.5 t/h, corresponding to a smaller plume and that of a large plume with an emission rate of 25 t/h. Values above 1500 ppb for (a) and 8000 ppb (b) are shown in a single bin for visual purposes.

The distribution of these simulated plumes show heavier tails than those of the matched filter, but do not confirm to those retrieved by SICOR either. One thing that does change significantly is that centre of the density peak shifts towards higher enhancements with greater emissions. An interesting observation is that SICOR does show a higher density for large enhancements, which is more in line with the simulated results. It must be noted that these results are only taken for a few cases and that a conclusive answer to which retrieval method more closely resembles the actual density distribution of enhancements can only be given if more tests are done. The results do show however that the simulated distribution lies in between the two retrieval methods.

7.4. Application

The goal of this thesis project was to extend the capabilities of methane retrieval with PRISMA. To this end two methods were developed to verify which one was better: the matched filter and a PRISMA adapted version of SICOR. From the previous comparisons, it could be seen that the matched filter is less susceptible to noise than SICOR, but that SICOR has greater flexibility and estimates higher enhancements and quantification of emissions. How can these two models be used in the future for methane emission detections?

The matched filter excels in quick analysis of a scene since it can perform a retrieval within a few minutes. Because of its ability to keep noise low, it is ideal for plume mask generation, with a plume being more easily separable from background noise than with retrieved enhancements from SICOR. From experiments, it can be seen that SICOR retrieves higher enhancement and emission quantification estimates. Also for emissions over areas with strong correlations between albedo and methane, it is sometimes better to use SICOR as it allows for filtering of these high correlated areas.

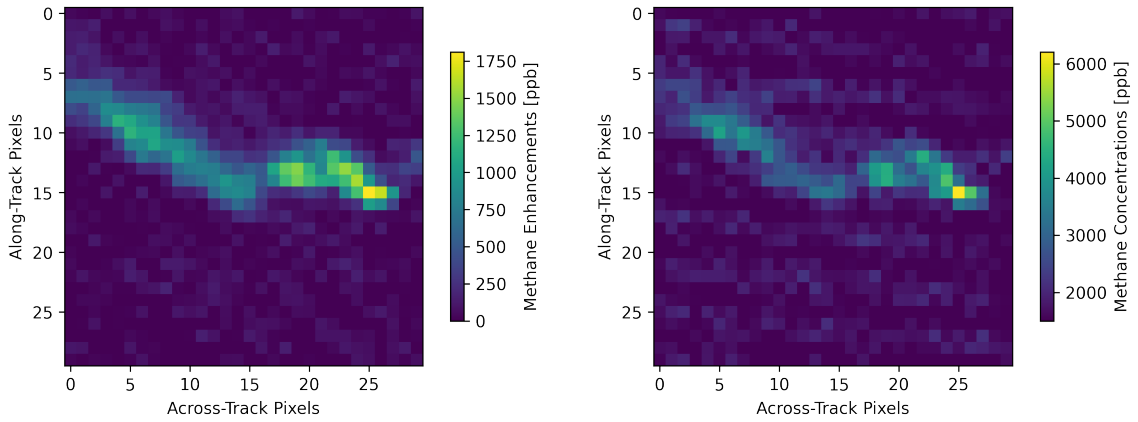

(a) Matched Filter Plume Mask.

(b) SICOR Plume Mask.

Figure 7.7: A comparison between the matched filter and SICOR for a scene in Turkmenistan (Turkmenistan 21), where the contrast between the two in the source is clearly visible.

In Figure 7.7 the difference between the two methods is clearly shown. SICOR clearly estimates that there is a single strong source, with methane concentration values being much lower in the tail. This is much less apparent in the matched filter retrieval, which reinforces the idea that it underestimates methane enhancements for strong sources. A combination between the matched filter and SICOR is can be most optimal, as the matched filter allows for a quick visualization and SICOR can provide a more accurate estimate of the source localization and source enhancement estimation. An example of this tandem configuration is shown in Figure 7.8 and Figure 7.9

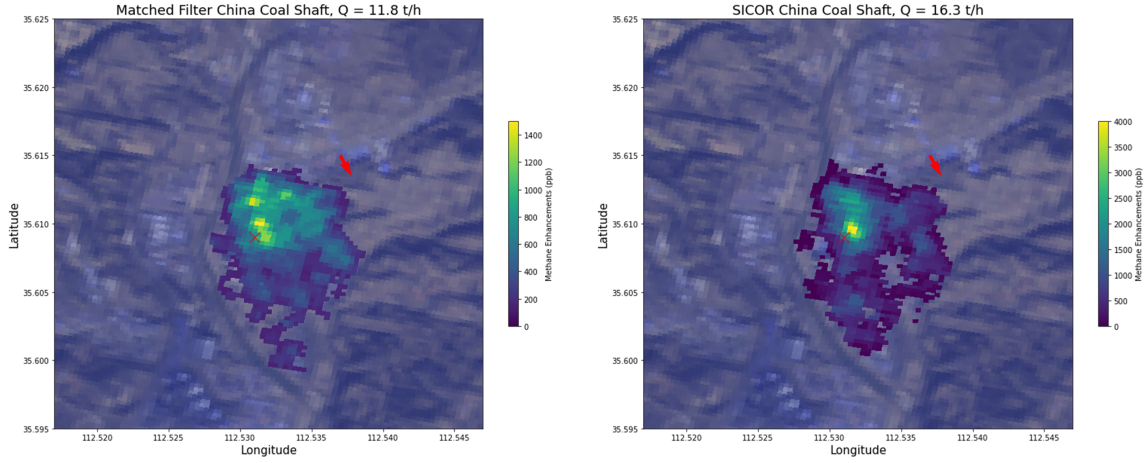

(a) Matched Filter Plume Mask.

(b) SICOR Plume Mask.

Figure 7.8: An example of how the matched filter and SICOR can be used together to locate a source. The matched filter was used to identify a plume mask, which showed spread out enhancements, SICOR was then used to show that there is a central source. Notice the difference in color scales, which shows the greater flexibility that SICOR has with fitting high enhancements to the measured data of PRISMA.

Figure 7.9: A Google maps image of a possible source, that shows a facility. The red circle indicates the location of this facility and the likely shaft where emissions originate from, which is indicated with a red cross in Figure 7.8

Here the scene was first analyzed with the matched filter, but no clear source could be spotted, but there was clear presence of a plume. The retrieval with SICOR showed that there was evidence that there was a single source and when looking at the location in Google Maps showed that there was a facility that could be the source. It must be noted that this approach is only possible if the data does not suffer too much from the radiance pattern as discussed earlier. Using the matched filter a wide variety of emissions have been detected, ranging from large gas emissions in Turkmenistan to concentrated emissions from landfills in Argentina. It helps to take into account where the expected emissions are coming from, for example using other sources to identify the location of a landfill. The presence of artefacts can make it difficult to identify emissions without any a priori information. Nevertheless, many detections have been made, both over locations that have already been known to be possible to detect with PRISMA, as well as new ones. An overview of the locations of all detected emissions is shown in Figure 7.10 and important statistics of all emissions can be found in Appendix A and Appendix B.

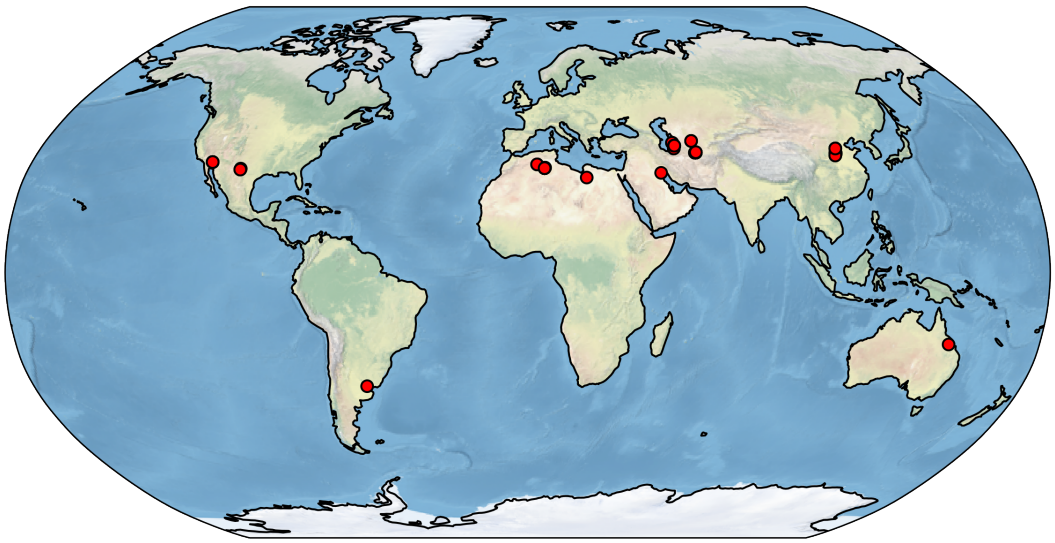

Figure 7.10: Overview of methane emissions spotted using the current setup with PRISMA. The red dots indicate a single detection, with some locations having more than one detected emission.

These results have shown that both methods have promise and there are other leads that might improve the capabilities of PRISMA. When comparing PRISMA again to the other satellites that monitor methane there is a clear difference in that PRISMA is more dependent on what type of scene it can observe. Because the radiance measurements are taken with a lower spectral resolution it is only able to detect very concentrated emissions from regions where more artefacts are present due to surface features. It is however important to remember that PRISMA was not designed for these capabilities, but that together with other methane observing satellites such as Sentinel-5P, Sentinel-2 and the GHGSat constellation, PRISMA can help to map methane emissions and to provide a framework with which climate mitigation can be planned.

7.5. K-means Clustering and Sparsity Prior Extension

Currently a problem in both retrieval methods is the presence of large albedo changes over the spectrum that is used for retrieval. These albedo changes are not uniform over the entire scene as each surface type (vegetation, rock, buildings) are different. SICOR can fit an albedo profile for each individual pixel, but this is not always sufficient and the matched filter does not incorporate any albedo profile in its retrieval. Hyperspectral imagers however are very effective at surface classification and this information could be used to better incorporate information about the type of surface that PRISMA is measuring for retrievals.

K-means clustering is an unsupervised classification algorithm, that can be used to group hyperspectral data into similar clusters [56]. It does this by starting with a set of points within the hyperspectral data (starting clusters) and tries to group the hyperspectral data around these clusters so that the sum of squares within each square is minimized. It was used to cluster spatial pixels together based on radiance data from 1100-2100 nm. The assumption is that the albedo profile can be estimated by grouping pixels that have a similar radiance spectrum. This can then be used to calculate what the absorption is for each individual pixel based on their cluster albedo profile. This absorption was used for the matched filter instead of calculating the mean spectrum of each along-track data column. A test was run over a location in Turkmenistan with a lot of albedo artefacts, caused by the presence of dunes, shown in Figure 7.11

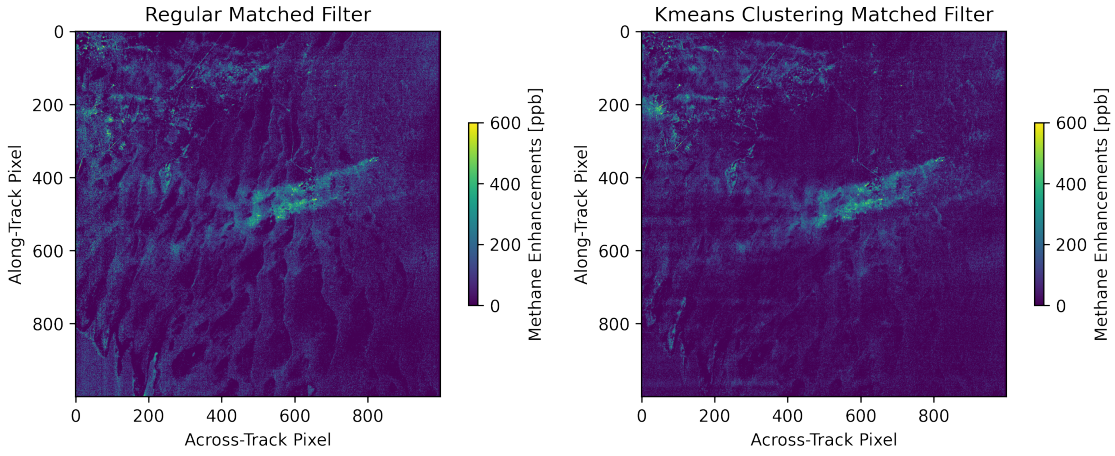

(a) RMS 95 ppb

(b) RMS 76 ppb

Figure 7.11: Example of the K-means Clustering Matched Filter on the right, with the original matched filter implementation shown on the left.

From this result it can be seen that correcting for specific albedo profiles can result in a better retrieval. The current method allows for large artefacts, such as the presence of sand dunes to be corrected, with more advanced methods roads and buildings might also be detected and their specific albedo spectra corrected for. SICOR might also benefit from this clustering approach, but the current implementation of SICOR does not allow for an input albedo spectrum. Adapting SICOR to include an apriori estimate for albedo would most likely be an effective addition to the model. A last extension to this clustering is applying a sparsity prior to the methane enhancements [13]. This limits the allowed enhancements by penalizing the total enhancements by making use of a l1 term. This method was implemented earlier in the process but a downside of the method is that it cannot distinguish between artefacts and methane emissions and can therefore also remove significant parts of a methane plume. By applying a K-means clustering step in between many artefacts are already removed, thereby negating the risk of removing methane emissions significantly. A comparison is made between the matched filter, the k-means clustered matched filter and the k-means clustered sparsity prior (MAG1C) matched filter in Figure 7.12.

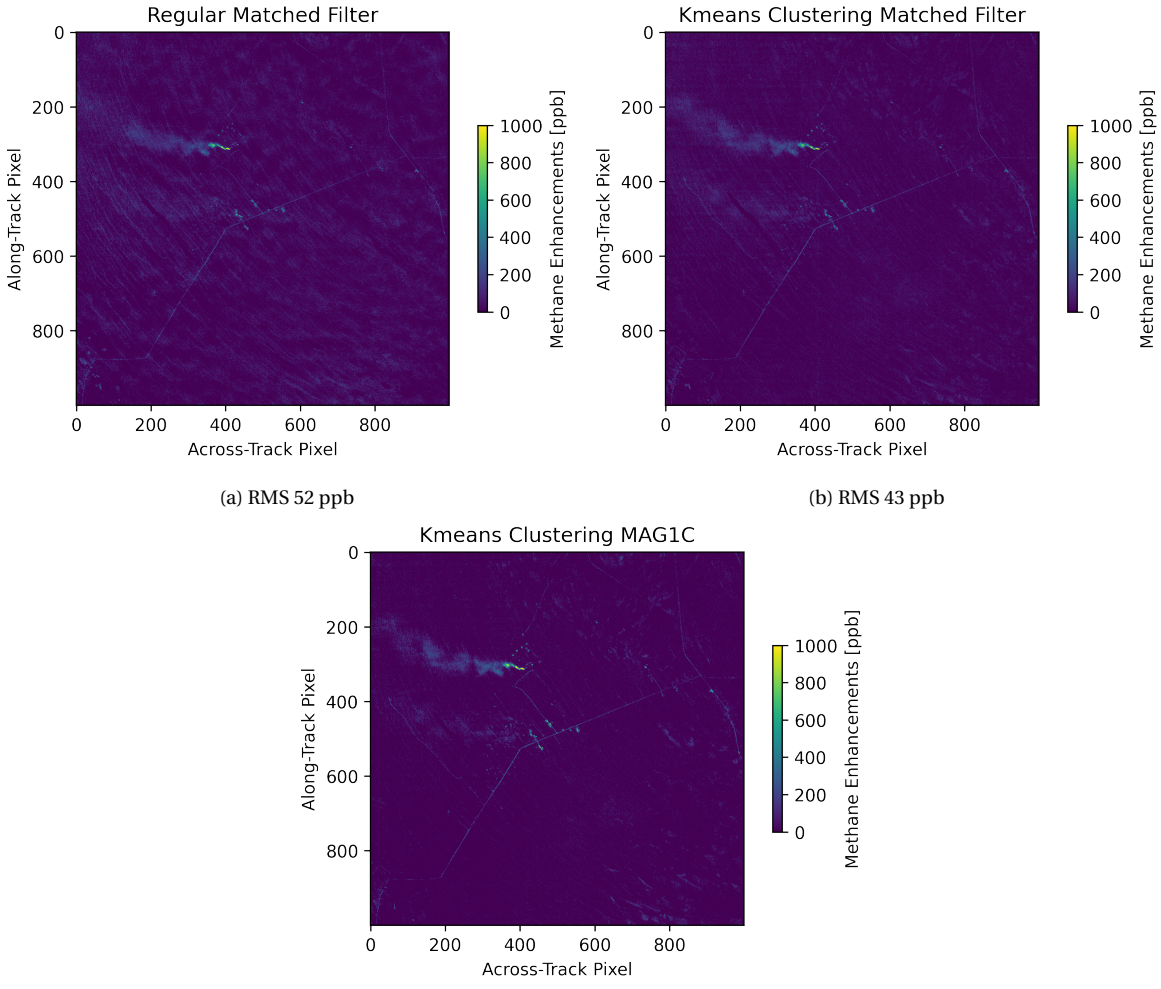

(a) RMS 52 ppb

(b) RMS 43 ppb

(c) RMS 40 ppb

Figure 7.12: Overview of successive improvements in removing noise and isolating plume enhancements over Turkmenistan, using the same plume that was used in Figure 5.9 and Figure 7.7. It can be seen that by applying the Kmeans clustering, some albedo artefacts can be removed by calculating cluster specific means for the matched filter algorithm. By applying the MAG1C algorithm the results can be improved even more [13].

Also important is to look at what the sparsity prior allows to do further. One of the steps that is necessary to make the sparsity prior work is to re-estimate the covariance successively. For all three methods shown in Figure 7.12, the enhancements have been shown, similar to Figure 5.9, to show the effect of this successive covariance estimation, the results of which are shown in Figure 7.13:

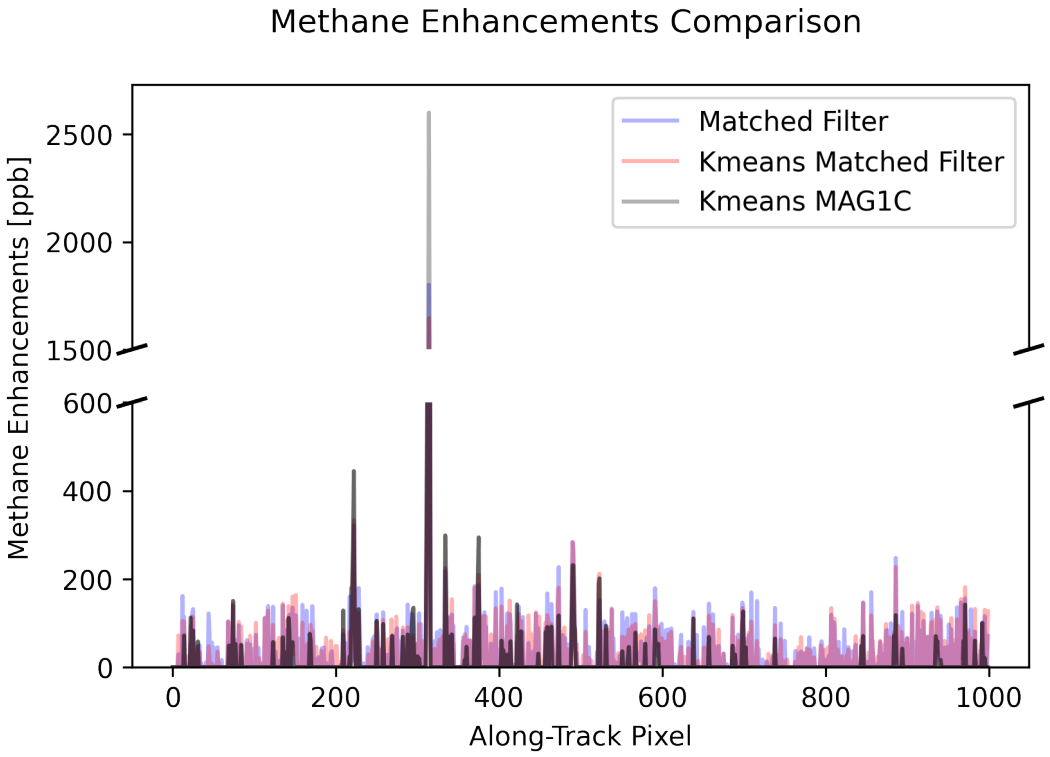

Figure 7.13: Comparison of enhancements for across-track detector-column 589. It can be seen that the k-means matched filter improves over the matched filter in terms of noise, but that it has a slightly lower maximum enhancement and the k-means MAG1C improves over both of them, with lower noise and a higher maximum enhancement.

From these results it is clear that the k-means matched filter improves over the matched filter in terms of noise (RMS), but that it also estimates the highest enhancement (likely source) slightly lower. The k-means MAG1C matched filter improves over both of them in terms of noise (RMS) and the maximum enhancement, which comes close to the maximum enhancement retrieved with the high enhancement covariance matched filter experiment. However it is also visible that MAG1C cannot make a distinction between artefacts and methane, as the enhancements around along-track pixel 200 are higher than the other two methods.

7.6. Conclusion

This chapter started with an analysis into pre-processing techniques such as hyperspectral denoising and spectral calibration. These were tested to estimate their effectiveness in improving the quality of a methane retrieval using PRISMA. Hyperspectral denoising using NAILRMA was found to be effective in reducing the noise found in retrieval, more so for SICOR than for the matched filter, but it also decreased the average enhancement in a plume mask. The overall net effect (plume enhancement vs. noise) is positive. Hyperspectral denoising might be useful for generating more accurate plume masks. Spectral calibration was found to be less useful, with the spectral calibration resulting in a slightly worse fit, with higher noise for SICOR and a reduced plume to noise ratio for the matched filter.

In this chapter a comparison was made between the two developed retrieval methods, the matched filter and the PRISMA adapted version of SICOR. In this comparison, it could be seen that the two models responded differently to various types of scenes, with the matched filter being more stable when faced with noisy data and SICOR being less sensitive to some of the albedo artefacts that have been present in matched filter methane retrievals. With the current setup the matched filter beats SICOR in terms of plume detection performance, as it is significantly faster and easier to use and provides better SNR and is able to detect plumes that SICOR is not. A deeper analysis was made concerning how the distributions of enhancements within plumes compare between the two methods. It was found that the matched filter has very similar distributions for different types of sources, while SICOR has a distribution that depends more on the type of emission. This reinforces the hypothesis that SICOR is more flexible than the matched filter. When comparing these distributions, both show characteristics of a simulated distribution, but neither matches perfectly.

With regard to quantifications and the quality metrics, it was seen that SICOR estimates higher source rates for the detected plumes. It suffers from higher noise in its enhancement estimates, but it has greater flexibility. This can mainly be seen in the fact that it can estimate the source pixel enhancements with greater independence, depending on the source type. The matched filter consistently estimates the source enhancement around 1000-1500 ppb, with only the strongest sources exceeding these enhancements. The rest of the plume masks, as shown with the median enhancement value of the plume mask differ much less from the matched filter.

A combination of the two retrieval methods can be useful, for the application of detection and quantification of methane emissions using PRISMA. This is because SICOR is better equiped to detect high methane enhancements, which can lead to a source, whereas the matched filter can be used to detect the general outline of the plume. Using the matched filter emissions have been found in several countries.

A final extension to the retrieval using PRISMA was made by utilizing an unsupervised classification algorithm, called k-means clustering to group spatial pixels together. This way an albedo corrected matched filter could be created, that together with a sparsity prior is able to significantly reduce noise and artefacts and also able to detect source enhancements with a magnitude comparable to results obtained with the covariance experiment from chapter 5.

8

Conclusion and Future Work

Conclusion

The main research question for this thesis as discussed in section 3.3 is:

> **"Does a full inversion of a radiative transfer model improve over the matched filter for methane retrievals using hyperspectral PRISMA data and for what other tracers can it be used?"**

It can be concluded from this research, the obtained results and the analysis done that the full inversion of a radiative transfer model can improve over the matched filter concerning retrieval flexibility, but that the matched filter remains better in plume detection and noise mitigation, according to the designed metrics. The matched filter can be used for other tracers such as carbon dioxide, but carbon monoxide remains too challenging to detect with PRISMA, for both the matched filter as well as a full inversion retrieval. The various sub-questions, that helped in answering the main research questions will be answered below:

A literature study was done on the properties of methane in the atmosphere and the problems that it is causing to the climate through radiative forcing. Significant sources of methane emissions are concentrated super-emitters, due to oil and gas exploitations. Monitoring methane from space is an effective way of spotting point-source emissions, which can be done using the hyperspectral imager PRISMA. Currently PRISMA is limited in viewing primarily strong emitting sources over heterogeneous scenes. That is why two retrieval methods were analyzed, the matched filter, which was the original method used for PRISMA methane retrievals and a full inversion retrieval method, based on SICOR, the operational algorithm in use for TROPOMI carbon monoxide retrievals. The reason that this comparison will be made is that the full inversion retrieval method should have more flexibility than the matched filter and might improve over the matched filter in some regards.

To answer the research question a good approach was necessary with which to design a framework that could consistently assess the quality of a retrieval. A pipeline was created that could handle the PRISMA hyperspectral data, perform pre-processing steps, execute the retrieval and calculate important metrics. Currently, PRISMA methane retrievals are limited over heterogeneous areas to only the largest emissions as the high noise prohibits small sources from being visible. That is why the focus of the research is

on lowering the noise and to try and make small sources more visible. Estimations for noise and the SNR have been found by focusing on the RMS of enhancements.

The matched filter was the first retrieval method employed for methane retrievals using PRISMA. It works by correlating the radiance measurements to a reference methane signal. With it, methane emissions can be detected from various types of sources. Plume mask dilation methods have been used to separate methane plumes from background noise and to quantify the source rate of emissions. Two methods for emission quantification were implemented and tested. A limitation of the matched filter is that it uses a linearized reference signal for methane absorption, which in reality behaves in a non-linear way. Two adaptations were made to the original method of the matched filter, by adapting an iterative matched filter and pixel iterative matched filter, in increasing order of flexibility. These showed that increasing flexibility can improve the original matched filter, but not significantly so that new sources can be detected. From tests done that use different bands for PRISMA retrievals, it was found that the original band of 2110-2450 nm was the best suited for retrievals, based on the measure for noise and stability of the retrieval. Quantification estimates for known emission scenes were in line to those found in literature. When comparing results to another methane monitoring satellite, Sentinel-2, retrieved quantification estimates are similar, albeit slightly lower for PRISMA for several observations over Algeria. An analysis was done to the matched filter as a least-squares estimator, which can cause high enhancement pixels to be underestimated. By changing the way the covariance was taken into account in the matched filter it was shown that this might be indeed the case, giving extra reason to find out what a full inversion of a radiative transfer model will do to PRISMA enhancements. When testing other trace gases it was shown that carbon monoxide is too difficult to retrieve with the matched filter, because the absorption is too faint with the spectral resolution of PRISMA, but that carbon dioxide is possible to retrieve with the matched filter, detecting several plumes over a power plant.

For a full inversion model, SICOR was used, which is the operational algorithm for carbon monoxide retrieval using TROPOMI data. It includes a step which also retrieves methane. In order to make it compatible with PRISMA the settings and input files were changed. Most importantly the ISRF was simulated using a Gaussian Spectral Response Function (SRF), along with LUTs that were needed for the radiative transfer model. Tests were done to determine the optimal settings for SICOR and it was found that these settings should not be equal for all types of scenes. With the adapted SICOR methane emissions could be retrieved for similar scenes as the matched filter. It was discovered that PRISMA suffers from fixed pattern noise, which is especially problematic for SICOR, with it being most likely caused due to electronic issues, that might stem from a high frame rate. From emission quantification tests it was concluded that concentration and emission quantification estimates were higher than those of the matched filter, but still comparable to results found in literature. Tests done for other trace gases delivered similar results, with carbon monoxide being too difficult to retrieve with PRISMA with current methods.

When comparing the two retrieval methods it became clear that the matched filter has lower values for noise than the retrieval done with SICOR, but that SICOR does allow for more flexibility. When comparing the enhancement estimates for likely sources of emissions SICOR, shows the ability to fit maximum enhancements more freely, depending on the magnitude and concentration of the source. This also results in slightly higher emission quantification estimates. Hyperspectral denoising can be used as a preprocessing step, removing noise from the measurements, which was shown for both re-

trieval methods, but it does decrease the average enhancement retrieved in a plume. Spectral calibration did not help with retrievals, for both methods.

In the end, both models have their own strengths, with the matched filter being a fast retrieval method that is excellent for noise suppression. It does lack however flexibility in estimating the enhancements for measurements where emissions do appear. That is why a combination of the two methods is likely the best approach, with the matched filter being useful as a plume identification and plume mask generation step, methods such as hyperspectral denoising can help with this. SICOR can then be used to determine the source concentrations and help in estimating the emission source rate. As a last extension the possibility of using k-means clustering to group pixels together in an effort to perform albedo corrections was explored. This showed that albedo artefacts can be removed by using the hyperspectral image to classify data. This albedo correction allowed a sparsity prior to be used, which can give the matched filter more flexibility to estimate high enhancement sources more accurately.

Recommendations for Further Research

Several opportunities for improvements were identified while working on this thesis, which are listed below:

- It was identified in chapter 5 that the matched filter suffers from source enhancement underestimation. This is because the matched filter is a least-squares estimator and is designed to minimize noise. As shown if the covariance estimation changes so do the retrieved enhancements. The sparsity prior proposed in the algorithm MAG1C is a way of fixing this, but this might be too restrictive as it forces enhancements to zero. Another approach might be to use a weighted least squares approach, which can correct for heterogeneity in the dataset, but the matched filter would need to be rewritten for this.
- As seen in both retrievals, PRISMA suffers from albedo artefacts. Differences in the surface reflectance over a spectrum are picked up by the retrieval algorithms as methane. The matched filter does not have a way of correcting for this and SICOR tries to estimate it by including albedo as in its state vector. Unfortunately, SICOR still suffers from albedo artefacts. Having information about the surface reflection spectrum can help correct these artefacts. PRISMA is a hyperspectral imager and is often used for surface classification, which if coupled with a spectral library could allow for correcting the data. This is currently explored by using an unsupervised classification algorithm to group pixels together and infer a rough spectral profile of each group. It would be even better to couple a trained classification algorithm, such as a Support Vector Classifier (SVC) to couple spatial pixels to a spectra library, so that more accurate albedo corrections can be done, for both the matched filter as well as SICOR.
- Increasing the number of pixels to be simultaneously used in the SICOR retrieval can help to reduce the noise found currently in the retrieval. The spatial resolution of PRISMA is high enough that there is a high correlation between spatial pixels concerning surfaces and albedo profiles. This can be achieved by extending the state vector to include the states of multiple pixels, but the code for the retrieval would have to be rewritten.
- The emission quantification of PRISMA for the matched filter currently estimates lower than results obtained with Sentinel-2 and the controlled release experiments.

Performing additional experiments and verifying that the effective wind speed is properly calibrated can help in asserting that the quantification estimates are consistent.

- The fixed radiance pattern is currently partially removed by applying a 2D Fast Fourier Transform over the data. Later it was discovered that the pattern is different for all the eight parts of the data. It is recommended to perform the FFT separately for all parts of the data to improve the performance.
- Currently only the fixed pattern noise was addressed in the instrument analysis of PRISMA, but there are more sources of noise that affect the measurements. It would be helpful to receive measurements of complete darkness (used for calibration) and images of the Internal Calibration Unit (ICU) to determine what sources of noise are most problematic. This way a bottum-up analysis can be done to verify if the required SNR is met by the design [29]. Other factors to think about is the effect of polarization of light within PRISMA and straylight, which can decrease the image contrast.

A

Plume Overview

A.1. Algeria

Table A.1: Overview of retrieved plumes in Algeria.

Plume Title	Date	Lat	Lon	Max [ppb]	Median [ppb]	RMS [ppb]	Q [t/h]
Algeria 1	22/06/2021	31.778	5.997	650	130	43	1.6±0.6
Algeria 2	22/06/2021	31.769	6.003	654	95	43	1.8±0.7
Algeria 3	19/08/2021	31.77	6.006	786	109	50	4.2±1.5
Algeria 4	19/08/2021	31.78	5.998	509	84	50	1.6±0.6
Algeria 5	30/08/2020	31.769	6.002	577	113	42	1.7±0.7
Algeria 6	09/07/2021	31.77	6.001	954	191	46	4.4±1.7
Algeria 7	21/07/2021	31.779	5.995	596	103	47	3.9±1.5
Algeria 8	07/08/2021	31.78	5.996	407	105	43	1.4±0.6
Algeria 9	08/04/2020	32.841	3.244	934	116	40	2.8±1.1
Algeria 10	31/08/2021	32.843	3.242	308	113	44	2.0±0.9
Algeria 11	19/08/2021	31.807	6.157	374	89	50	1.9±0.7
Algeria 12	19/08/2021	31.807	6.144	485	102	50	1.5±0.5
Algeria 13	07/08/2021	31.771	6.003	465	78	43	3.7±1.5

A.2. China

Table A.2: Overview of retrieved plumes in China.

Plume Title	Date	Lat	Lon	Max [ppb]	Median [ppb]	RMS [ppb]	Q [t/h]
China 1	06/02/2021	36.247	112.99	1670	165	93	6.1±2.4
China 2	06/02/2021	36.258	112.923	985	228	93	9.6±3.8
China 3	06/02/2021	35.619	112.61	1371	216	111	9.1±3.6
China 4	28/04/2020	37.742	113.683	830	177	103	3.6±1.4
China 5	30/03/2021	36.172	112.984	759	150	105	1.7±0.5
China 6	06/02/2021	36.233	112.947	1273	153	93	7.9±3.2
China 7	22/12/2021	35.609	112.532	2167	340	138	11.8±4.2
China 8	28/04/2020	37.744	113.551	1260	153	103	4.4±1.7
China 9	28/04/2020	37.735	113.679	901	246	103	9.4±3.5

A.3. Controlled Release Experiments

Table A.3: Overview of retrieved plumes from the controlled release experiments by Stanford.

Plume Title	Date	Lat	Lon	Max [ppb]	Median [ppb]	RMS [ppb]	Q [t/h]
Controlled Release 1	21/10/2021	33.63	-114.49	794	143	113	3.5±1.6
Controlled Release 2	27/10/2021	33.63	-114.489	900	195	121	4.5±2.5
Controlled Release 3	16/10/2021	33.626	-114.489	596	123	113	1.8±0.7

A.4. Permian

Table A.4: Overview of retrieved plumes over the Permian in Texas, USA.

Plume Title	Date	Lat	Lon	Max [ppb]	Median [ppb]	RMS [ppb]	Q [t/h]
Permian 1	06/03/2021	31.527	-103.478	681	117	62	2.7±1.0
Permian 2	06/03/2021	31.353	-103.684	1321	246	61	4.5±1.7
Permian 3	06/03/2021	31.348	-103.668	840	191	61	2.4±0.9

A.5. Turkmenistan

Table A.5: Overview of retrieved plumes in Turkmenistan.

Plume Title	Date	Lat	Lon	Max [ppb]	Median [ppb]	RMS [ppb]	Q [t/h]
Turkmenistan 1	22/06/2020	38.558	54.21	710	83	48	7.0±3.1
Turkmenistan 2	22/06/2020	38.507	54.201	638	104	48	3.8±1.7
Turkmenistan 3	22/06/2020	38.493	54.2	778	85	48	6.4±2.8
Turkmenistan 4	31/07/2021	36.412	61.478	597	91	36	3.2±1.3
Turkmenistan 5	31/07/2021	36.485	61.637	525	84	36	2.9±1.2
Turkmenistan 6	31/07/2021	36.478	61.625	801	80	36	3.7±1.5
Turkmenistan 7	31/07/2021	36.49	61.623	826	77	36	2.1±0.9
Turkmenistan 8	31/07/2021	36.607	61.679	570	81	36	3.3±1.4
Turkmenistan 9	11/08/2021	36.477	61.427	811	111	44	1.9±0.7
Turkmenistan 10	11/08/2021	36.47	61.433	472	95	44	1.5±0.6
Turkmenistan 11	11/08/2021	36.474	61.457	802	115	44	2.5±0.9
Turkmenistan 12	11/08/2021	36.427	61.477	474	74	44	1.6±0.6
Turkmenistan 13	11/08/2021	36.369	61.556	648	129	44	2.7±1.0
Turkmenistan 14	19/04/2020	38.557	54.204	1247	81	50	6.5±1.3
Turkmenistan 15	13/02/2021	40.051	61.042	723	52	36	3.6±1.3
Turkmenistan 16	13/02/2021	40.025	61.054	820	46	36	5.3±1.5
Turkmenistan 17	13/02/2021	40.013	60.934	590	132	36	3.6±1.2
Turkmenistan 18	31/07/2021	36.472	61.462	673	97	36	5.5±2.3
Turkmenistan 19	21/09/2021	36.612	61.675	880	40	32	8.4±3.0
Turkmenistan 20	03/07/2020	38.556	54.198	1320	101	46	8.1±3.3
Turkmenistan 21	21/07/2020	38.558	54.202	1809	109	52	16.0±5.9
Turkmenistan 22	23/01/2021	39.368	53.744	949	207	95	28.5±9.0
Turkmenistan 23	19/12/2021	37.771	53.917	1653	312	82	10.2±2.2
Turkmenistan 24	19/12/2021	37.763	53.966	590	216	82	4.4±1.0
Turkmenistan 25	23/01/2021	39.498	53.637	628	176	95	3.1±1.1
Turkmenistan 26	23/01/2021	39.464	53.625	747	175	95	5.9±2.0
Turkmenistan 27	27/03/2022	38.558	54.2	1713	110	60	9.1±2.9
Turkmenistan 28	27/03/2022	38.499	54.2	1651	167	60	14.1±4.5

A.6. Miscellaneous

Table A.6: Overview of retrieved plumes from various single locations.

Plume Title	Date	Lat	Lon	Max [ppb]	Median [ppb]	RMS [ppb]	Q [t/h]
Australia 1	19/07/2021	-21.887	147.996	1299	243	115	3.1±1.1
Libya 1	07/01/2022	28.912	20.963	469	75	29	2.2±0.7
Iraq 1	14/08/2021	30.27	47.748	571	116	60	5.8±2.4
Argentina 1	11/01/2022	-34.524	-58.62	919	296	120	10.3±3.7

B

Plume Masks

Overview of plume masks from plumes from Appendix A.

B.1. Algeria

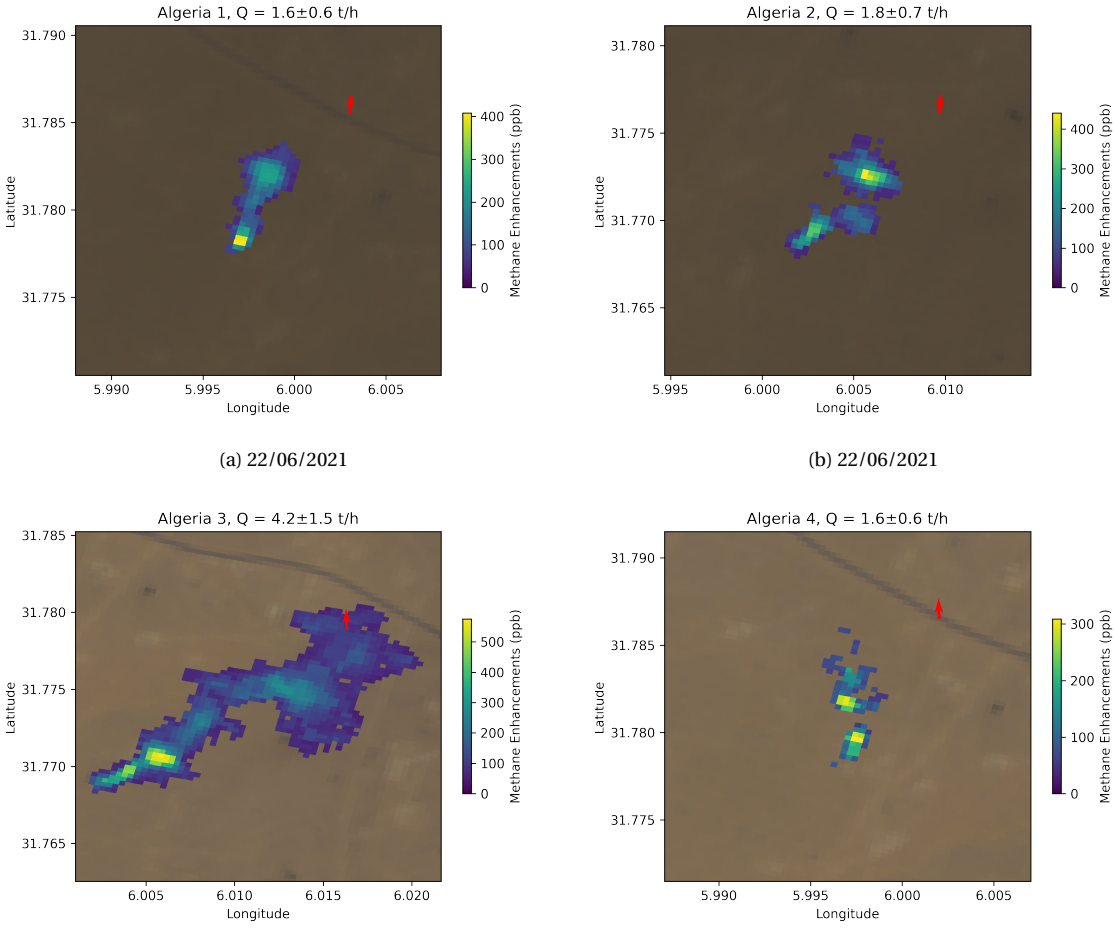

(a) 22/06/2021

(b) 22/06/2021

(c) 19/08/2021

(d) 19/08/2021

Figure B.1

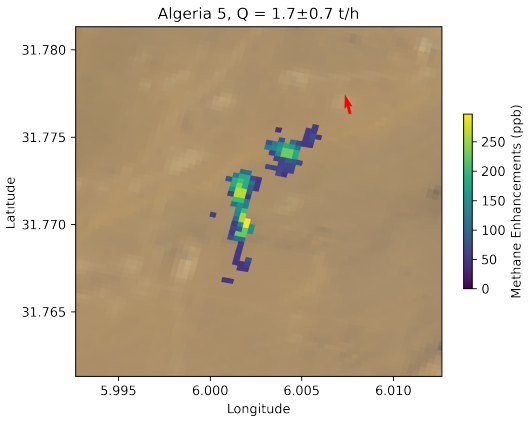

(a) 30/08/2020

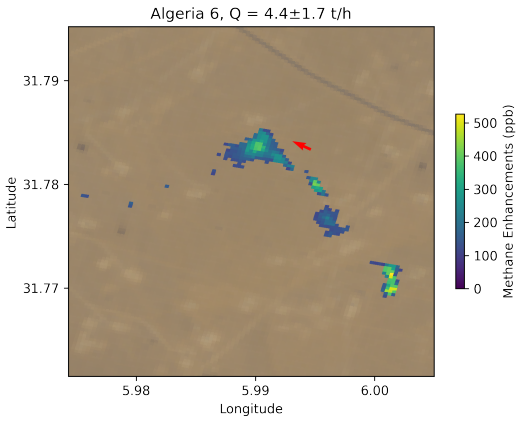

(b) 09/07/2021

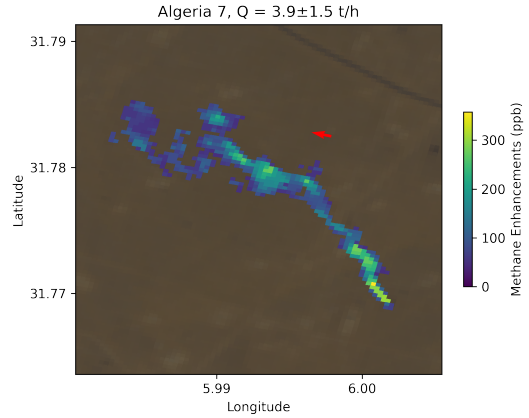

(c) 21/07/2021

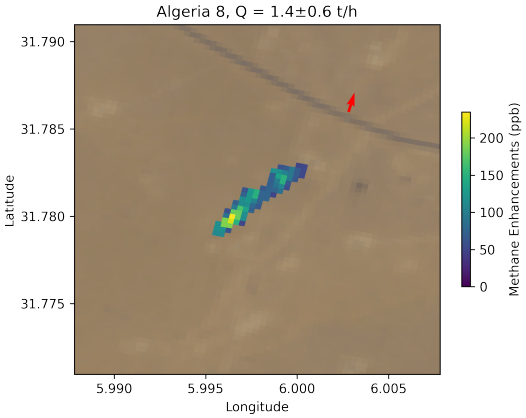

(d) 07/08/2021

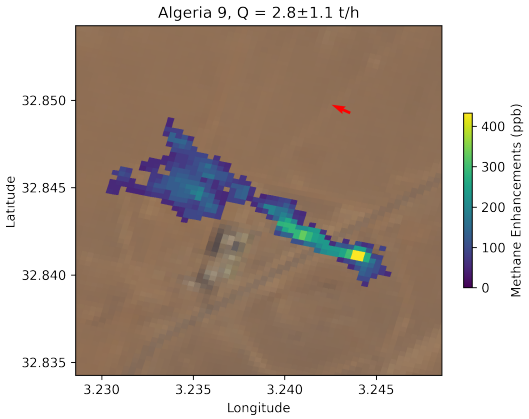

(e) 08/04/2020

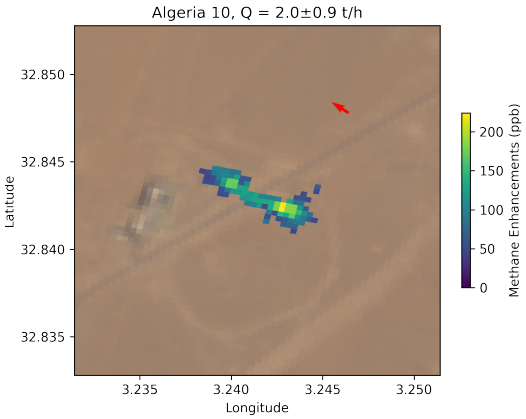

(f) 31/08/2021

Figure B.2

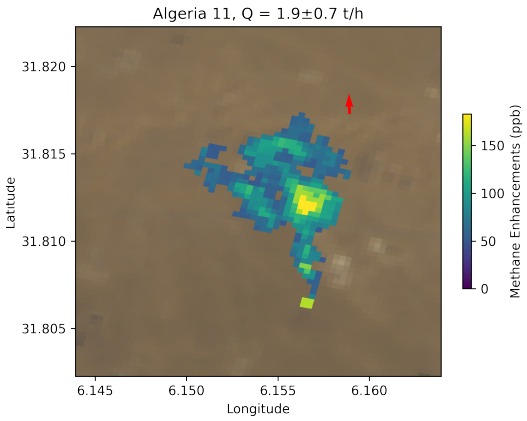

(a) 19/08/2021

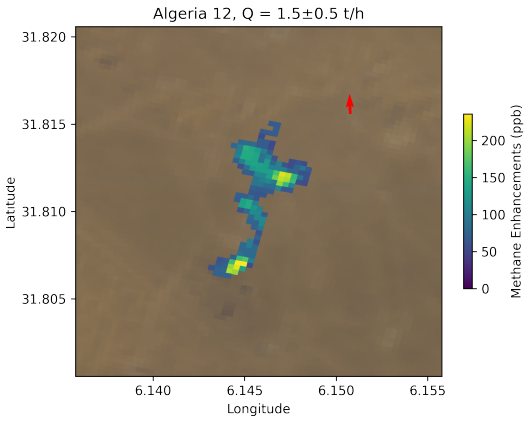

(b) 19/08/2021

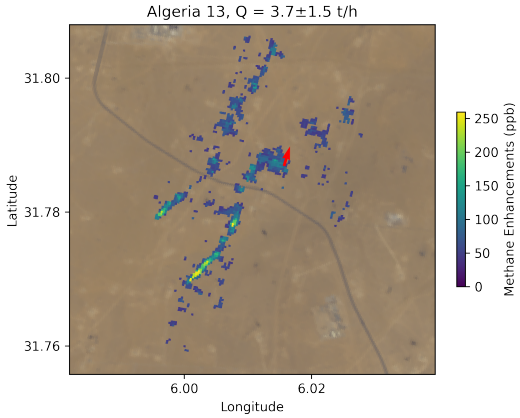

(c) 07/08/2021

Figure B.3

B.2. China

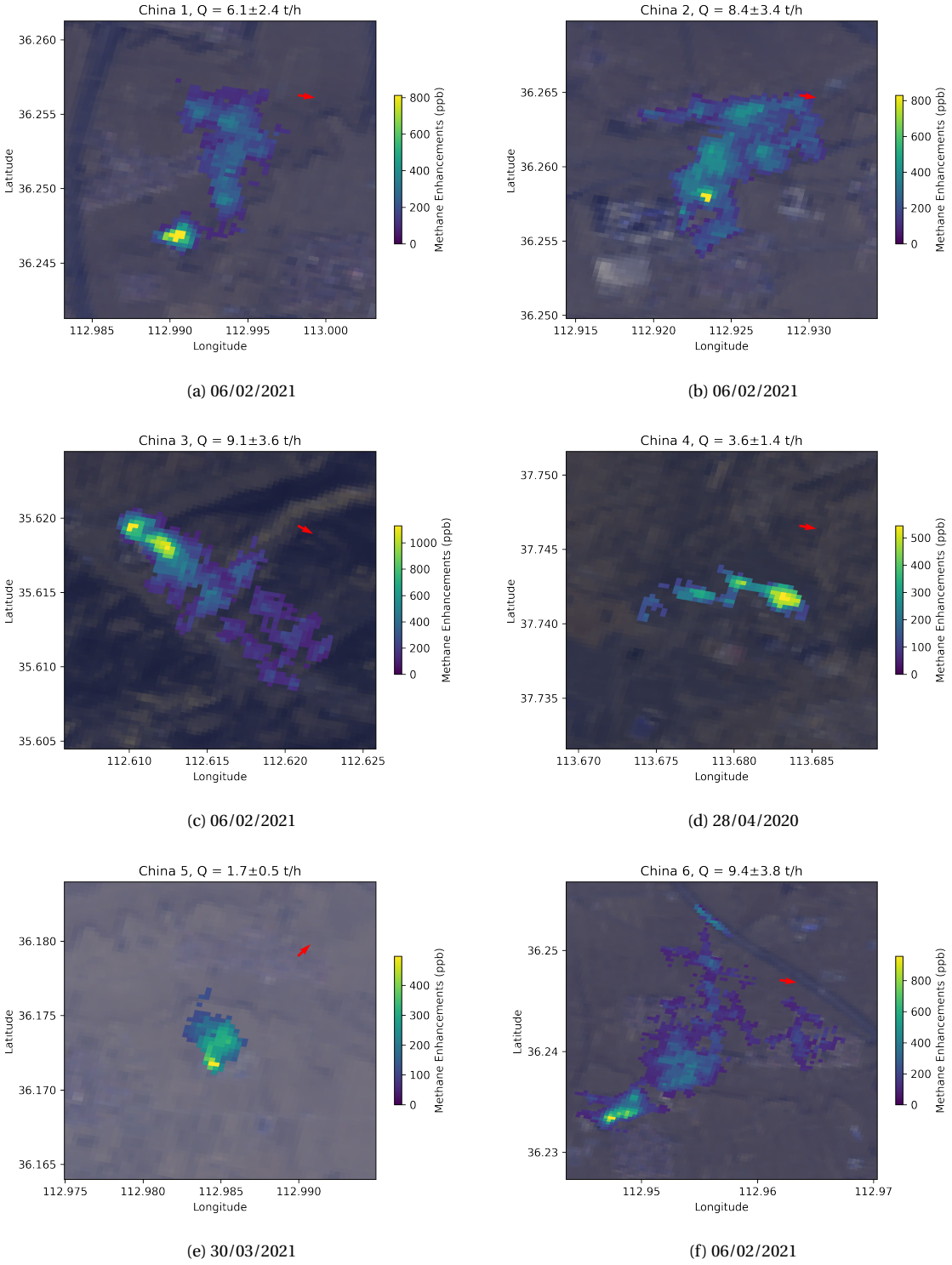

(a) 06/02/2021

(b) 06/02/2021

(c) 06/02/2021

(d) 28/04/2020

(e) 30/03/2021

(f) 06/02/2021

Figure B.4

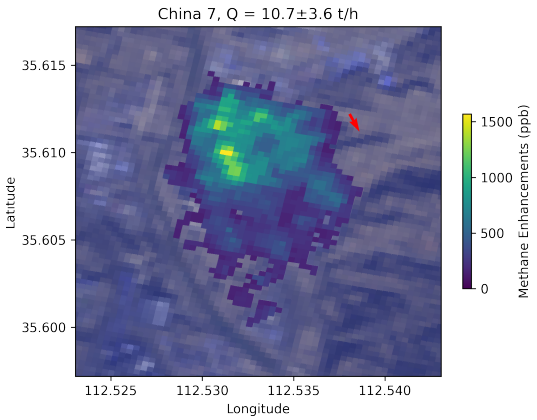

(a) 22/12/2021

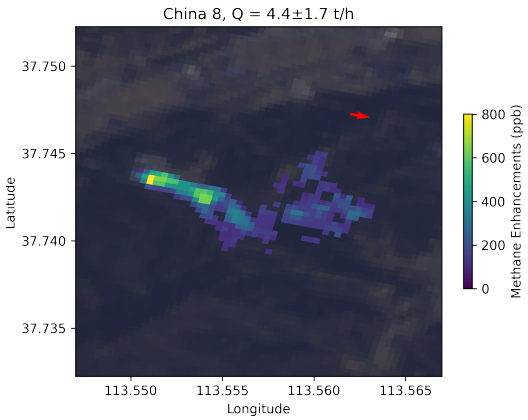

(b) 28/04/2020

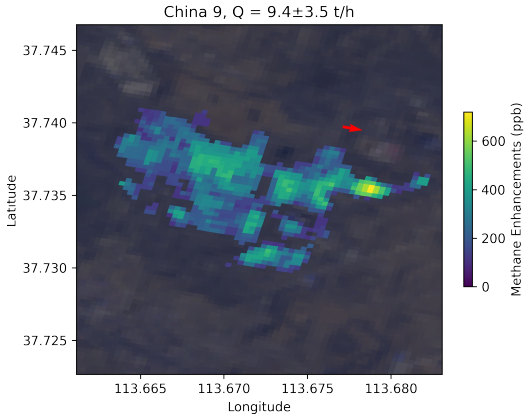

(c) 28/04/2020

Figure B.5

B.3. Controlled Release Experiments

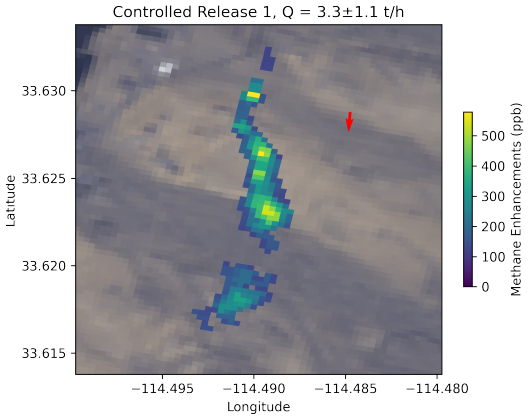

(a) 21/10/2021

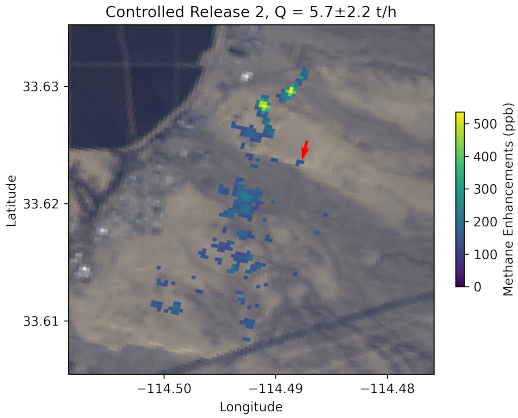

(b) 27/10/2021

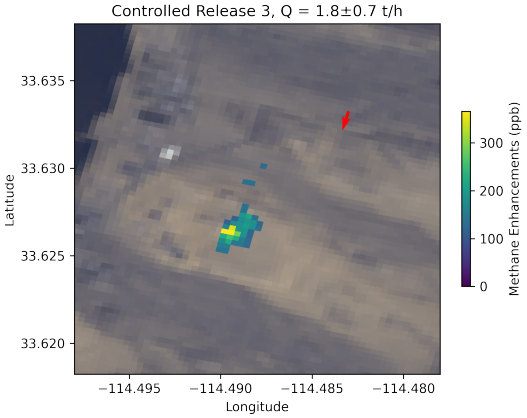

(c) 16/10/2021

Figure B.6

B.4. Permian

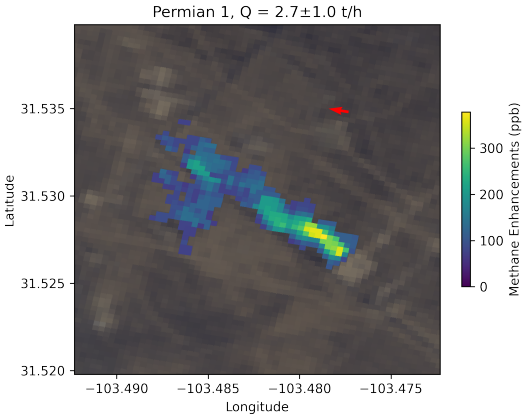

(a) 06/03/2021

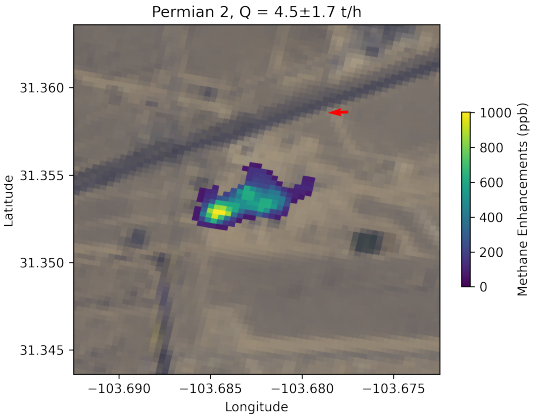

(b) 06/03/2021

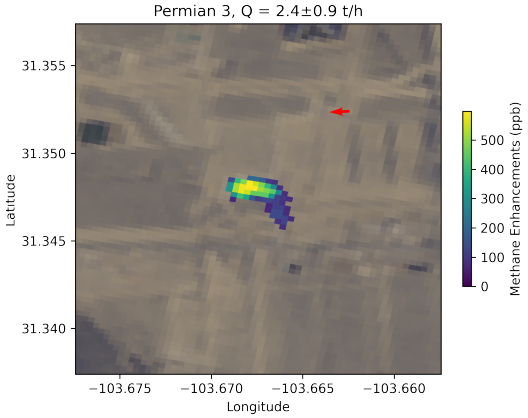

(c) 06/03/2021

Figure B.7

B.5. Turkmenistan

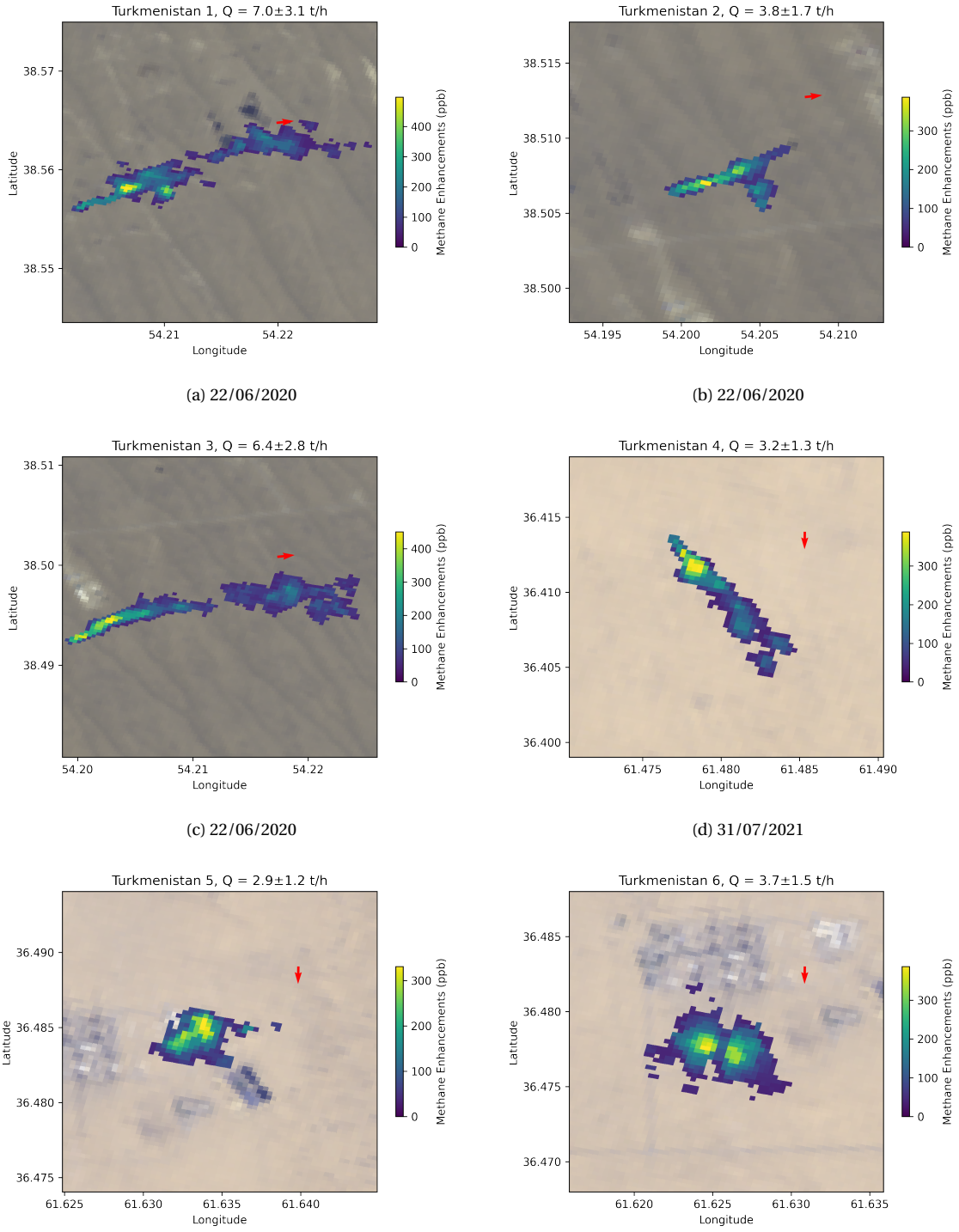

(a) 22/06/2020

(b) 22/06/2020

(c) 22/06/2020

(d) 31/07/2021

(e) 31/07/2021

(f) 31/07/2021

Figure B.8

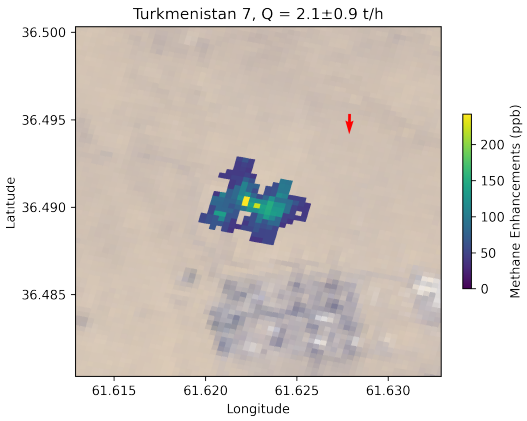

(a) 31/07/2021

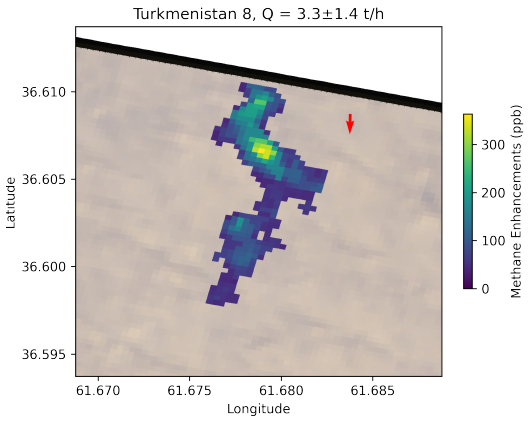

(b) 31/07/2021

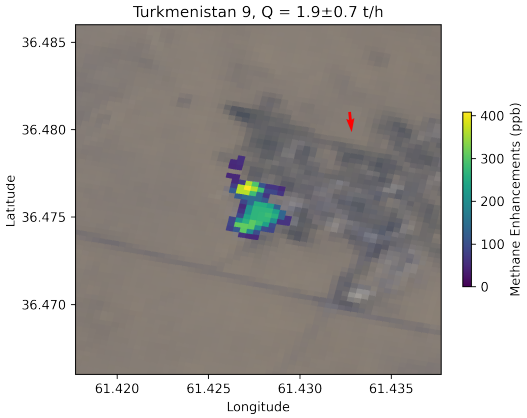

(c) 11/08/2021

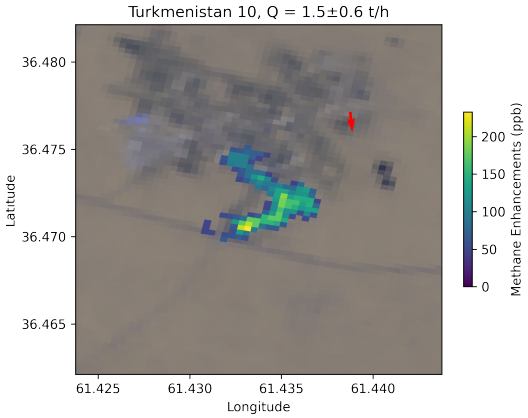

(d) 11/08/2021

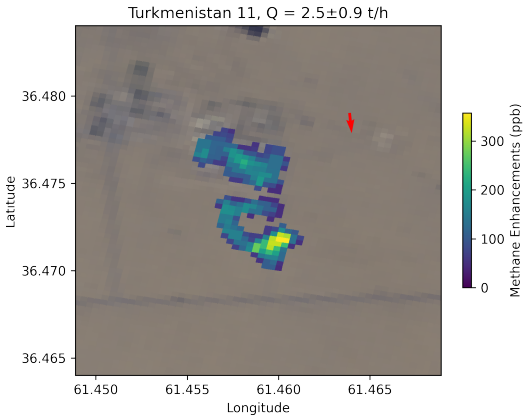

(e) 11/08/2021

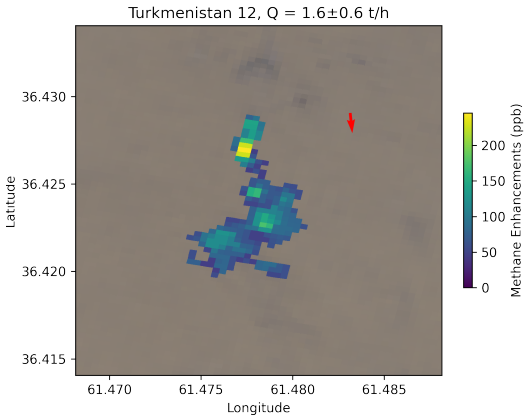

(f) 11/08/2021

Figure B.9

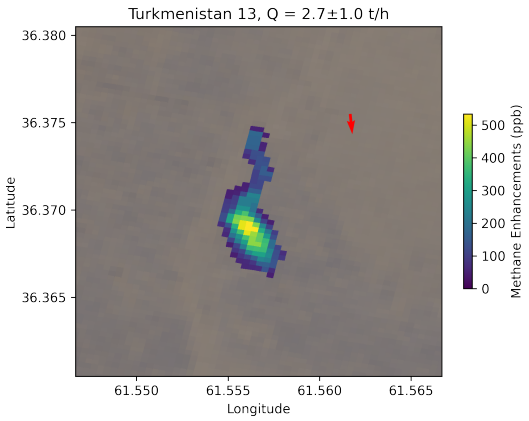

(a) 11/08/2021

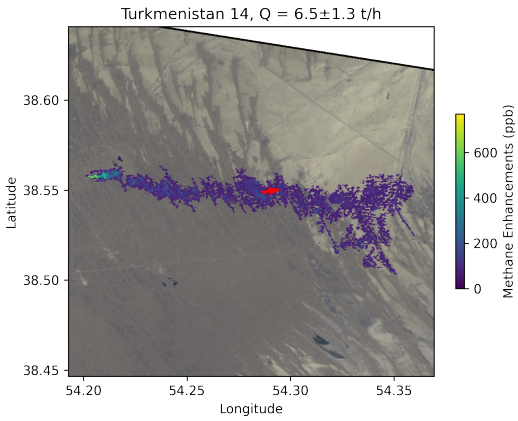

(b) 19/04/2020

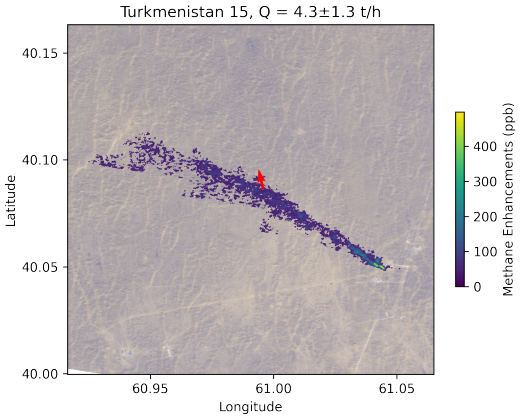

(c) 13/02/2021

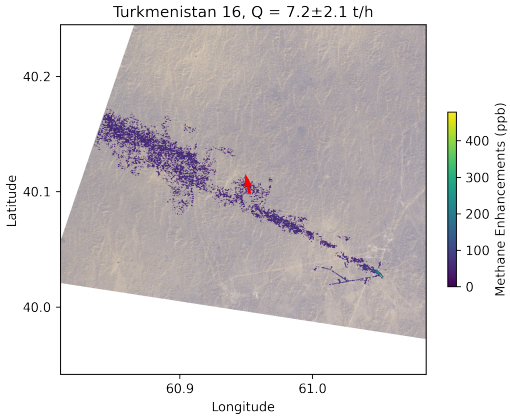

(d) 13/02/2021

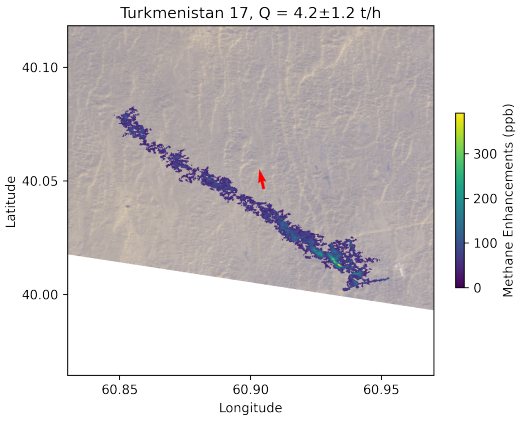

(e) 13/02/2021

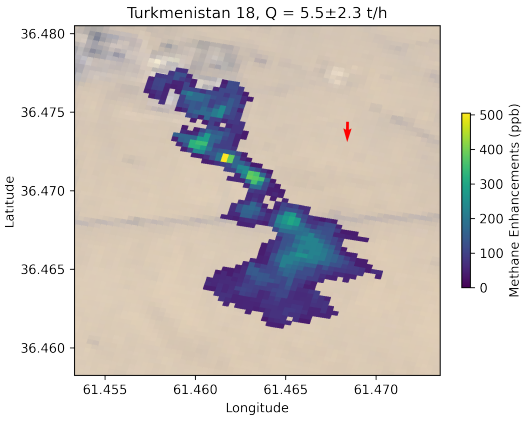

(f) 31/07/2021

Figure B.10

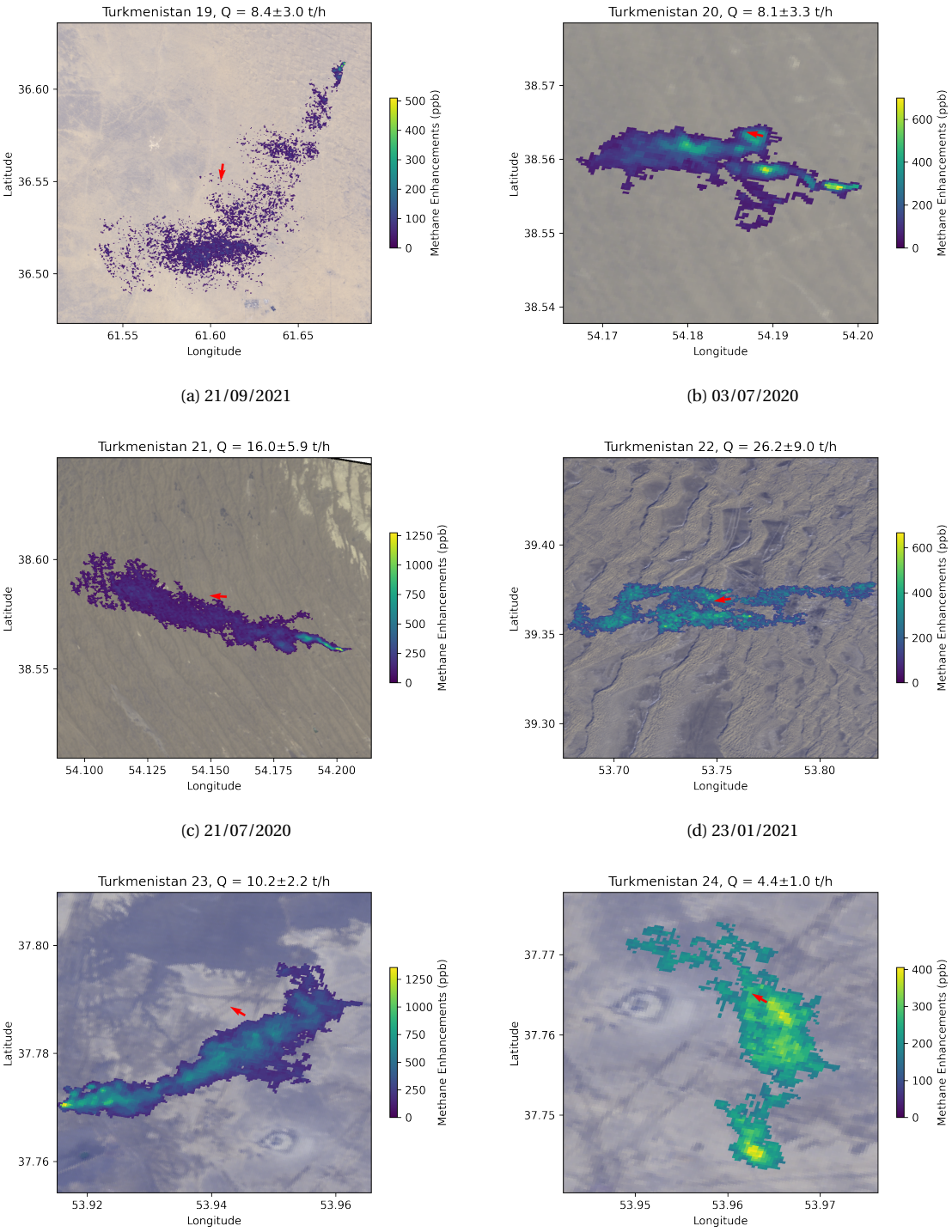

(a) 21/09/2021

(b) 03/07/2020

(c) 21/07/2020

(d) 23/01/2021

(e) 19/12/2021

(f) 19/12/2021

Figure B.11

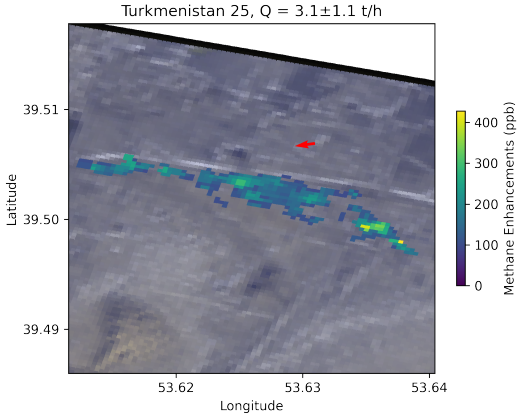

(a) 23/01/2021

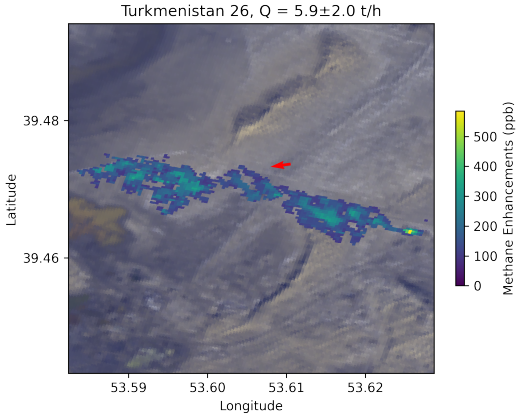

(b) 23/01/2021

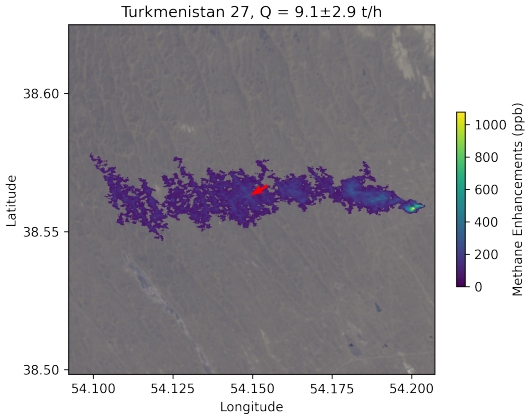

(c) 27/03/2022

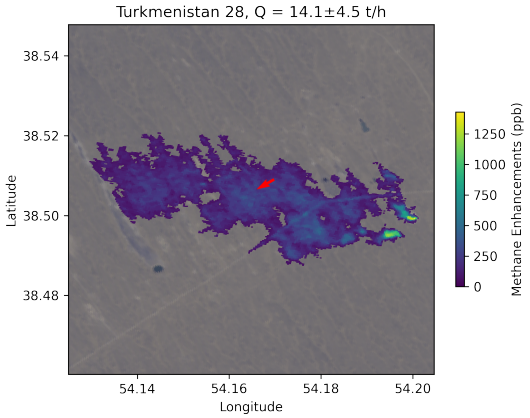

(d) 27/03/2022

Figure B.12

B.6. Miscellaneous

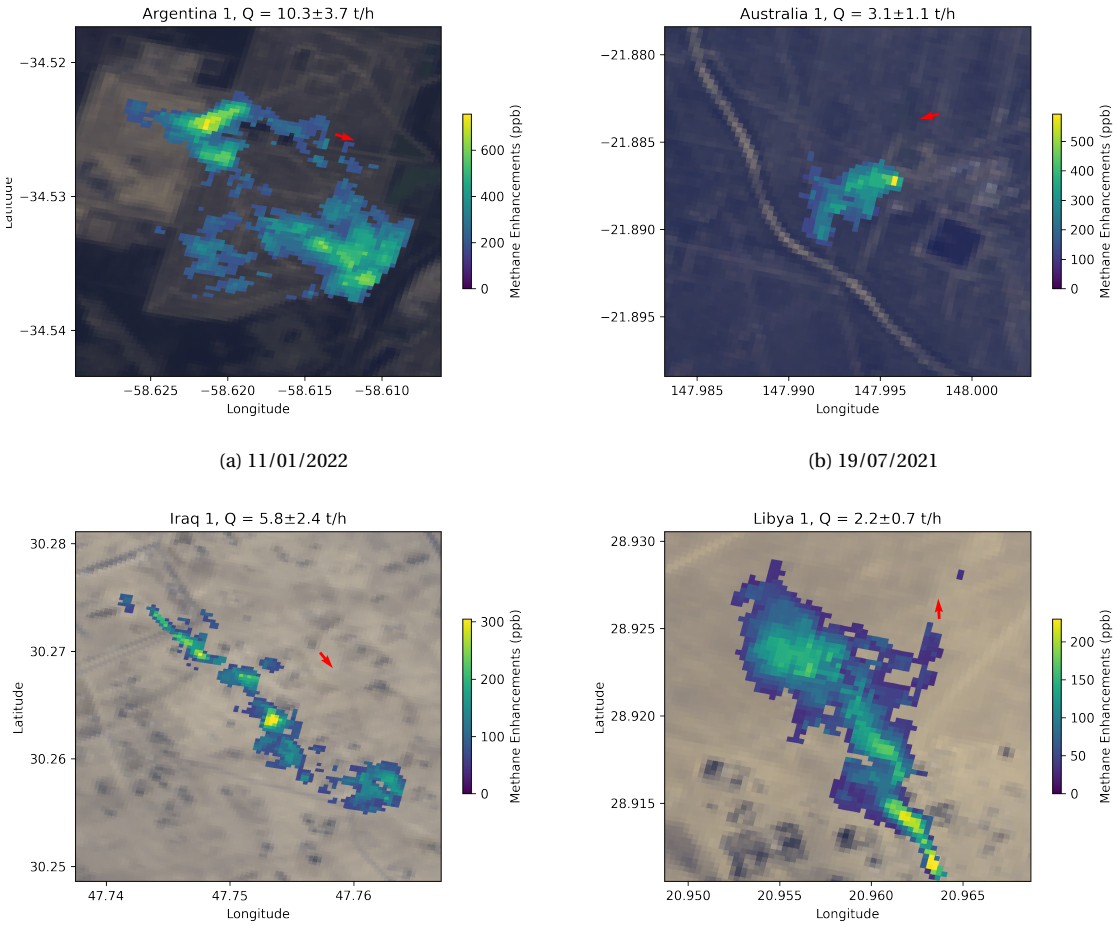

(a) 11/01/2022

(b) 19/07/2021

(c) 14/08/2021

(d) 07/01/2022

Figure B.13

Bibliography

[1] A Berk et al. “MODTRAN® 6: A major upgrade of the MODTRAN® radiative transfer code”. In: *2014 6th Workshop on Hyperspectral Image and Signal Processing: Evolution in Remote Sensing (WHISPERS)*. 2014, pp. 1–4. DOI: 10.1109/WHISPERS.2014.8077573.

[2] Helmut Bürgmann. “Methane Oxidation (Aerobic)”. In: *Encyclopedia of Geobiology* (2011). DOI: https://doi.org/10.1007/978-1-4020-9212-1{_}139.

[3] Guangyi Chen and Shen En Qian. “Denoising of hyperspectral imagery using principal component analysis and wavelet shrinkage”. In: *IEEE Transactions on Geoscience and Remote Sensing* 49.3 (Mar. 2011), pp. 973–980. ISSN: 01962892. DOI: 10.1109/TGRS.2010.2075937.

[4] Daniel H. Cusworth et al. *Multisatellite Imaging of a Gas Well Blowout Enables Quantification of Total Methane Emissions*. Jan. 2021. DOI: 10.1029/2020GL090864.

[5] Daniel H. Cusworth et al. “Quantifying Global Power Plant Carbon Dioxide Emissions With Imaging Spectroscopy”. In: *AGU Advances* 2.2 (June 2021). ISSN: 2576-604X. DOI: 10.1029/2020av000350.

[6] Digital Globe. *WorldView-3 Data Sheet Collection scenarios Design and specifications Panchromatic*. Tech. rep. 2014. URL: www.digitalglobe.com.

[7] G. Dochossois. “FIRST EUROPEAN REMOTE SENSING SATELLITE (ERS-1): OVERALL DESCRIPTION, POTENTIAL APPLICATIONS AND USERS.” In: *European Space Agency, (Special Publication) ESA SP*. 1983, pp. 25–36.

[8] D L Donoho. “Compressed sensing”. In: *IEEE Transactions on Information Theory* 52.4 (2006), pp. 1289–1306. DOI: 10.1109/TIT.2006.871582.

[9] Riley M. Duren et al. “California’s methane super-emitters”. In: *Nature* 575.7781 (Nov. 2019), pp. 180–184. ISSN: 14764687. DOI: 10.1038/s41586-019-1720-3.

[10] W. Emery and A. Camps. *Introduction to satellite remote sensing: Atmosphere, ocean, cryosphere and land applications*. 2017, pp. 1–860. ISBN: 9780128092545. DOI: 10.1016/C2015-0-04517-8.

[11] Xavier Faïn et al. “Northern Hemisphere atmospheric history of carbon monoxide since preindustrial times reconstructed from multiple Greenland ice cores”. In: *Climate of the Past Discussions* (2021), pp. 1–28. ISSN: 1814-9324. DOI: 10.5194/cp-2021-28.

[12] Bruno Fieque et al. “Status of space activity and science detectors development at Sofradir”. In: SPIE-Intl Soc Optical Eng, July 2019, p. 121. ISBN: 9781510630772. DOI: 10.1117/12.2536041.

[13] Markus D. Foote et al. “Fast and accurate retrieval of methane concentration from imaging spectrometer data using sparsity prior”. In: *IEEE Transactions on Geoscience and Remote Sensing* 58.9 (Sept. 2020), pp. 6480–6492. ISSN: 15580644. DOI: 10.1109/TGRS.2020.2976888.

[14] Luis Guanter, Rudolf Richter, and José Moreno. “Spectral calibration of hyperspectral imagery using atmospheric absorption features”. In: *Applied Optics* 45.10 (Apr. 2006), pp. 2360–2370. ISSN: 15394522. DOI: 10.1364/AO.45.002360.

[15] Luis Guanter et al. “Mapping methane point emissions with the PRISMA spaceborne imaging spectrometer”. In: *Remote Sensing of Environment* 265 (Nov. 2021), p. 112671. ISSN: 00344257. DOI: 10.1016/j.rse.2021.112671. URL: https://linkinghub.elsevier.com/retrieve/pii/S0034425721003916.

[16] Luis Guanter et al. *Scene-based spectral calibration assessment of high spectral resolution imaging spectrometers References and links*. Tech. rep. 2009. URL: http://www.fz-juelich.de/icg/icg-3/cefles/.

[17] Nathan Hagen and Michael W. Kudenov. “Review of snapshot spectral imaging technologies”. In: *Optical Engineering* 52.9 (Sept. 2013), p. 090901. ISSN: 0091-3286. DOI: 10.1117/1.oe.52.9.090901.

[18] Wei He et al. “Hyperspectral Image Denoising via Noise-Adjusted Iterative Low-Rank Matrix Approximation”. In: *IEEE Journal of Selected Topics in Applied Earth Observations and Remote Sensing* 8.6 (June 2015), pp. 3050–3061. ISSN: 21511535. DOI: 10.1109/JSTARS.2015.2398433.

[19] “IPCC AR6 WGI Chapter 3: Human influence on the climate system”. In: (2021).

[20] *IPCC AR6 WGI Chapter 7 Supplementary Material*. Tech. rep. 2021. URL: https://github.com/IPCC-WG1/Chapter-7.

[21] *IPCC AR6 WGI Chapter 7: The Earth's energy budget, climate feedbacks, and climate sensitivity*. Tech. rep. 2021.

[22] *IPCC AR6 WGI Climate Change 2021 The Physical Science Basis*. Tech. rep.

[23] Itziar Irakulis-Loitxate et al. “Satellites unveil easily-fixable super-emissions in one of the world's largest methane hotspot regions 2 3”.

[24] Daniel J Jacob. *Introduction to Atmospheric Chemistry*. 1999.

[25] Daniel J Jacob et al. “Quantifying methane emissions from the global scale down to point sources using satellite observations of atmospheric methane”. In: (2022). DOI: 10.5194/acp-2022-246. URL: https://doi.org/10.5194/acp-2022-246.

[26] Daniel J. Jacob et al. “Satellite observations of atmospheric methane and their value for quantifying methane emissions”. In: *Atmospheric Chemistry and Physics* 16.22 (Nov. 2016), pp. 14371–14396. ISSN: 16807324. DOI: 10.5194/acp-16-14371-2016.

[27] Safieh Javadinejad, Saied Eslamian, and Kaveh Ostad-Ali-Askari. “Investigation of monthly and seasonal changes of methane gas with respect to climate change using satellite data”. In: *Applied Water Science* 9.8 (Nov. 2019). ISSN: 2190-5487. DOI: 10.1007/s13201-019-1067-9.

[28] Dylan Jervis et al. “The GHGSat-D imaging spectrometer”. In: *Atmospheric Measurement Techniques* 14.3 (Mar. 2021), pp. 2127–2140. ISSN: 18678548. DOI: 10.5194/amt-14-2127-2021.

[29] Ir A Kamp. *Space Instrumentation Engineering Lecture Notes ae4-880 Faculty of Aerospace Engineering Space Instrumentation Engineering*. Tech. rep. 2007.

[30] Stefanie Kirschke et al. *Three decades of global methane sources and sinks*. Oct. 2013. DOI: 10.1038/ngeo1955.

[31] Demetrio Labate et al. “The PRISMA payload optomechanical design, a high performance instrument for a new hyperspectral mission”. In: *Acta Astronautica* 65.9-10 (Nov. 2009), pp. 1429–1436. ISSN: 00945765. DOI: 10.1016/j.actaastro.2009.03.077.

[32] J Landgraf et al. *Sentinel 5 L2 Prototype Processors, Algorithm Theoretical Baseline Document: Carbon Monoxide Retrieval*. Tech. rep. 2019.

[33] Jochen Landgraf and Joost Aan De Brugh. *Sicor-S5 for Sentinel 5 Operational Processor Software Release Note*. Tech. rep.

[34] Jochen Landgraf et al. “Carbon monoxide total column retrievals from TROPOMI shortwave infrared measurements”. In: *Atmospheric Measurement Techniques* 9.10 (Oct. 2016), pp. 4955–4975. ISSN: 18678548. DOI: 10.5194/amt-9-4955-2016.

[35] R Lasaponara et al. *The Prisma Hyperspectral Mission*. Tech. rep. 2020.

[36] Antje Ludewig et al. “In-flight calibration results of the TROPOMI payload on board the Sentinel-5 Precursor satellite”. In: *Atmospheric Measurement Techniques* 13.7 (July 2020), pp. 3561–3580. ISSN: 18678548. DOI: 10.5194/amt-13-3561-2020.

[37] Michael Lustig, David Donoho, and John M. Pauly. “Sparse MRI: The application of compressed sensing for rapid MR imaging”. In: *Magnetic Resonance in Medicine* 58.6 (Dec. 2007), pp. 1182–1195. ISSN: 07403194. DOI: 10.1002/mrm.21391.

[38] Andrea Molod et al. *Technical Report Series on Global Modeling and Data Assimilation, Volume 28 The GEOS-5 Atmospheric General Circulation Model: Mean Climate and Development from MERRA to Fortuna*. Tech. rep. 2012. URL: http://www.sti.nasa.gov.

[39] Yoanna-Reine Nowicki-Bringuier and Philippe Chorier. “Sofradir SWIR hyperspectral detectors for space applications”. In: *Proc SPIE* (Sept. 2009). DOI: 10.1117/12.830721.

[40] Stefano Pignatti et al. “PRISMA L1 and L2 Performances within the PRISCAV Project: The Pignola Test Site in Southern Italy”. In: *Remote Sensing* 14.9 (Apr. 2022), p. 1985. ISSN: 2072-4292. DOI: 10.3390/rs14091985. URL: https://www.mdpi.com/2072-4292/14/9/1985.

[41] *PRISMA Product Specifications*. Tech. rep. ASI, Mar. 2020.

[42] Behnood Rasti et al. “Noise reduction in hyperspectral imagery: Overview and application”. In: *Remote Sensing* 10.3 (Mar. 2018). ISSN: 20724292. DOI: 10.3390/rs10030482.

[43] Elena Sánchez-García et al. “Mapping methane plumes at very high spatial resolution with the WorldView-3 satellite”. In: (). DOI: 10.5194/amt-2021-238. URL: https://doi.org/10.5194/amt-2021-238.

[44] Marielle Saunois et al. “The global methane budget 2000-2017”. In: *Earth System Science Data* 12.3 (July 2020), pp. 1561–1623. ISSN: 18663516. DOI: 10.5194/essd-12-1561-2020.

[45] Kersten Schmidt, Núria Tous Ramon, and Marco Schwerdt. “Radiometric accuracy and stability of sentinel-1A determined using point targets”. In: *Journal of the Royal Asiatic Society* 10.5-6 (June 2018), pp. 538–546. ISSN: 14740591. DOI: 10.1017/S1759078718000016.

[46] Mark R. Schoeberl et al. “Overview of the EOS aura mission”. In: *IEEE Transactions on Geoscience and Remote Sensing* 44.5 (May 2006), pp. 1066–1072. ISSN: 01962892. DOI: 10.1109/TGRS.2005.861950.

[47] Francois Spoto et al. “Overview Of Sentinel-2”. In: *2012 IEEE International Geoscience and Remote Sensing Symposium*. 2012, pp. 1707–1710. DOI: 10.1109/IGARSS.2012.6351195.

[48] D. R. Thompson et al. “Real-time remote detection and measurement for airborne imaging spectroscopy: A case study with methane”. In: *Atmospheric Measurement Techniques* 8.10 (Oct. 2015), pp. 4383–4397. ISSN: 18678548. DOI: 10.5194/amt-8-4383-2015.

[49] A. K. Thorpe et al. “Mapping methane concentrations from a controlled release experiment using the next generation airborne visible/infrared imaging spectrometer (AVIRIS-NG)”. In: *Remote Sensing of Environment* 179 (June 2016), pp. 104–115. ISSN: 00344257. DOI: 10.1016/j.rse.2016.03.032.

[50] Andrew K. Thorpe et al. “Airborne DOAS retrievals of methane, carbon dioxide, and water vapor concentrations at high spatial resolution: Application to AVIRIS-NG”. In: *Atmospheric Measurement Techniques* 10.10 (Oct. 2017), pp. 3833–3850. ISSN: 18678548. DOI: 10.5194/amt-10-3833-2017.

[51] Richard M. Van Hees et al. “Determination of the TROPOMI-SWIR instrument spectral response function”. In: *Atmospheric Measurement Techniques* 11.7 (July 2018), pp. 3917–3933. ISSN: 18678548. DOI: 10.5194/amt-11-3917-2018.

[52] Daniel J. Varon et al. “High-frequency monitoring of anomalous methane point sources with multispectral Sentinel-2 satellite observations”. In: *Atmospheric Measurement Techniques* 14.4 (Apr. 2021), pp. 2771–2785. ISSN: 18678548. DOI: 10.5194/amt-14-2771-2021.

[53] Daniel J. Varon et al. “Quantifying methane point sources from fine-scale satellite observations of atmospheric methane plumes”. In: *Atmospheric Measurement Techniques* 11.10 (Oct. 2018), pp. 5673–5686. ISSN: 18678548. DOI: 10.5194/amt-11-5673-2018.

[54] J. P. Veefkind et al. “TROPOMI on the ESA Sentinel-5 Precursor: A GMES mission for global observations of the atmospheric composition for climate, air quality and ozone layer applications”. In: *Remote Sensing of Environment* 120 (May 2012), pp. 70–83. ISSN: 00344257. DOI: 10.1016/j.rse.2011.09.027.

[55] J. Vidot et al. “Carbon monoxide from shortwave infrared reflectance measurements: A new retrieval approach for clear sky and partially cloudy atmospheres”. In: *Remote Sensing of Environment* 120 (May 2012), pp. 255–266. ISSN: 00344257. DOI: 10.1016/j.rse.2011.09.032.

[56] Zimichev E.A. and Kazanskiy N.L. *Spectral-spatial classification with k-means++ particional clustering*. Tech. rep. 2014, p. 2.